UNIVERSITY OF CALIFORNIA, SAN DIEGO

Design and Fabrication of Efficient Electrodes for Dye Sensitized Solar Cells

A dissertation submitted in partial satisfaction of the
requirements for the degree
Doctor of Philosophy

in

Materials Science and Engineering

by

Jirapon Khamwannah

Committee in charge:

Professor Jan Talbot, Chair
Professor Ratnesh Lal
Professor Yu-Hwa Lo
Professor Patrick Mercier
Professor Yu Qiao

2015

The dissertation of Jirapon Khamwannah is approved, and it is acceptable in quality and form for publication on microfilm and electronically:

_____

_____

_____

_____

_____

Chair

University of California, San Diego

2015

DEDICATION

I dedicate my dissertation to my beloved family, Jaras and Lamai Khamwannah who have given me immeasurable love and support all along the way. I would have not come this far without you.
To Prin mana-aporn and his family for always being by my side.
Also,to Karina for purring around and making me happy.

EPIGRAPH

It is never too late to be what you might have been.

—*George Eliot*

TABLE OF CONTENTS

LIST OF FIGURES

LIST OF TABLES

ACKNOWLEDGEMENTS

First of all, I would like to express my sincere gratitude to the Jacobs School of Engineering and the Materials Science and Engineering program for giving me the opportunity to fulfill my dream as a PhD student here. I also would like to thank Professor Sungho Jin for providing me ideas, guidance, and inspiration for the projects through many years. To my committee chair, Professor Jan B.Talbot, I'm extremely grateful for your encouragement and support. Thank you for believing in me and pushing me further than I thought I could go. Also, I would like to thank my committee members, Professor Ratnesh Lal, Professor Yu-Hwa Lo, Professor Patrick Mercier and Professor Yu Qiao for helpful discussion on my research. My deepest appreciation also goes to the Ministry of Science and Technology, Royal Thai Government for their financial support through my entire graduate study. Cosmo and Cosmo-America, Iwama fund, and National Research Foundation (NRF) grant for financial support of the research.

To all of my past and present colleagues in the Jin lab who have also made a great contribution toward my graduate study. Dr.Leon Chen, Dr.Chulmin Choi, Dr.Hyunsu Kim, Dr.Taekyoung Kim, Dr.Cyrus Rustomji, Dr.Isaac Liu and Dr.Gary Johnston, their willingness to help as well as their invaluable ideas and suggestion are always impressed me. I would like to thank to my wonderful friends : Sun Young Noh, YanYan Zhang and my San Diego Thai friends for their awesome friendship. Thank you for helping and cheering me up!

Last but not least, without my family, I would have not come this far. Thank you my parent for their sacrifice in order to put me to the highest education.

Chapter 2, in full, is a reprint of the material as it appears in Nano Energy, Volume 1, 2012. Jirapon Khamwannah, Yanyan Zhang, Sun Young Noh, Hyunsu Kim, Christine Frandsen, Seong Deok Kong and Sungho Jin.The dissertation author was the primary investigator and author of this paper.

Chapter 3, in full, is a reprint of the material as it appears in J. Renewable Sustainable Energy, vol.4, 2012. Jirapon Khamwannah, Sun Young Noh, Christine Frandsen, Yanyan Zhang, Hyunsu Kim, Seong Deok Kong, and Sungho Jin. The dissertation author was the primary investigator and author of this paper.

Chapter 4, in full, is a reprint of the material as it appears in Nanotechnology, vol.24, 2012. Yanyan Zhang, Jirapon Khamwannah, Hyunsu Kim, Sun Young Noh, Haibin Yang, Sungho Jin. The dissertation author was the primary investigator and co-author of this paper.And partly, is a reprint of the material as it appears in Journal of Nanoscience and Nanotechnology, vol.13, 2013. Jirapon Khamwannah, Hyunsu Kim, Yanyan Zhang, Tae Kyoung Kim and Sungho Jin. The dissertation author was the primary investigator and author of this paper.

VITA

2006	B. E. in Materials Engineering, King's Mongkut University of Technology Thonburi,Thailand
2010	M. S in Materials Science and Engineering, University of California, San Diego
2010-2014	Research Assistant, University of California, San Diego
2015	Ph. D. in Materials Science and Engineering, University of California, San Diego

PUBLICATIONS

Jirapon Khamwannah, Yanyan Zhang, Sun Young Noh, Hyunsu Kim, Christine Frandsen, Seong Deok Kong, and Sungho Jin. "Enhancement of dye sensitized solar cell efficiency by composite TiO_2 nanoparticle/8nm TiO_2 nanotube paper-like photoelectrode." *Nano Energy* 1, no. 3 (2012): 411-417.

Jirapon Khamwannah, Sun Young Noh, Christine Frandsen, Yanyan Zhang, Hyunsu Kim, Seong Deok Kong, and Sungho Jin. "Nanocomposites of TiO_2 and double-walled carbon nanotubes for improved dye-sensitized solar cells." *Journal of Renewable and Sustainable Energy* 4, no. 2 (2012):023116.

Jirapon Khamwannah, Hyunsu Kim, Yan Yan Zhang, Tae Kyoung Kim, and Sungho Jin. "Control of nanogeometry for advanced energy applications." *Journal of nanoscience and nanotechnology* 13, no. 12 (2013): 8199-8206.

Yanyan Zhang, **Jirapon Khamwannah**, Sun Young Noh, Haibin Yang, Sungho Jin, "Improved Dye Sensitized Solar Cell Performance in Larger Cell Size by Using TiO_2 Nanotubes", *Nanotechnology*,24, 045401 (2013).

Kim, Hyunsu, Kunbae Noh, Chulmin Choi, **Jirapon Khamwannah**, Diana Villwock, and Sungho Jin. "Extreme superomniphobicity of multiwalled 8 nm TiO_2 nanotubes." *Langmuir* 27, no. 16 (2011): 10191-10196.

Kim, Hyunsu, **Jirapon Khamwannah**, Chulmin Choi, Calvin J. Gardner, and Sungho Jin. "Formation of 8nm TiO_2 nanotubes on a three dimensional electrode for enhanced photoelectrochemical reaction." *Nano Energy* 2, no. 6 (2013): 1347-1353.

Kim, Hyunsu, Chulmin Choi, **Jirapon Khamwannah**, Sun Young Noh, Yanyan Zhang, Tae-Yeon Seong, and Sungho Jin. "Plasmonic Au nanoparticles on 8 nm TiO 2 nanotubes for enhanced photocatalytic water splitting." *Journal of Renewable and Sustainable Energy* 5, no. 5 (2013): 053104.

Ni, Jia-Hua, Christine Frandsen, Li-Han Chen, Yan-Yan Zhang, **Jirapon Khamwannah**, Guo He, Ting-Ting Tang, and Sungho Jin. "Fabrication of Gradient TiO_2 Nanotubes on Ti Foil by Anodization." *Advanced Engineering Materials* 15, no. 6 (2013): 464-468.

Kong, Seong Deok, Weizhou Zhang, Jun Hee Lee, Chulmin Choi, **Jirapon Khamwannah**, Michael Karin, and Sungho Jin. "Externally triggered on-demand drug release and deep tumor penetration." *Journal of Vacuum Science & Technology B* 30, no. 2 (2012): 02C102.

Kong, Seong Deok, Chulmin Choi, **Jirapon Khamwannah**, and Sungho Jin. "Magnetically Vectored Delivery of Cancer Drug Using Remotely On–Off Switchable NanoCapsules." *Magnetics, IEEE Transactions on* 49, no. 1 (2013): 349-352.

Choi, Chulmin, Kunbae Noh, Duyoung Choi, **Jirapon Khamwannah**, Chin-Hung Liu, Daehoon Hong, Li-han Chen, and Sungho Jin. "Geometrically Planar Ion-Implant Patterned Magnetic Recording Media Using Block Copolymer Aided Gold Nanoisland Masks." Magnetics, *IEEE Transactions on* 48, no. 11 (2012): 3402-3405.

Kim, Tae Kyoung, Bryan VanSaders, Jaeyun Moon, Taewoo Kim, Chin-Hung Liu, **Jirapon Khamwannah**, Dongwon Chun, Duyoung Choi, Alireza Kargar, Renkun Chen, Zhaowei Liu and Sungho Jin. "Tandem structured spectrally selective coating layer of copper oxide nanowires combined with cobalt oxide nanoparticles." *Nano Energy* 11 (2015): 247-259.

ABSTRACT OF THE DISSERTATION

Design and Fabrication of Efficient Electrodes for Dye Sensitized Solar Cells

by

Jirapon Khamwannah

Doctor of Philosophy in Materials Science and Engineering

University of California, San Diego, 2015

Professor Jan Talbot, Chair

Dye sensitized solar cells (DSSCs) represent a cheap and clean technology to harnesses solar energy efficiently. To further decrease the production cost while improving the device performance is a bottleneck for large scale application and commercialization of DSSCs. The thesis focuses on the development of economically competitive photoelectrodes with the motivation to further enhance energy conversion efficiency of DSSCs. Practical and scalable device fabrication is also proposed and studied in details.

In this research, several novel structures of TiO_2 photo-anode beside the TiO_2 nanoparticls thin film have been prepared. A composite of TiO_2 nanoparticles/8 nm TiO_2 nanotubes was successfully fabricated as a stand-alone, paper-like

structure for a photoanode of dye-sensitized solar cells by using a simple pressing method. The best power conversion efficiency of 5.38% was obtained on micropaper with a combination of TiO_2 nanospherical particles and a 1D nanostructure.

Incorporation of double-walled carbon nanotubes (DWCNTs) into a TiO_2 photo-anode layer has been studied. A significant improvement in the performance in the DSSC was obtained from the DWCNTs-TiO_2 photoanode. Comparing to the standard TiO2 anode, the carbon nanotube-containing TiO_2 anode with 0.2 wt.% DWCNTs has boosted up the photocurrent density (J_{sc}) by 43%.

In order to mitigate the severe performance deterioration in larger size DSSC solar cells, the use of anodized TiO_2 nanotubes was introduced on Ti foil. Instead of FTO glass, the photoanode was made of Ti foil. Elimination of the highly resistive FTO glass in the anode structure, as well as the enhanced charge collection via the nanotube-coated Ti substrate, resulting in improving mechanical and electrical connections, electron conduction and possibly improving the light trapping.

Chapter 1

Introduction

1.1 A brief history of photovoltaics

In 1839, 19-year-old French physicist Edmond Becquerel observed a phenomenon of light-energy conversion. He noticed that two electrodes in an electrolyte could produce small amount of electric current when exposed to light [2].This was later called the "Photovoltatic (PV) effect". In 1873, the photoconductivity of selenium was measured by Willoughby Smith. In his experiment he found that the conductivity of the selenium increased from 15 to 100 percent, increasing with the intensity of light [3]. The first selenium solar cell construction was then built in 1877 with the light-to-electricity efficiency of 1-2%. However, the selenium deteriorated very quickly when exposed to strong light and with its very low efficiency, it was not a promising material for large-scale solar devices.

In 1904, the theory explanation of the "photovoltaic effect" was first explained by Albert Einstein. He published a simple description of "light quanta" (later called "photons") which is the basis for all photovoltaic devices and in common semiconductors [4]. In 1921, he won the Nobel Prize for this theoretical explanation.This theory was proven in practice by Robert Millikan's experiment in 1916. Since then, a variety of concepts and devices had been developed to harvest sunlight to produce electricity. A breakthrough in photovoltaic devices started when a Polish scientist Jan Czochralski discovered a method for monocrystalline silicon production, which enabled monocrystalline solar cell production in 1918 [5].

The Czochralski process was adapted for producing highly purity crystalline silicon by Bell Laboratories. The the first crystalline silicon photovoltaic cell was constructed and the efficiency of 4% for light-to-energy conversion was reached.

One of the major milestones in the development of the photovoltaic solar cell was when the researchers at Bell Laboratories created the near-surface p-n junction of solar cell by treating an n-type silicon wafer with boron trichloride which greatly increased the charge separation of the devices, which then increased the conversion efficiency to 6% by Chapin in the 1950s [6]. This was 50-times the efficiency of the selenium solar cell produced in the 1930s. Other types of thin-film heterojuction solar cells such as GaAs,InP ,CdS and CdTe were also studied for higher efficiency. However, with the high production cost (several $100 per watt), the photovoltaic solar cell at that time was only usable for space applications.

In 1970s, when the worldwide oil crisis became a serious concern, many countries looked for the alternative renewable energy sources, including photovoltaic solar cells. It was during this period that the second generation photovoltaic solar cells, such as polycrystalline and amorphous silicon, thin-film deposits of silicon, CdTe, $CuInSe_2$, (CIS) and $Cu(In,Ga)Se_2$ (CIGS), as well as multijunction cell technology were emerged. These devices were not only designed for achieving higher efficiency but also to cut down the production cost compared to the traditional single crystalline silicon devices.The first thin-film solar cell with over 10% efficiency was produced in 1980 based on Cu_2S/CdS. Many photovoltaic companies also established in this period, such as Solar Power Corporation (1970), Solarex Corporation (1973), Solec International (1975) and Solar Technology International (1975).

In 1989, the first commercial thin-film photovoltaic module was produced by ARCO Solar. The photovoltaic market kept growing rapidly. The worldwide production of photovoltaics reached 100MW per year in 1997.In the mean times, the third generation photovoltaic solar cells were realized. These devices included dye-sensitized solar cells, polymer solar cells and nano-crystalline solar cells. The third generation photovoltaic solar cells are different from the first and second generations, which rely on a p-n junction to separate charges. On the other hand,

they form a “bulky” junction for charges to separate. Moreover, they could be made from low-cost materials with ease of device fabrication. These are expected to be a promising technologies among others in the photovoltaic solar cells areas [7], [8].Figure 1.1 shows the evolution in photovoltaics efficiency since 1975 to present.

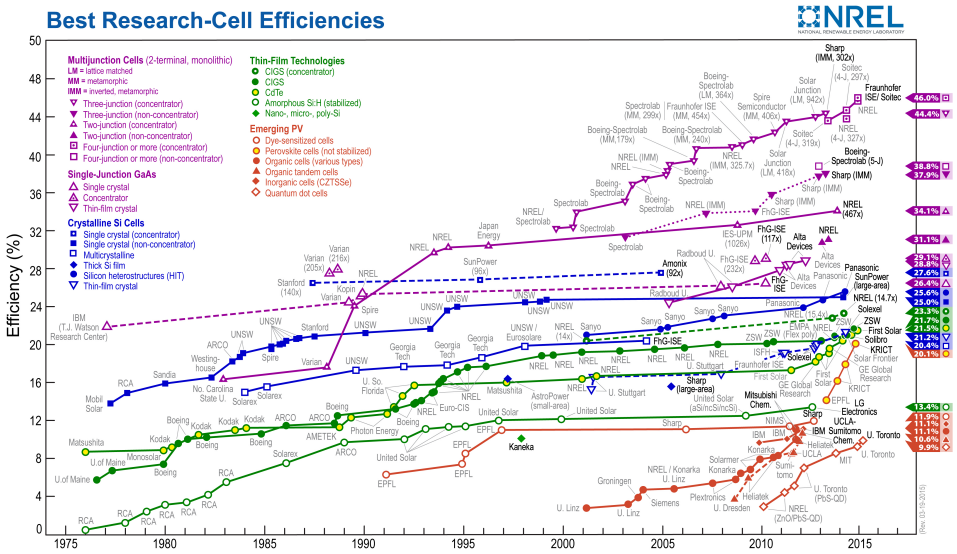

Figure 1.1: Evolution of photovoltaics conversion efficiency overtime (from [9]).

Presently, the photovoltaic market still depends mostly on the conventional first generation of solar cell which is a p-n junction using monocrystalline silicon (85% in the market) [10]. The current researches shows that the efficiency of this solar cell can gain up to 30% [11] with a much lower cost. These gains have been achieved partly through research development and demonstration and partly through the market stimulation. In late 2010, the best-in-class installed photovoltaic costs for utility-system were recorded at about $3.80 per watt [12] and the prices were predicted to continue decreasing due to the continuous price and performance improvements. Efforts were then moved toward ways to cut the costs further and make the price comparable to traditional energy sources. Some established semiconductor-based technologies are gallium arsenide tin film solar cells (GaAs, $\eta \approx 24\%$), copper–indium–gallium–diselenide (CIGS, $\eta \approx 20\%$), cadmium–telluride (CdTe, $\eta \approx 17\%$) and amorphous/nanocrystalline silicon ($\eta \approx 10\%$) solar cells [13]. These devices, which are the second generation of thin film tech-

nologies, are believed to have an important role in increasing the PV installation capacity by 2015. However, they share the same performance and cost limitations as in the first generation devices. Therefore, to bring the cost down even further and more rapidly, breakthrough technologies and processes are required to decrease the cost of the photovoltaic modules. The long-term goal for photovoltaic market is to produce 34% of the total world electricity production by 2050 [14].

1.2 Dye sensitized solar cell

The dye sensitized solar cells (DSSCs) was developed in 1991 by O'Regan and Grätzel [15].This type of solar cell attains a relatively high efficiency (∼11% at full sunlight) and is made of cheap components that are non-toxic and abundant. This is considered to be very promising photovoltaic technology since it offers many exclusive features such as semi-transparency, multi-color range possibilities, flexibility and lightweight applications, and also good performance under low light conditions and different solar incident angles [16] [17] [18]. Figure 1.2 illustrates the exmaples of DSSC uses in real life. The unique characteristics of DSSC open the possibility for building integration in photovoltaic windows and facades as well as applications in small, flexible and low-power consumer devices.

Figure 1.2: DSSC uses in real life (Top) G24:solar charging for mobile devices (from [1]) (Bottom) Solaronix' multicolored transparent photovoltaic facade at the SwissTech Convention Center, EPFL, Switzerland (from [19]).

1.2.1 Structure of a dye sensitized solar cell

The key parts of the standard dye sensitized solar cell (DSSC) are illustrated in Figure 1.3. The cell is composed of mainly five components: a transparent conducting substrate, a nanostructured/nanoporous wide-band gap semiconductor thin film, a photosensitizer/sensitizing dye adsorbed on the nanostructured-layer, a redox electrolyte and a counter electrode.The components of DSSC will be described in more detail.

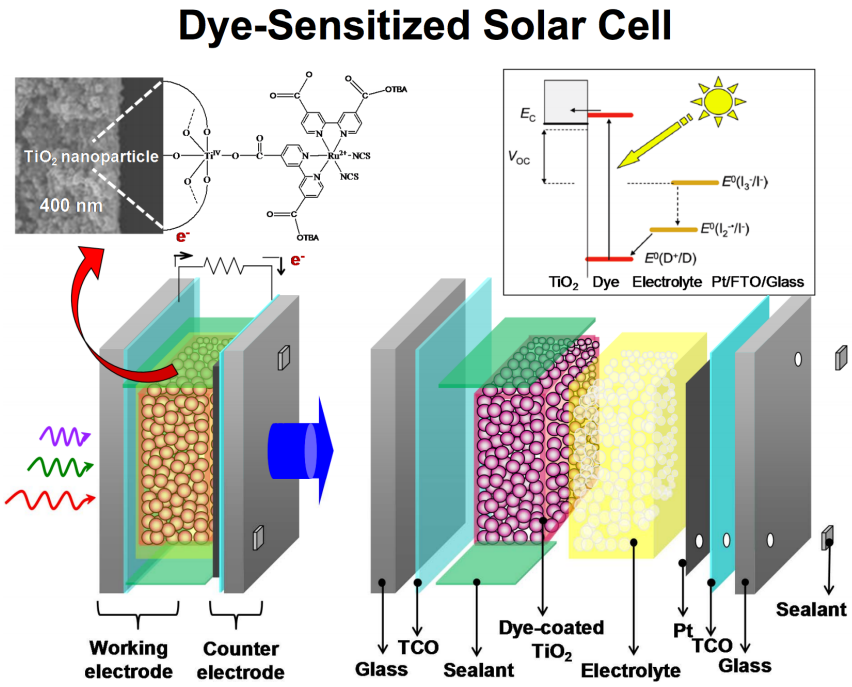

Figure 1.3: Schematic diagram of conventional DSSC structure.

1.) Transparent conducting substrate

The transparent conducting substrate or TCO glass is commonly used as the DSSC substrate because of their relatively low cost, abundance, and high optical transparency in the visible and infrared region of the solar spectrum. The TCO glass is made of bare glass doped with a metal oxide thin film to make it electrically conductive. The most common type of TCO coating are florine-doped tin oxide-FTO (SnO_2:F, FTO) and indium tin oxide-ITO (In_2O_3:Sn, ITO). In gen-

eral, fluorine-doped tin oxide (FTO) glass is used in DSSCs instead of indium tin oxide (ITO) coated glass because of its better thermal stability at high temperatures. This conducting film sheet resistance of the TCO substrate is typically 10-20Ω per square area. However, to select the suitable sheet resistance of the TCO substrate, the one factor that is needed to be taken into account is the transmittance of the substrate: a higher conductance (lower resistance) results in a lower transmittance. Moreover, the TCO substrates transmittance level is further reduced after a deposition of nanostructured material. Figure 1.4 shows a typical transmittance measurement of conductive glass electrode before and after being coated with nanostructured TiO_2 layer. Besides its role as a current collector, the TCO substrates are used as a support for the nanostructured wide-bandgap as a photoanode, a Pt counter electrode and as well as a sealing layer for the DSSC cell.

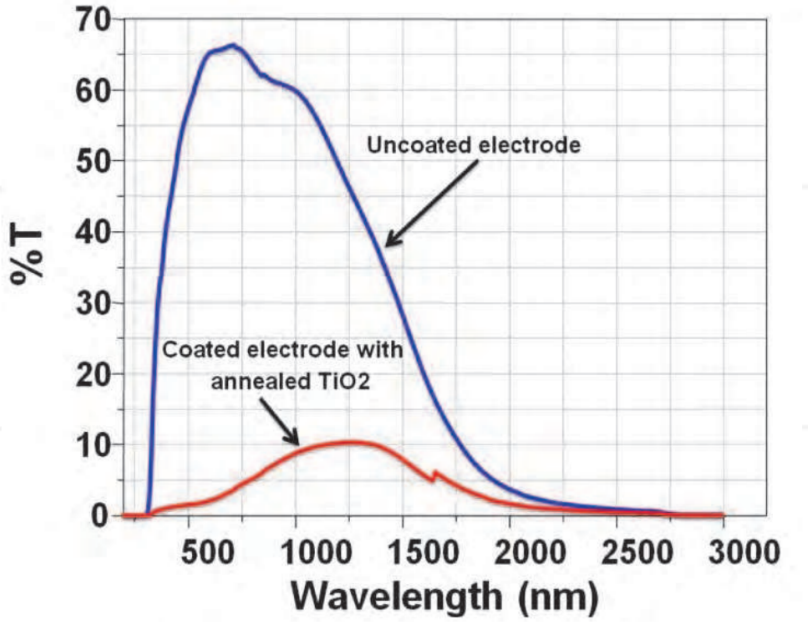

Figure 1.4: Transmittance of a conductive glass electrode before and after being coated with nanostructured TiO_2 layer (from [20]).

2.) A wide-band gap nanostructured semiconductors thin film as a photoelectrode

The photoelectrode (or photoanode) in a DSSC is made from a thin layer of sensitized wide-band gap nanostructured semiconductor (typically TiO_2, ZnO, SnO_2 and Sb_2O_5) deposited onto the TCO substrate. In order to achieve high light-harvesting efficiency (LHE), the nanostructured semiconductor layer must provide a large surface area (high roughness) to permit the adsorption of a large amount of sensitizer molecules [21] [15].

Among the several choices of wide-band gap semiconductors for DSSC, titanium dioxide(TiO_2) is the most efficient materials and attracted great attention because it is cheap, plentiful, non-toxic and has good chemical stability [22]. The preparation of TiO_2 nanoparticles/film is quite simple and requires no vacuum. Titanium dioxide, also known as titania, can be applied to many fields other than photovoltaics. It can be used as pigments, a cosmetic ingredient (sunscreen), environmental purification, electronic devices, gas sensors and photocatalyst [23] [24]. TiO_2 exists in three crystalline structure depending on the annealing temperature : anatase, rutile and brookite [25] [26] [27]. Rutile is stable while anatase and brookite are metastable. However, only rutile and anatase polymorphs are considered important for photocatalytic activity since brookite is very difficult to synthesis [28]. Figure 1.5(a) depicts a three-dimensional representation of the arrangement of TiO_6 octahedra in anatase and rutile showing 4 edge sharing connectivity in anatase and 2 edge sharing connectivity in rutile. Anatase to rutile transformation usually occurs in the temperature range of 400-700° C. The XRD pattern of TiO_2 anatase and rutile is shown in Figure 1.5 (b). The band gap of anatase is 3.2 eV and for rultile 3.0 eV, therefore making TiO_2 active to UV light. Mixed-phase photocatalysts with rutile–anatase compositions have been reported to exhibit enhanced photo-activity compared to the pure phases [29]. However, pure anatase exhibits a higher photocatalytic activity than pure rutile [30].

Conventional photoelectrode thin films usually contain TiO_2 mesoporous structure, produced by the sintering of a TiO_2 thin film at a temperature >400°C. The TiO_2 thin film is a TiO_2 paste consisting of 10-25 nm spherical particles

in an acidic solution and binder.After sintering, the binder evaporates and the TiO_2 nanoparticles are connected forming TiO_2 network. A scanning electron microscope image of the TiO_2 nanoparticles after sintering is shown in Figure 1.6.

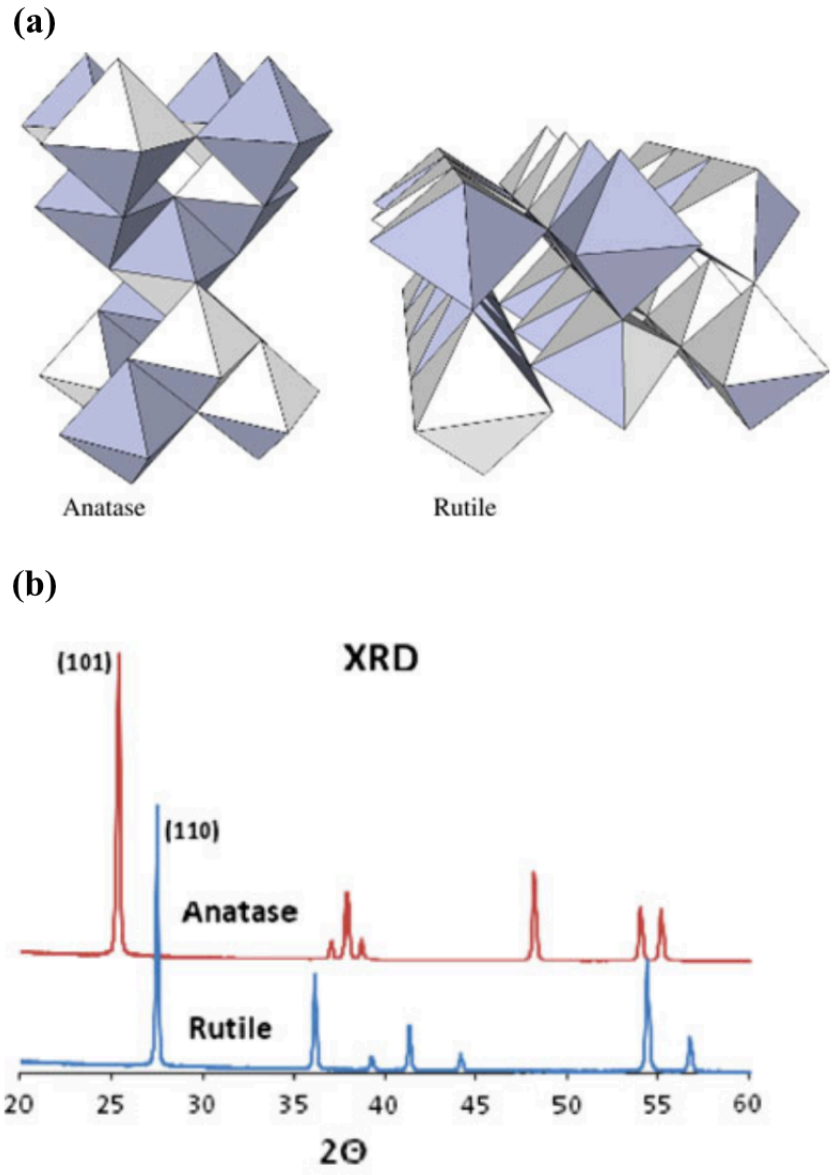

Figure 1.5: (a) Three-dimensional representation of the arrangement of anatase and rutile. (b) XRD pattern of TiO_2 anatase and rutile phases (from [31]).

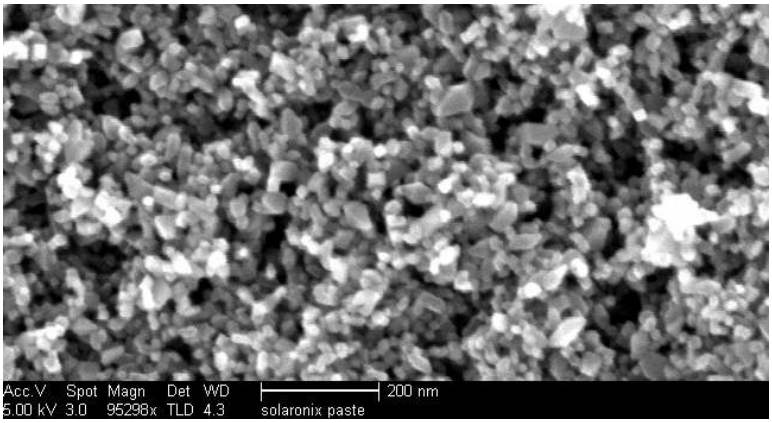

Figure 1.6: Scanning electron microscope (SEM) images of TiO_2 nanoparticles.

The synthetic route for TiO_2 nanoparticles is simple and chemically stable and has low materials cost. However, the weakness of this TiO_2 nanoparticle thin film is a small diffusion coefficient (D_n) and a slow electron transport that greatly limits the choice of redox couple in the electrolyte and thus, limits the photovoltage and constrains the choice of dye [32].

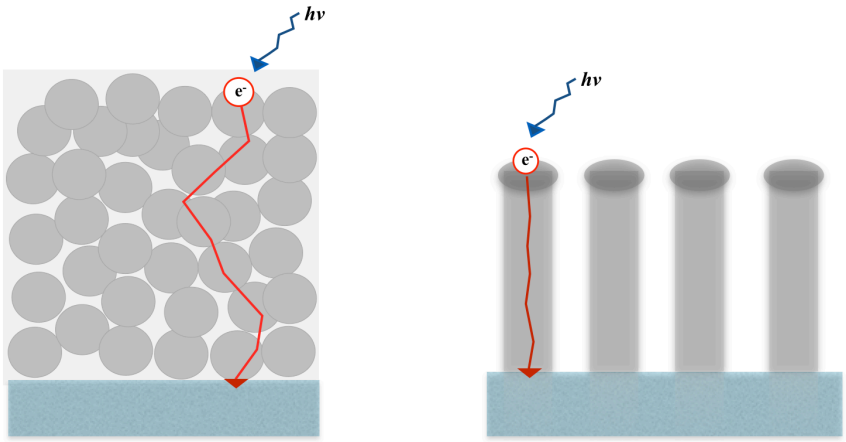

Figure 1.7: Illustration of charge transport pathways in (a) 3D randomly packed TiO_2 nanoparticles and (b) aligned one-dimensional TiO_2 Nanotubes .

As illustrated in Figure 1.7, it is also possible to apply 1-D nanostructures such as nanotubes [33] [34], nanowires [35] and nanorods [36]or the combination of both TiO_2 nanoparticles and a 1-D nanostructure which can increase cell per-

formance due to the higher surface area for dye adsorption and faster electron transportation [37] [38].

3.) Photosensitizer/Dye

Dye molecules are used to sensitized the wide-bandgap nanostructured photoelectrode. Upon illumination, an electron from the ground stated (S^0) of a dye molecule gets boosted to the excited state (S^*) and then injected into the conduction band of the nanostructured TiO_2. Based on the principle of a DSSC, the dye molecules should meet the some essential requirements in order to promote a high light-to-energy conversion efficiency. The dye molecules must bind strongly to the surface of TiO_2 nanostructure to ensure efficient electron injection into the TiO_2 conducting band and to prevent gradual leaching from the electrolyte [39]. The excited state of the dye must be slightly higher than the conduction band of TiO_2 but enough to have a driving force in energy for efficient charge injection into the TiO_2, and the ground state must be sufficiently low in energy for efficient regeneration of the oxidized dye by the redox electrolyte. The dye should absorb light in the visible or near-IR region, preferably covering a broad range of wavelengths. The process of electron transfer from the dye to the TiO_2 must be fast enough to compete with unwanted recombination to the ground state of the dye [39] [40].

Numerous metal complexes and organic dyes have been synthesized and utilized as sensitizers. However, the outstanding solar light absorber and charge-transfer sensitizer is the cis-Di(thiocyanato)bis(2,2'-bipyridyl)-4,4'-dicarboxylate) ruthenium(II), coded as N3, N-719 and black dyes (structure are shown in Figure 1.8. This type of dye has achieved conversion efficiency above 10% [21] [41].

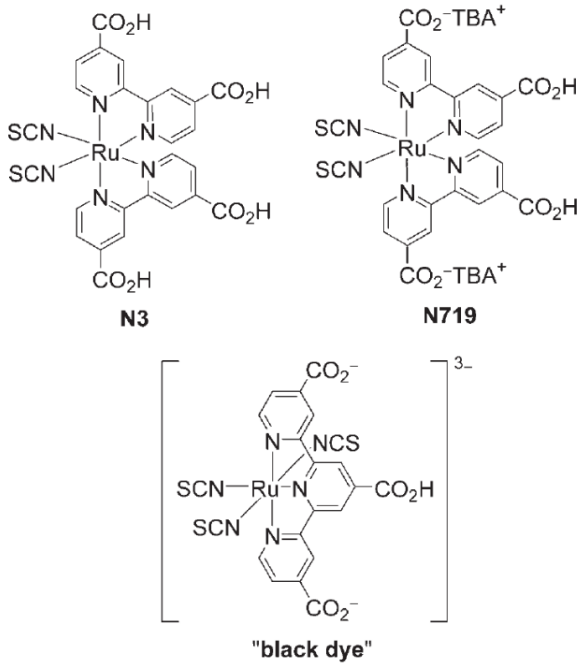

Figure 1.8: Examples of some Ru–polypyridyl dyes used in DSSCs that give cell efficiencies of over 10 %. TBA = tetra-n-butylammonium (from [42]).

4.) Redox electrolyte

In DSSC, the electrolyte is needed for dye regeneration and to complete the electron transportation between the photo electrode and the counter-electrode. The electrolyte is a liquid consisting of a redox couple (I^-/I_3^-) and some additives dissolved in an organic solvent, typically acetonitrile (ACN). The choice of solvent used in the electrolyte is impactful. There are several studies on various kinds of solvents for the electrolyte, such as alcohols, propylene carbonate, γ-butyrolactone, tetrahydrofuran, N, N-dimethylformamide [43] [44] [45], as well as different types of nitrile solvent [46]. However, acetronitrile has proved to be the most successful and efficient one so far. Acetronitrile has low viscosity and good solubility to dissolve the electrolyte components, including iodine salt and additives. The conversion efficiency recorded for an ACN-based DSSC is up to 12%. [47] [48].

A redox couple also plays a crucial role in determining the DSSC performance. The task of the redox couple is to promote the reduction of the oxidized

(S^+) dye as fast as possible to avoid recombination. Thus, the ideal redox couple should meet the following requirements: (1) the redox couple potential should be less negative than the oxidized energy level of the dye molecule meanwhile maintaining a sufficient driving force for dye regenerations; (2) slow electron recombination kinetics at the interface; (3) absence to the visible wavelength to prevent absorption of the incident light; (4) fast electron transfer kinetics at the counter electrode; (5) good diffusion properties for efficient mass-transport; (6) completely solubility in the solvent to ensure a high concentration of charge carriers in the electrolyte; and (7) chemically inert toward other components of the cell [49].

Iodide/triiodide (I^-/I_3^-) in a solvent is commonly used as an electrolyte in a DSSC since it has been proven to be one of the most versatile redox couple and also has good long-term stability [50]. However, the nature of this chemical is very corrosive and thus limits the choices for other components in the cell. Therefore, research has moved toward to find the alternative iodine-free redox couples. In 2011, a DSSC made of a cobalt-based electrolyte, in combination with a porphyrin dye, has achieved a conversion efficiency up to 12% [48]. An outstanding long-term stability over 1000 h under light soaking conditions has recently been confirmed by Gao et al. [51].

5.) Counter electrode

The Counter electrodes (CEs) is one of the most crucial parts in a DSSC. The role of the counter electrode is to reduce the redox species, which are the mediators for regenerating the sensitizer (dye) after electron injection. Usually, (I^-/I_3^-) is used as a redox couple.The regeneration of the dye produces triiodine (Equation1.4)and it will be reduced to iodide ion at counter electrode(Equation1.6).

Generally, a DSSC counter electrode is prepared from a small amount of platinum(Pt) catalyst deposited onto a TCO glass. Pt is the materials of choice due to its high catalytic activity and stability toward the iodide electrolyte [52] [53] [54]. This element unfortunately is very expensive and limited in supply. A great deal of effort has been devoted to identify alternative CE materials to replace Pt. Several alternative CEs are, for example, carbon materials, conducting polymers, and

transition metals [55].

1.2.2 DSSC's operational principle

The operation of dye sensitized solar cell is illustrated in Figure 1.9 and is described as follows,

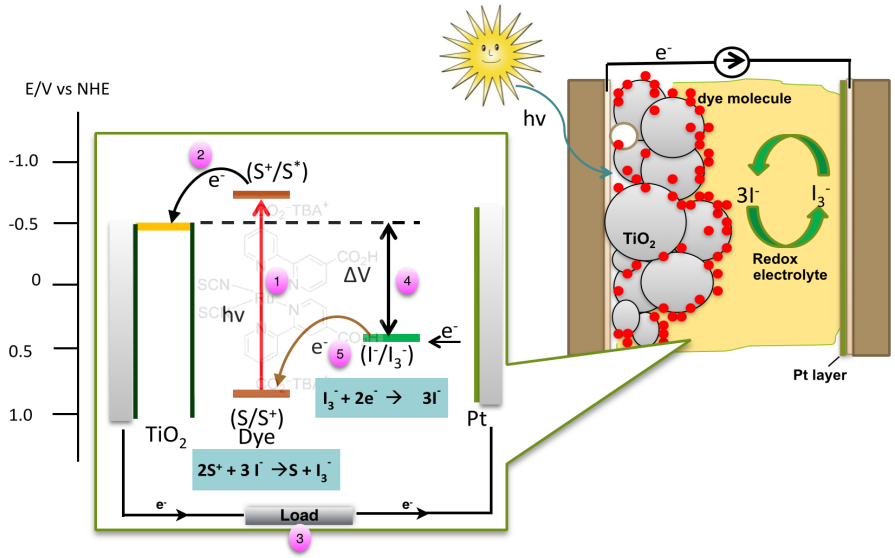

Figure 1.9: A schematic presentation of the operating principles of the DSSC.

1.) Upon light irradiation, a photon is absorbed by a sensitizer.This leads to the excitation of the sensitizer to the excited state (S^*).

$$S + h\upsilon = S^* \tag{1.1}$$

Light absorption by a dye molecule

2.) The excited electrons are injected into the conduction band (CB) in the TiO_2. The excited sensitizer is oxidized to S^+.

$$S^* \rightarrow S^+ + e^-_{cb}(TiO_2) \tag{1.2}$$

Charge injection)

3.) In the meantime, electrons diffuse through the nano-crystalline TiO_2 layer to the back contact of the conducting substrate and flow through the external circuit to the counter electrode.

$$e^-(TiO_2) \rightarrow e^-(CE) \tag{1.3}$$

Charge transportation

4.) The original state of the sensitizer (S) is subsequently restored by the electron from the electrolyte through the reduction of iodide. However, there are two major (unwanted) recombination reactions that lower the conversion efficiency of the DSSC: The excited electron in TiO_2 can directly recombine with the oxidized sensitizer or with the oxidized redox couple in the electrolyte.

$$2S^+ + 3I^- \rightarrow 2S + I_3^- \tag{1.4}$$

Dye regeneration

$$S^+ + e^-(TiO_2) \rightarrow S \tag{1.5}$$

Recombination

5.) The iodide is in turn regenerated at the counter electrode by reducing tri-iodide

$$I_3^- + 2e^-/3I^- \tag{1.6}$$

Iodine regeneration

Upon illumination, the sensitizer is photoexcited in a femtosecond and the electron injection from the excited state dye (S^*) into the TiO_2 conduction band (CB) is a very fast process on the sub-picosecond scale. The reduction rate of oxidized dye by the redox electrolyte occurs in about the nanoseconds timescale. Recombination of photoinjected CB electrons with the oxidized dye molecules or with the oxidized form of the electrolyte redox couple ($I_3^- ions$) takes place in microseconds [22]. To achieve good quantum yield, the charge injection rate should be in the picosecond range or below. In conclusion, fast recovery of the sensitizer is important for attaining long term stability to maintain a long-lasting charge separation which is crucial for the performance of the DSSC [56].

1.2.3 Basic parameters to evaluate the performance of DSSCs

The performance of DSSCs is evaluated by the following four parameters:

1.) Open circuit photovoltage ($\mathbf{V}_{oc}$) : If the output current is zero, the cell is at open circuited and the voltage of the cell is called the open circuit voltage. The open-circuit voltage is related to the energy difference between the quasi-Fermi level of electrons in the semiconductor and the chemical potential of the redox mediator in the electrolyte.

2.) Short circuit photocurrent ($\mathbf{I}_{sc}$): If the output voltage is zero, the cell is said to be short circuited. The short circuit current is equal to the absolute number of photons converted to hole-electron pairs. The I_{sc} is dependent upon the area of the solar cell, the number of photons which is directly related to the light intensity, the optical properties of the solar cell and the collection probability of the surface passivation and carrier lifetime. In general, it is presented in the form of the short circuit current density (J_{sc}) which is defined the short circuit photocurrent (I_{sc}) divided by the active cell area.The short-circuit photocurrent (I_{sc}) is essentially related to the amount of sunlight harvested in the visible part of the solar spectrum by the sensitizer.

3.) Fill factor (FF): The fill factor is an important part of the efficiency of the cell. High V_{oc} and I_{sc} are essential in achieving high efficiencies, but paired with a low fill factor, the overall efficiency of the cell will remain low. The ratio of peak output power $P_{max} = V_{max}$,I_{max} to V_{oc} I_{sc} is called the fill factor (FF) of a solar cell.

$$FF = \frac{I_{max} \times V_{max}}{I_{sc} \times V_{oc}} = \frac{P_{max}}{sc \times V_{oc}} \tag{1.7}$$

where I_{max} and V_{max} are the current and voltage at the maximum power on the I-V curve of the cell, as shown in Figure 1.10).

4.) Conversion efficiency (η): The energy conversion efficiency of the solar cell is defined as the maximum power produced by the cell (P_{max}) divided by the power of the incident light on the representative area of the cell (P_{light}).

$$\eta = \frac{I_{max} \times V_{max}}{P_{light}} = FF \times \frac{I_{sc} \times V_{oc}}{P_{light}} \tag{1.8}$$

The efficiency of the solar cell depends on the temperature of the cell and even more on the quality of the illumination, i.e. the total light intensity and the spectral distribution of the intensity. For this reason, a standard measurement condition has been developed to generalize the testing of solar cells at any laboratory. The standard condition that is used to test a terrestrial solar cell is light intensity of 1000 W/m^2 at AM 1.5 when the temperature of the cell is at 25 °C. The power output of the solar cell at these conditions is the nominal power of the cell, or module, and is reported in peak watts (W_p).

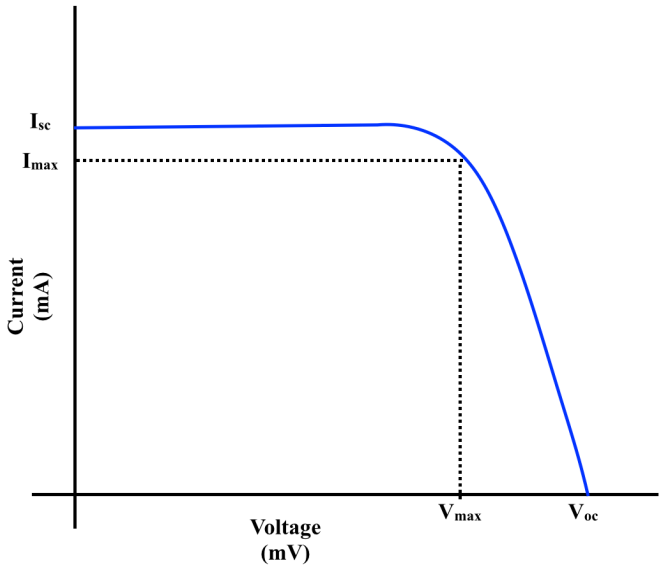

Figure 1.10: Characteristic I-V curve of a DSSC.

1.2.4 Characterization techniques for DSSCs

The basic techniques to characterize of DSSCs are described as follows.

1.) Current-voltage (I-V) measurement : The current-voltage measurement of a DSSC is the most important and conventional technique for evaluating the photovoltaic performance. It is performed on a Keithley 2400 source meter under simulated sunlight. A standard illumination of air-mass 1.5 global (AM1.5) with the irradiance of 100 mW/cm^2 is generally used. A typical I-V curve is shown in Figure 1.10. From the I-V measurement, four parameters mentioned above (V_{oc},

J_{sc}, FF and η) can be determined.

2.) Incident photon-to-electron conversion efficiency,(IPCE) measurement: The sensitivity of a DSSC varies with the wavelength of the incident light. Incident photon-to-electron conversion efficiency (IPCE) measures the ratio of the number of electrons generated by the solar cell to the number of incident photons on the active surface under monochromatic light irradiation:

$$IPCE\lambda = \frac{numberofcollectedelectrons}{numberofincidentphoton} = \frac{h \cdot c \cdot J_{sc}}{P_{in} \cdot \lambda \cdot e} \tag{1.9}$$

where I (λ) is the photocurrent (μA cm^{-2}) given by the cell under monochromatic illumination at wavelength λ (nm), P_{in} is the input optical power (W m^{-2}) at wavelength λ, e is the elementary charge, h is the Plank's constant, υ is frequency of light, c is the speed of light in vacuum. If not specified differently, the IPCE is measured under short circuit conditions and displayed graphically versus the corresponding wavelength in a photovoltaic action spectrum. IPCE measurement is also useful for indirect determination of the short circuit photocurrent of a DSSC.

3.) Electrochemical impedance spectroscopy,(EIS) : Electrochemical impedance spectroscopy measurement is used for characterizing the process of electron transport and ion diffusion at difference interfaces of a DSSC. Impedance is measured both under illumination and under dark conditions. Under illumination the cell is illuminated with a range of intensities and impedance is measured at open-circuit condition. In the dark a bias potential is applied. From EIS, several parameters can be obtained, such as charge-transfer resistance at the CE, electron recombination resistance at the TiO_2/dye/electrolyte interface as well as diffusion resistance in the electrolyte

1.3 Recent progress in dye sensitized solar cell research

After almost two decades of the breakthrough discovery of DSSCs, numerous efforts have been on the improvment of DSSCs performance. Studies have

reported several different methods to improve the efficiency of DSSCs, such as the use of 1-D or 3-D nanostructures of TiO_2, novel organic and natural sensitizers, alternative flexible substrates, a quasi solid state electrolyte, or an inexpensive catalyst for the counter electrode. However, the effect of improving a single part on a whole system must be considered. For example, it has to be realized that the performance of the photoanode can only be improved when done in parallel with a suitable redox couples and counter electrodes. When seeking for the improvement of the DSSCs, one should understand about the crucial phenomena in the cell. Sometimes, rethinking the overall DSSC architecture may be the way to achieve improvement. The following section will highlight the selected recent advances and alternative architectures of DSSCs.

1.) Alternative nanostructured photoelectrodes

To date, the most common and efficient DSSCs are made of thin films of TiO_2 nanoparticles. This thin film nanostructured is very important in many aspects. First of all, the large surface area of TiO_2 nanoparticles is for dye adsorption. Since photons are only absorbed on dye-TiO_2 interface, this means an extremely large surface area is required to increase the contact between the sensitizer molecules and TiO_2 layer. Secondly, after dye excitation and the electron injection through the TiO_2 layer, the excited dye has to be quickly reduced to the ground state by the electrolyte. The electrolyte then must be able to penetrate through the TiO_2 network in order to meet the dye molecule inside the TiO_2 layer. Therefore, a large enough pore size is also required in the TiO_2 network. Furthermore, the TiO_2 layer must provide a direct path for the flow of electrons to transport to the external load. Finally, the TiO_2 layer must maintain a high level of transparency for maximum light harvesting. Thus, designing the photoanode to serve all of these requirements is very challenging [57].

In recent years, alternative anode nanostructures for DSSC have been intensively studied. 1-D nanostructures such as nanorods, nanotubes, nanowires or nanofibers of TiO_2, ZnO and SnO_2have received considerable attention [58], [59] [60] [61]. As compared to the conventional mesoporous TiO_2, a 1-D nanostructures

are believed to provide a direct pathway for charge transportation [60] [61]. The high crystallinity along with fewer grain boundaries characteristic in 1-D nanostructures can accelerate the electron transport and reduce the chance of interfacial electron recombination.

In 2005, the first well-aligned ZnO nanowires were employed by Law et al. [62].The arrays of ZnO nanowires were synthesized by a seed-growth process on FTO glass. They produced the ZnO arrays with a hight of 20-15 μm and diameter of 130-200 nm as shown in Figure 1.11. The electron diffusivity was calculated as D_n = 0.05–0.5 cm^2 s^{-1} for single dry nanowires. This value is several hundred times larger than the typical electron diffusion coefficients in 5×10^{-5} cm^2 s^{-1} [63]. However, the roughness factor (defined as the ratio of actual surface area to the projected surface area) of the ZnO array is about 5 times smaller ($\sim$1000). The inadequate surface area of ZnO significantly limits the dye adsorption capacity, giving an overall power conversion efficiency that is relatively low ($\sim$1.5%) [62].

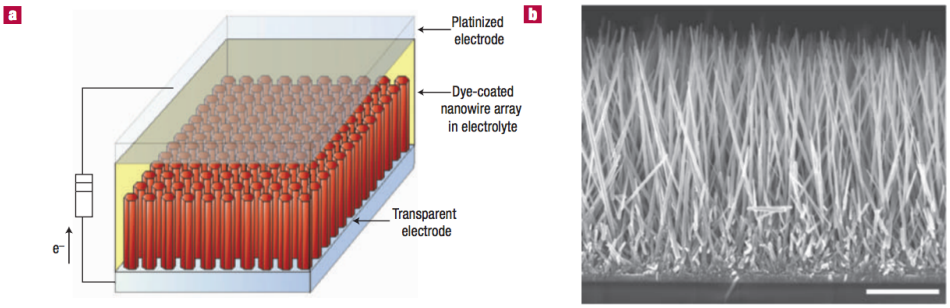

Figure 1.11: The nanowire dye-sensitized cell, based on a ZnO wire array: (a) Schematic diagram of the cell. Light is incident through the bottom electrode. (b) Typical scanning electron microscopy cross-section of a cleaved nanowire array on FTO. The wires are in direct contact with the substrate, with no intervening particle layer. Scale bar, 5 μm (from [62]).

To overcome the roughness factor limitation , an array of TiO_2 nanotubes on FTO glass was prepared by using electrochemical anodization [64]. The arrays were found to consist of closely packed NTs, several micrometers in length, with typical wall thicknesses and intertube spacings of 8-10 nm and pore diameters of about 30 nm.The thin film of TiO_2nanotubes has roughness factor over 1000.

Nonetheless, the best efficiency of TiO_2 naotubes-based DSSC was only approached 3% [64].

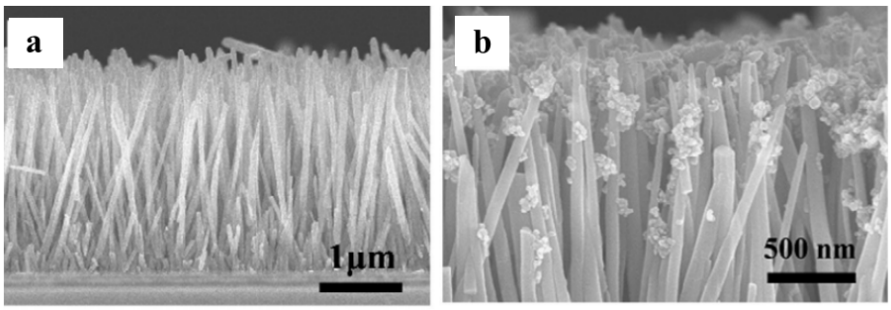

Figure 1.12: Vertically aligned nanowires: (a) without and (b) with NP attached to its surface and the correspondent DSC performance values and diffusion coefficients (from [65]).

As shown in Figure 1.12A hybrid nanotstructure combining vertically aligned ZnO nanowires (NW) with attached TiO_2 nanoparticles (NP) took advantage of both structures. Gan et al. [65] showed that current density increased from 1.60 to 3.54 mA cm^{-2} with this structure. The hybrid cell gave a diffusion coefficient D_n= 6.92× 10^{-4} cm^2 s^{-1}. The value falls between those of the bare ZnO film (2.8 × 10^{-3} cm^2 s^{-1}) and the TiO_2 NP electrode (≈5 ×10^{-5} cm^2 s^{-1}). This confirmed that the hybrid electrode combines the advantages of both structures: improved electron transport of the aligned ZnO nanowires and increased surface area of the TiO_2 nanoparticles. However, the surface area of the hybrid structure was still low compared to a similar thickness of the TiO_2 nanoparticles due small coverage of the nanowires with nanoparticles as shown in Figure 1.12(b). The performance of the hybrid structures is still far from the efficiency of TiO_2 nanoparticles-based cell [65].

Another interesting approach to manipulate the nanostructure of the photoanode is called 3-D template-based backbone. In this approach, tunably sized polystyrene spheres (PS) is used as a template to coat a thin layer of TiO_2. The resulting PS template is removed with heat treatment to obtain a crystalline TiO_2 inverse opal structure (see Figure 1.13). A block-copolymer can be incorporated into the structure to control the structural dimensions, pore size, porosity and charge-

transport properties of the photo-anode layer. Figure 1.13 depicts the synthesis method and scanning electron microscope images of TiO_2 inverse opal structure proposed by Kue et al. [66], the TiO_2 nanostructured was assembled in a DSSC configuration, yielding a J_{sc} of 8.2 mA cm^{-2}, a V_{oc} of 720 mV, a FF of 0.62 and an efficiency of η of 3.7%. Guldin et al. also reached a power conversion efficiency (η) of 4.0% by using a block-copolymer-assembled solid state DSSC [67].

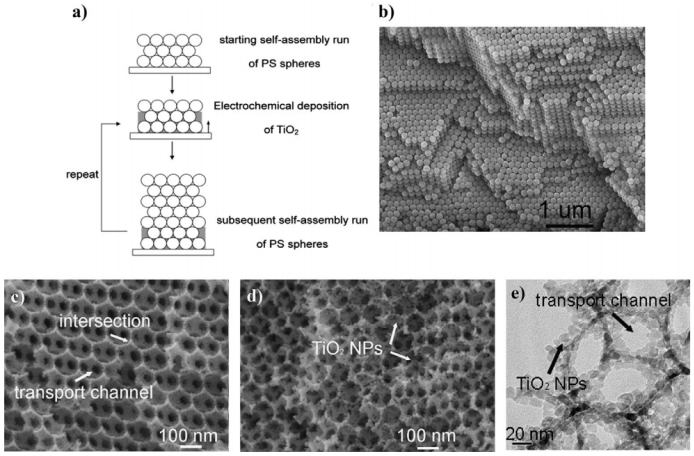

Figure 1.13: (a) Schematic representation of the synthesis method of a highly ordered multi-scale nanostructure of TiO_2 proposed by Kuo et al. ; (b) film composed of the polystyrene opals revealing their close packing; SEM micrographs of the TiO_2 inverse opal (c) before and (d) after $TiCl_4$ treatment; (e) TEM images of the TiO_2 nanoparticle decorated inverse opal revealing the coating of the macroporous transport channels (from [66]).

2.) Flexible DSSCs

A key issue in the commercialization of DSSCs is reducing the production cost further while keeping adequate efficiency and lifetime. The total expense of volume DSSCs production principally depends on the materials cost and the fabrication methods. Surprisingly, the conducting glass substrate (FTO/ITO) is the most costly part in a DSSCs which is in excess of 60% of the aggregate expense of all parts in DSSCs [68].The DSSCs fabrication can be switched from traditional glass substrates to a cheap and flexible substrate, such as plastic,metal, paper or textiles that can be fabricated in different combinations [69] [70] [71] [72].Flexible solar cells are lightweight, thin and bendable. Therefore, they have opened new

and emerging applications in the mobile and wearable electronic industries.

DSSCs fabricated with plastic substrates, such as polyethylene terephthalate (PET) or polyethylene naphthalate (PEN), however shows poor solar conversion efficiencies compared to traditional glass based DSSCs [73] [74]. The main problem of a plastic substrate is that it has low heat resistance (±150°C) and therefore can not stand the high temperature sintering process of TiO_2 (450-550 °C). Without the sintering process, chemical bonding between TiO_2 nanoparticles is limited. Many different approaches has been conducted to modify the TiO_2 paste preparation conditions and different methods to apply TiO_2 onto the plastic substrate at lower temperature, such as chemical sintering, vacuum sealing and pressing and hydrothermal treatment [75] [76] [77] [78] [79]. Yamaguchi et al. applied a "lift off" process of a sintered TiO_2 layer that was transferred to a plastic substrate. By using an optimized mechanical pressing process, an efficiency of 7.6% was achieved [75]. Figure 1.14 shows the schematic diagrams of flexible DSSCs based on conductive plastic, metal foil and metal mesh.

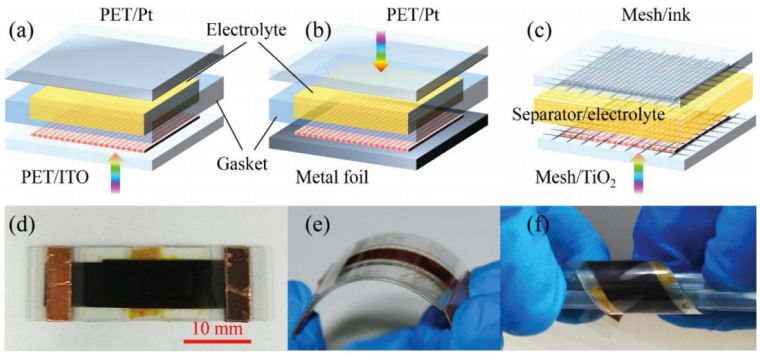

Figure 1.14: Schematic diagrams of flexible DSSCs (a) based on PET/ITO substrates, (b) based on the metal foil and (c) flexible double mesh based DSSCs. (e, f) Photographs showing that the device has very good flexibility (from [80]).

Another concept for flexible DSSCs is the use of thin metal sheets as photoelectrode substrates. The metal-based photoelectrode offers the advantage of high temperature sintering processes, which is a key requirement for high quality TiO_2 nanoparticle film. In 2006, Grätzel et al. [81] reported highly efficient (7.2%) flexible DSSCs with a Ti-metal substrate attaining 100 mW/cm^2 .Park et al. [82]

also reported an efficiency of 8.6% using SiO_x and ITO-coated stainless-substrates. However, the stability is a critical issue of the stainless steel as the cell performance dropped just couple hours after illumination [71]. Unlike the metal sheet, using metal mesh as a substrate is also another option for flexible DSSCs since it is giving much better bending performance and also allowing some light to penetrate [83].

3.) Quantum dot sensitized solar cell (QDSSC)

Improvement of the photosensitization is a key factor in enhancing the performance of DSSCs. The ideal sensitizer should be highly absorbing across the entire solar light spectrum, bind strongly to the TiO_2 surface, and efficiently inject photoexcited electrons into the TiO_2 conduction band. Many efforts have been devoted to explored the sensitizers that meet all of these requirements but it could be realized by co-adsorption of a different dyes for absorption at different solar spectra [80] [84]. Quantum dot (QD, semiconductor nanocrystal) sensitized solar cell is an emerging solar cell technology. The principle of QDSSC is shown in Figure 1.15.Basically it is similar to DSSC but instead of using dyes as light absorbers, the inorganic semiconductors are used [85].The QDs are the semiconductor materials and are small enough to observe the effect of the quantum confinement (particle radius <the Bohr radius).The QD band gaps can be tunable, so this has opened an alternative path for harvesting light energy from visible to infrared (IR) regions of the solar spectrum [86].The most commonly used QDs are a) large band gap (E_g>1.5 eV) cadmium-chalcogenide such as CdS, CdSe and CdTe; b) low band gap (E_g <1.5 eV) lead-chacogenide including PbS ,PbSe and c) antimony sulfide Sb2S3 (E_g = 6.5 eV) [87].

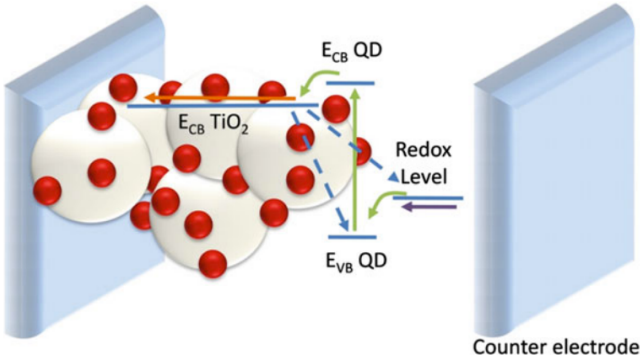

Figure 1.15: The fundamental principles of QD sensitized solar cells. Light photoexcites electron-hole pairs at the QD. Photoexcited electron is injected into the CB of the wide bandgap semiconductor, while hole is regenerated from the redox level of the liquid electrolyte. Electron is transported to the electron contact. Redox sytem is regenerated at the counter electrode and electrons diffuse to the working electrode (from [88]).

Among the QDs materials mentioned above, lead-chalcogenide QD-based solar cells have attracted increasing interest in sensitizers. The studies in recent years show the highest efficiency of 7.4% [89]. However, Sb_2S_3 may also be another attractive candidate due to its nontoxic composition, abundance and the high efficiency of its corresponding solar cells (6.3%) [90]. The challenge for the QDSC is the low open circuit voltage and fill factor due to the charge loss at TiO_2/QD and TiO_2 and electrolyte interfaces [87].

4.) Perovskite-based sensitized solar cells

Organometal halide perovskites as a visible light absorber for solar cells have attracted considerable attention during the past few years. The halide perovskite $CH_3NH_3PbX_3$ (X = Cl, Br, or I) has shown excellent light-harvesting characteristics with a narrow band-gap (E_g = 1.5 eV) with an optical absorption edge of 820 nm [87]. In 2009, Kojima et al. was the first team to report the perovskite-sentized solar cell [91]. Their cell was constructed by combining the $CH_3NH_3PbX_3$ and deposited TiO_2 electrode ($CH_3NH_3PbX_3$-TiO_2) as the photo electrode (anode) and a Pt-coated FTO glass as the counter electrode (cathode) and used lithium halide and halogen as a redox couple in a liquid electrolyte.The

performance showed an efficiency of 3.81%.The improvement was further made by Im et al. in 2011 which showed an efficiency of 6.5% [92]. This research has progressed with improved performance [93] [94] [95]. Recently, in early 2014, the efficiency of perovskyte $CH_3NH_3PbX_3$-based solar cells was further boosted up to 16.7% [96]. The efficiency of 20% is expected to be achieved in the near term [97].

1.4 Research Goals

The propose of this research was to develop well-designed and cost effective DSSC components to further enhance the energy conversion efficiency of DSSCs.The major emphasis was on the modification of the photoelectrode materials with approach to be as simple and with as low cost fabrication as possible. The efforts have also been devoted to the optimization of the device fabrication procedures to enhance the device performance along with the understanding of the relationship between the developed materials and the corresponding device performance.

1.5 Dissertation overview

Chapter 1 has provides a brief introduction to the principle of dye sensitized solar cell, recent progress in DSSCs and the purpose of this research. **Chapter 2** will demonstrate a novel approach of using a composite structure of TiO_2 nanoparticles and high-aspect-ratio, 8nm diameter TiO_2 nanotubes, as a photoelectrode. **Chapter 3** will describe the preparation and characterization of the double-wall carbon nanotubes (CNT) incorporated with TiO_2 nanoparticles and will explain the effect of the incorporated CNT on the TiO_2 photo-anodes. **Chapter 4** will illustrate the fabrication of a fluorine-doped tin oxide (FTO)-free photoanode and compare the performance of the scaled-up DSSC devices. **Chapter 5** will summarize the research presented and describe the potential direction for further DSSC improvement.

Chapter 2

Enhancement of dye sensitized solar cell efficiency by composite TiO_2 nanoparticle/8nm TiO_2 nanotube paper-like photoelectrode

2.1 Introduction

Dye-sensitized solar cells (DSSC) have been intensively studied as promising, third generation solar cells since the first report in 1991 by O'regan and Grätzel [15]. Due to their simple and inexpensive manufacturing procedures yet relatively high conversion efficiencies, DSSCs have gained much attention from many researchers nowadays [98] [99] [100] [32] [101] [102]. Nonetheless, the highest DSSC efficiency achieved so far is 11-12% [56] [48]. Various materials and process approaches have been applied to further enhance the DSSC power conversion efficiency [103] [104] [105] [106] [107] [108].

The TiO_2 layer is the key for the electron transport in DSSC. During the DSSC operation, electrons are generated by photo-excited dye molecules, which

are then injected into the conduction band of the Ti oxide. The electrons then get transported by diffusion through TiO_2 layer and are collected at the conductive electrode. While most electrons are efficiently collected, some might recombine with holes nearby or in the electrolyte and/or excited dyes, thus leading to reduced energy conversion efficiency. Therefore, improving charge collection efficiency of TiO_2 layer is one of the main areas worthy of further investigation. In general, porous TiO_2 nanoparticles are applied as an electron transport medium [109]. However the electrons diffuse through such porous nanoparticle assembly via slow mechanism, even much slower than in bulk crystal [110] [111] [112]. It has been assumed that electrons are trapped in grain boundaries or interfaces between nanoparticles, oxygen defects and TiO_2 amorphous layer [113] [114]. In order to improve electron transport by reducing the interfaces, one-dimensional TiO_2 nanomaterials having higher aspect ratio such as nanotubes, nanowires and nanorods should be preferable as easier electron transportation pathway [115].

In this paper, a novel approach of using composite structure of TiO_2 nanoparticles and high-aspect-ratio, 8nm diameter TiO_2 nanotubes is presented. A convenient micropaper configuration is adopted in this work. The simple and low cost of TiO_2 paper-like structure was obtained by compressive compaction of component mixed particles, yielding stand-alone TiO_2 micropaper which then can be transferred and attached onto the conductive glass, or alternatively and preferably utilized as an anode layer without even using a conductive glass substrate. Here the 8nm nanotubes TiO_2 are well mixed with the commercially available TiO_2 nanoparticles to form a thin nanocomposite structure as a photoelectrode of dye sensitized solar cell. This 1D nanostructure is expected to facilitate the electron transportation as well as to enhance mechanical interlink amount the particles within the TiO_2 nanoparticle layer, thus essentially eliminating the microcracking commonly observed in a dried layer from solvent containing mixture. The DSSC energy conversion efficiency is enhanced probably due to rapid electron movement along the 8nm TiO_2 nanotubes.

2.2 Experimental Procedure

TiO_2 paper-like structures were prepared by using high pressure pressing machine, in which the mixed TiO_2 nano-powders and nanotubes were pressed within a die into a micrometer thick disk (referred to a TiO_2 micropaper hereafter).

2.2.1 Synthesis of 8nm Titanium oxide nanotubes

Anatase TiO_2 nanotubes were prepared using a hydrothermal method [116] [117]. Two grams of P25 powder (Anatase TiO_2 25 nm diameter nanoparticles, procured from Sigma-Aldrich) was added to 20 ml of 10 M NaOH aqueous solution, which was vigorously stirred for 20 min followed by ultrasonication for 20 min. The solution was then transferred into PTFE (Polytetrafluoroethylene, Teflon)) liner and placed in a stainless steel hydrothermal vessel. The hydrothermal reaction was carried out at 130°C for 24 hours, after which the vessel was allowed to cool to room temperature. Light white colored precipitates were obtained after washing with 0.1 M HNO_3 solution and distilled water. The solids were separated from the washing solution by centrifuging. This process was repeated several times until the washing solution had pH 7. The precipitates were then dried in an oven at 70°C for 24 hours. The morphology and size of the 8 nm diameter TiO_2 nanotubes are depicted in Figure 2.1(a).

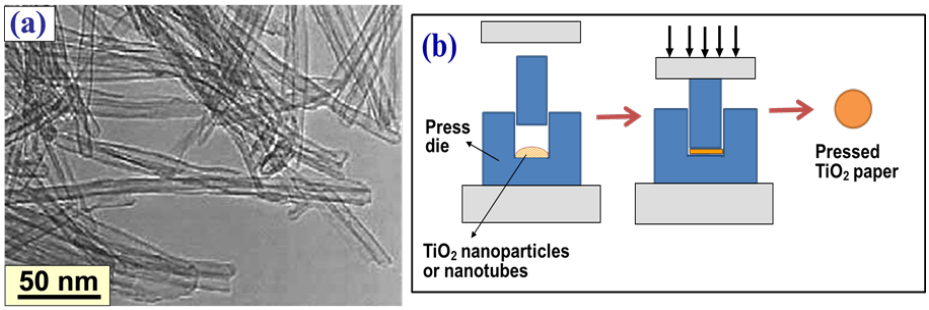

Figure 2.1: (a) SEM micrograph of 8 nm diameter TiO_2 nanotubes, (b) Fabrication schematic of TiO_2 paper-like structure (TiO_2 micropaper) by pressing machine.

2.2.2 Preparation of various types of TiO_2 micropaper

Three types of TiO_2 micropaper have been prepared for comparative studies on their DSSC performances.

Pure TiO_2 nanoparticle micropaper

TiO_2 nanoparticle paste (purchased from Solaronix) was used without modifications. The paste was dried at room temperature to remove the solvent and ground into fine powder, which was then placed in a cylindrical cavity pressing die (1 cm diameter) and pressed using ∼450 MPa pressure (Figure 2.1(b)). After releasing the sample from the die, approximately 30 μm thick paper-like disk was obtained, which was mechanical robust to be handled for assembly into DSSC cells. The thickness of the paper-like disk was indirectly controlled by adjusting the weight of the feed powder into the pressing die. For scale-up fabrications, a spacer array can also be used during pressing for geometrical control of the disk thickness.

TiO_2nanoparticle and nanotube mixed micropaper

Dried TiO_2 nanoparticle paste particles were mixed with 8 nm TiO_2 nanotubes at a weight ratio of 2:1. The mixed paste was then dried and ground into fine powder. The pressing process as described above was used to obtain 30μm thick, paper-liked TiO_2 samples.

TiO_2 nanotube micropaper

8 nm TiO_2 nanotube powder synthesized by hydrothermal process was washed and dried, then pressed to obtain 30 μm paper-like TiO_2. The TiO_2 micropapers were annealed at 450°C for 2 hour in air to burn away the polymer binder and solvent, and then treated with 0.04 M $TiCl_4$ aqueous solutions at 70°C for 30 min in order to make strong contact between the particles and nanotubes.

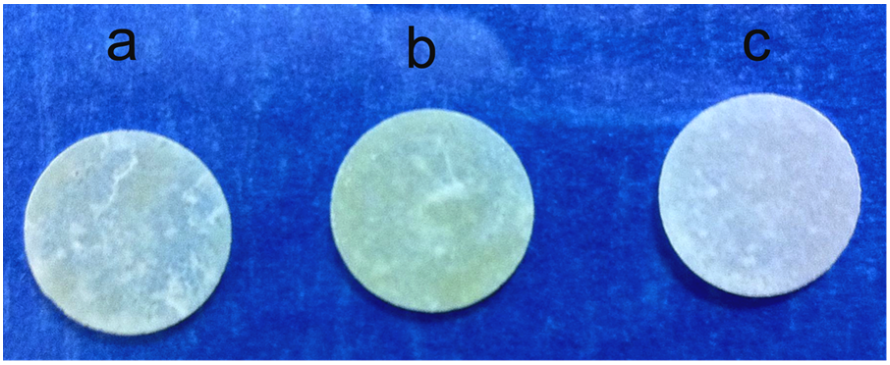

Figure 2.2: TiO_2 micropaper after pressing. The paper can be handled with tweezers and cut to size using a razor blade. (a) TiO_2 nanoparticles micropaper, (b) Mixed TiO_2 nanoparticles and 8 nm TiO_2 nanotubes, and (c) 8nm TiO_2 nanotube micropaper.

2.2.3 Preparation of TiO_2 micropaper photoelectrodes

The FTO (fluorine-doped tin oxide) conducting glass (Hartford; TEC 7, thickness 2.2 mm; resistivity 7 Ω cm^{-1}) was first scrubbed and ultrasonicated in detergent for 15 min, and subsequently ultrasonicated in ethanol for another 15 min and dried by flowing N_2. The cleaned FTO glass was treated with 0.04 M $TiCl_4$ aqueous solution at 70°C for 30 min in order to make good mechanical and electrical contact between the applied TiO_2 oxide layer and the FTO conducting layer. The prepared TiO_2 micropaper was cut into 0.2 cm $\times$ 0.2 cm square pieces (active area 0.04 cm^2) and transferred onto the $TiCl_4$ - treated FTO glass. A drop of homemade diluted Ti glue (polyethylene glycol+titanium isoproproxide+EtOH) was used to attach the TiO_2 micropaper to FTO glass [107]. The use of Ti glue followed by 500°C annealing (see below) produces TiO_2 interfacial bond layer, resulting in a well adhered disk on the FTO glass surface.

The photoanode was then gradually heated from room temperature to 500°C in air. (with a stepwise heating of 325°C for 5 min, 375°C for 5 min, 450°C for 15 min, 500°C for 15 min, with a 10min ramp between each). After being cooled down to $\sim$80°C , the anode was slowly immersed in 0.3 mM solution of N719 dye (solaronix) in dry ethanol and kept at room temperature for at least 12 hours to complete the sensitizer uptake onto the samples surface. The anode then

was washed with ethanol to remove excess dye material, followed by drying with N_2 before DSSC device fabrication.

2.2.4 Fabrication of dye-sensitized solar cells

The prepared photoanodes and counter electrodes were put together into a sandwich DSSC cell configuration and sealed with hot-melt sealing gasket (60μm thick Meltonix 1170-60, from Solaronix). The aperture of the sealing film frame was 2 mm larger than the active area. The internal space was filled with a drop of electrolyte and the cell was placed in a small vacuum chamber to remove inside air and let the electrolyte goes in. The electrolyte was composed of 0.6 M 1-butyl-3-methylimidazolium iodide (BMII), 0.03M I_2, 0.1M guanidinium thiocyanate, 0.5 M 4-tert-butylpyridine in acetonitrile and valeronitrile (85:15, v/v) [118].

An ultrahigh resolution scanning electron microscope (UHR SEM,FEI XL30) was employed to examine the surface morphology of TiO_2 micropapers. Phase transition and crystallization of annealed TiO_2 micropapers were confirmed by X-ray diffraction analysis data (Rigagu Gelgerflex model D/Max-IIB) using a maximum potential of 50 kV and current of 32 mA. The photocurrent density vs voltage (J-V) characteristics was measured using AM 1.5 G illumination with 450 Watt Xenon lamp equipped with an AM 1.5 global filter (Newport 81094). It should be noted that the DSSC performance was performed without masking [119]. Such DSSC measurements without masking introduce a slight reduction in the efficiency values as compared to the masked samples. All J-V measurements were carried out for comparative evaluation of DSSC behavior under identical conditions.

2.3 Results and Discussion

2.3.1 Morphology of TiO_2 micropapers

Figure 2.2 shows TiO_2 micropapers after pressing. The flat, round disks with thickness of $\sim$30-40 μm were obtained. The colors of the non-annealed micropapers were slightly different from each other. Figure 2.2(c), pure 8nm TiO_2

nanotube micropaper, shows white opaque appearance while semi-transparent yellowish color is observed from the pure TiO_2 nanoparticle micropaper (Figure 2.2(a)) and mixed TiO_2 nanoparticle nanotube micropaper (Figure 2.2(b)). The yellowish color probably comes from the polymer and binder present in the commercial paste. However, all organic additives were removed after annealing at 450°C for 2 hours. The X-ray diffraction (XRD) spectra of TiO_2 micropaper

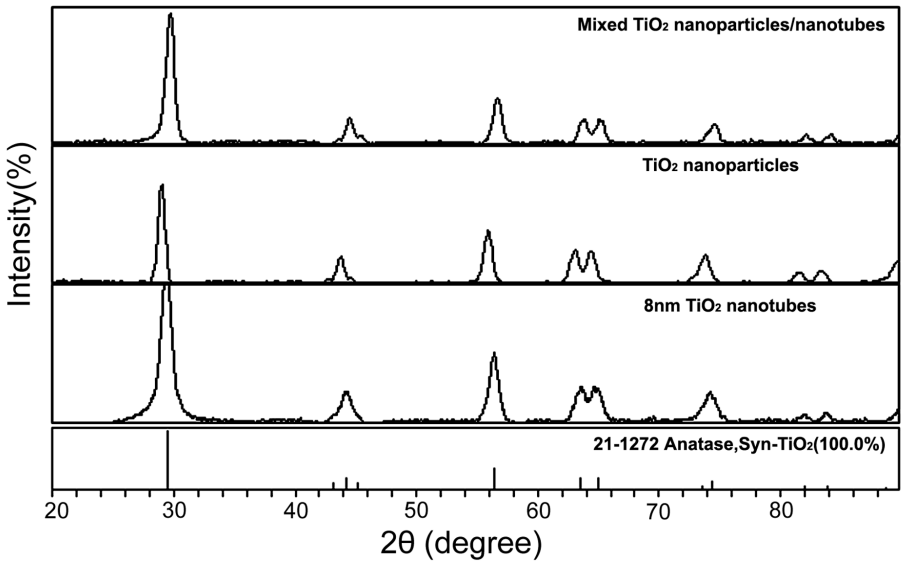

Figure 2.3: X-ray diffraction patterns for annealed TiO_2 micropapers compared with the standard anatase diffraction pattern (bottom curve).

Figure 2.3 indicates the predominant presence of anatase crystalline phase for all three TiO_2 micropapers. It has been reported that anatase is the preferred structure in DSSCs because it has a larger bandgap and higher conduction band edge energy compared to rutile structure, which means a higher Voc in DSSCs for the same conduction band electron concentration [120]. Figure 2.4(a-c) illustrates SEM microstructures of pure TiO_2 nanoparticle micropaper, 8nm TiO_2 nanotube micropaper, and mixed TiO_2 nanoparticle plus nanotube micropaper, respectively. The corresponding schematic microstructures are shown in Figure 2.4(d-f). For the same micropaper thickness, it was observed that the most brittle micropaper was the one made from pure TiO_2 nanoparticles.

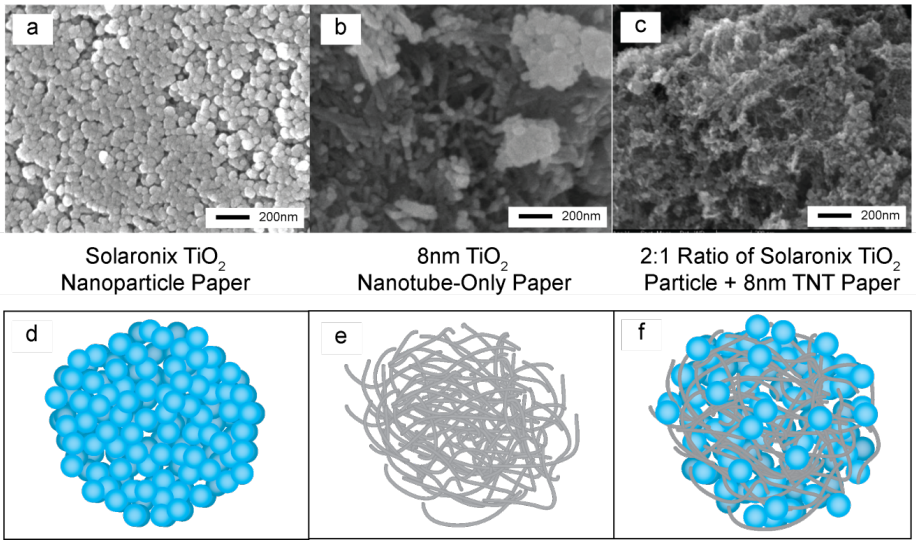

Figure 2.4: SEM micrographs and schematic illustrations showing the nanostructure configuration of (a) and (d) TiO_2 nanoparticles micropaper, (b) and (e) Mixed TiO_2 nanoparticle and 8 nm TiO_2 nanotube micropaper and (c) and (f) 8nm TiO_2 nanotube micropaper.

The SEM images in figure 2.4(a) and Figure 2.5(a) confirm that the loosely bonded structure between the TiO_2 sphered particles results in mechanical weakness in the micropaper. In the case of pure 8 nm TiO_2 nanotubes micropapers, the high aspect ratio nanotubes ($\sim$1-3 μm long) are probably tangled among themselves and provide mechanical locking, thus preventing microcracks to occur during annealing and cooling. The lack of many microcracks should help to minimize a loss of DSSC currents. It is also expected that long 1D structure provide faster electron path thus increasing the current density for the DSSC performance. However, there appears to be some loss of optical transparency in the micropaper made of 8 nm TiO_2 nanotubes micropaper, Figure 2.4(b), presumably due to the nature of the hydrothermally synthesized TiO_2 nanotubes not being as transparent as the spherical nanoparticles, possibly due to some altered stoichiometry, defect density, etc. Future improvement of the optical transparency of 8 nm TiO_2 nanotubes will be beneficial for higher DSSC performance.

Mixed TiO_2 nanoparticle and nanotube micropaper was prepared to optimize the benefit of the spherical TiO_2 nanoparticles and that of the 1D configured TiO_2 nanotube structure, shown in Figure 2.1(a). Figure 2.4(c) displays TiO_2

nanotube network in TiO_2 nanoparticles matrix, in which the presence of high-aspect-ratio TiO_2 nanotubes is expected to mechanically strengthen the overall structure while maintaining a reasonable level of optical transparency.

Figure 2.5(a) reveals the appearance of many microcracks on the surface of TiO_2 nanoparticle micropaper sample. These cracks most likely interrupt the continuous electron conduction and thus reduce the DSSC current density.Figure 2.5(b) represents an SEM micrograph for the mixed TiO_2 nanoparticle and 8nm TiO_2 nanotube micropapers. The micrograph shows very few microcracks on the surface of the sample, as compared to the TiO_2 nanoparticle based micropaper of Figure 2.5(a). By pressing of the composite containing high-aspect-ratio nanotubes, the powder was packed densely with interlocking nanotube networks which minimized the occurrence of undesirable microcracks.

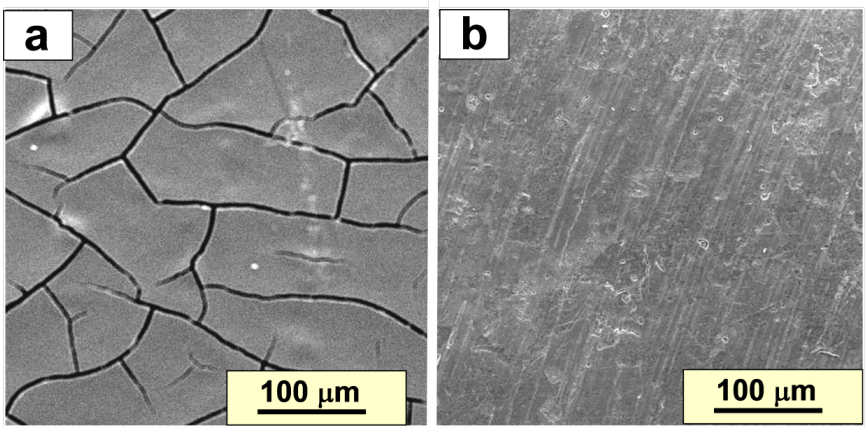

Figure 2.5: SEM images showing a dramatic difference in microcracking in photoanode samples.(a) TiO_2 nanoparticle micropaper after annealing, revealing many microcracks on the sample surface, (b) Mixed TiO_2 nanoparticle/nanotube micropaper after annealing, showing very few microcracks. The 8 nm TiO_2 nanotube only micropaper also exhibits few microcracks.

2.3.2 DSSC performance of TiO_2 Micropaper photoelectrodes

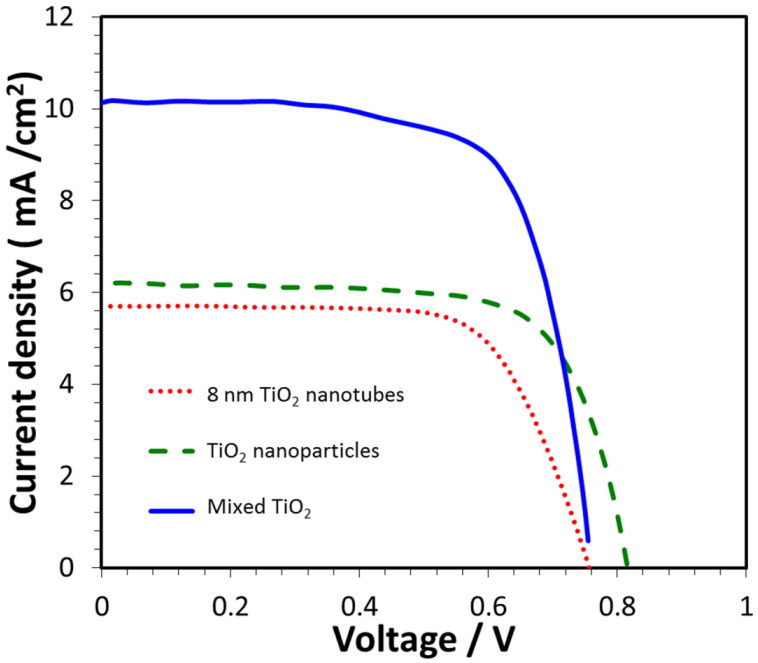

Figure 2.6: Current density vs voltage relationship (J-V curves) of the DSSCs with different types of TiO_2 micropapers.

Figure 2.6 shows the photocurrent density-voltage (J-V) characteristics of example DSSC devices based on TiO_2 micropaper photoelectrode. The comparative DSSC performance parameters for the three types of TiO_2 micropapers with V_{oc}, J_{sc}, conversion efficiency and fill factor data (average data for two or three samples for each type) are presented in Figure 2.7 and Table 2.1.

Table 2.1: V_{oc}, J_{sc}, conversion efficiency and fill factor data for the three types of DSSC micropaper.

Micropaper	V_{oc}(V)	J_{sc}(mA/cm^2)	Fill factor	Efficiency(%)
8 nm TiO_2 nanotubes	0.80	5.05	0.68	2.74
TiO_2 nanoparticles	0.77	5.98	0.72	3.35
Mixed TiO_2	0.76	10.76	0.66	5.38

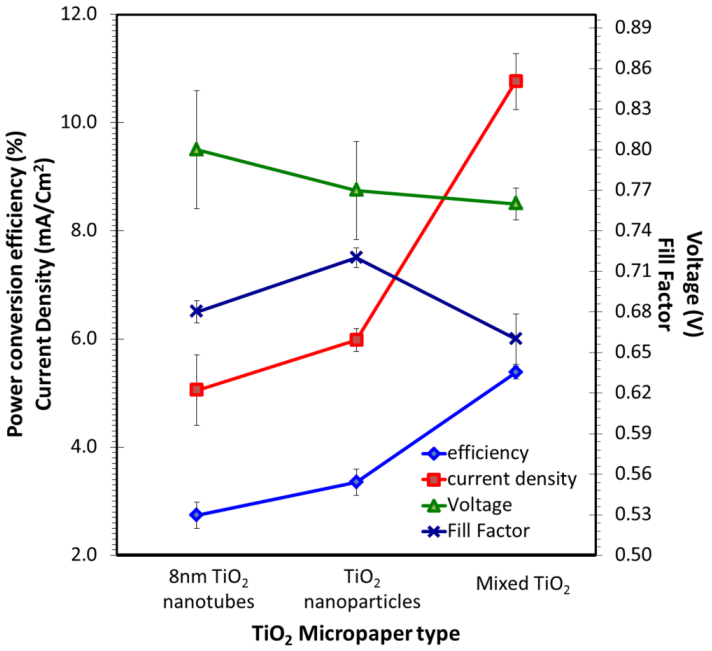

Figure 2.7: Comparative DSSC performance parameters for the three types of TiO_2 micropapers.

The mixed TiO_2 nanoparticle and nanotube micropaper achieved about twice higher photocurrent density (J_{sc}) value than that of both pure TiO_2 nanoparticle micropaper and pure TiO_2 8 nm nanotube micropaper. This resulted in high DSSC overall efficiency of average 5.38% while the pure TiO_2 nanoparticle micropaper and pure TiO_2 8 nm nanotubes produced 3.35% and 2.74% efficiency, respectively. (The average efficiency was obtained from 2-3 samples per each type of micropaper). This significantly improved photocurrent density in the nanoparticle-nanotube mixed structure could be related to the high-aspect-ratio, 1D nanostructure of TiO_2 8nm nanotubes which might help to interlink the TiO_2 nanoparticles matrix, thus providing faster pathways for electrons to transport with decreasing ohmic loss through 1D nanostructure [121] [122]. However, to support such a hypothesis, more thorough analysis such as the IPCE (incident photon to current efficiency) test should be conducted.

Another possibility is that a larger surface area within the anode samples could increase the number of sites for dye molecules to attach and thus enhance

the amount of dye adsorption [15]. A simple estimation of the surface areas for the average 17.5 nm diameter TiO_2 nanoparticles (the Solaronix paste used here contains 15-20 nm diameter particles) vs that for the 8 nm diameter x 2 μm long TiO_2 nanotubes (having identical volume as the spherical nanoparticles) yields a moderate surface area increase of 46% in the case of 8 nm nanotubes. However, only one-third of the spherical particle volume was replaced with nanotubes, and hence the resultant surface area increase is estimated to be on the order of 15%, a rather small change in surface area. Another important factor is the degree of microcracking in the TiO_2 anode layer as the extent of electrical connection could be reduced by such cracks. Since we observe a pronounced difference in the formation of microcracks (Figure 2.5 (a) vs (b)), the minimization of microcracks in the nanoparticle-nanotube mixed micropaper samples is believed to be the major factor for the improved DSSC performance.

From geometrical point of view, a higher degree of nanotube alignment along the electron transport direction (toward the current leads) would be more desirable since the electrical transport from the TiO_2 active material would benefit from the shorter distance to the current leads. Such an alignment could be attempted by mechanical alignment, for example by directional shear of the precursor paste containing the 8 nm nanotubes on removable substrate prior to drying and compaction. Further research is required to explore such possibilities.

In view of the significant and striking reduction in microcracking tendency in TiO_2 nanoparticles by the addition of high-aspect-ratio nanotubes (and the resultant increase in photocurrent density), it appears that this may have a more dominant effect on the DSSC performance than some of the other parameters. Additional detailed research can be performed to sort out the effect of various materials and process parameters on DSSC performance.

Another aspect to consider is the use of FTO glass. While the FTO glass type transparent conductive oxide layer is often used for the currently studied DSSC devices as a means of electron transport, it would be highly desirable to eventually eliminate the FTO glass for the purpose of reduced cost and ease of assembly. The free-standing nature of the TiO_2 micropapers reported here might

offer an intriguing possibility of direct electrical connection to the anode micropaper without the use of FTO glass, simply using inexpensive regular glass substrates. Further studies are required to explore such possibilities. While the mechanical flexibility is of less concern in the present case of rigid DSSC cells, the paper-like TiO_2 anode layer contains high-aspect-ratio, small-diameter TiO_2 nanotubes, which should result in an improved mechanical strength and mechanical flexibility that might be useful for future consideration of flexible DSSC assembly.

2.4 Conclusions

DSSC cells based on free-standing, paper-like TiO_2 structure have been demonstrated for the first time. Three types of TiO_2 micropaper photoanode were made and their microstructure and DSSC performances were compared. The measured photocurrent-voltage characteristics clearly indicate that the mixed of TiO_2 nanoparticle and 8 nm TiO_2 nanotube micropaper exhibits significantly improved photocurrent density (J_{sc}) as compared to the pure TiO_2 nanoparticle micropaper device, providing a much increased conversion efficiency. This enhanced efficiency is mainly attributed to the better interconnectivity among the TiO_2 nanoparticles due to the presence of high-aspect ratio 8 nm TiO_2 nanotubes, which provides easier pathways of electron transport, and also dramatically decreases the occurrence of microcracking in the micropaper anode layer. The free-standing nature of the micropaper TiO_2 structure offers an interesting possibility of future simpler anode assemblies without using the FTO glass.

2.5 Note

This chapter, in full, is a reprint of the material as it appears in Nano Energy, Volume 1, 2012. Jirapon Khamwannah, Yanyan Zhang, Sun Young Noh, Hyunsu Kim, Christine Frandsen, Seong Deok Kong and Sungho Jin.The dissertation author was the primary investigator and author of this paper

Chapter 3

Nanocomposites of TiO_2 and double-walled carbon nanotubes for improved dye-sensitized solar cells

3.1 Introduction

In the past decade, dye-sensitized solar cells (DSSC) have been extensively studied as a promising third-generation solar cell. With a relatively simple and low-cost fabrication process, yet with reasonably high conversion efficiency, DSSCs have gained much attention from many researchers in recent years [15] [98] [123] [124] [32] [101] [102] Nonetheless, the highest DSSC efficiency achieved thus far is only ∼11% [56]. As a result, many efforts to improve the DSSC performance are being studied throughout the world. However, no significant progress has been made in relation to further technical advancements and practical applications. The majority of research efforts have been devoted to the modification of the mesoporous semiconductor oxide film-TiO_2 [104] [107] [125] [108] [106]. Since the TiO_2 layer has been the most effective base material for DSSC due to its wide band gap and superior chemical stability.

During the DSSC operation, electrons are injected into the conduction band of TiO_2 upon photoexcitation of dye molecules. The electrons are then transported by diffusion through the TiO_2 layer and collected at the conductive electrode. As recombination of the electrons with species in electrolyte is a possible factor to limit the charge extraction from DSSCs [64], improved charge collection efficiency of the TiO_2 layer is a crucial aspect deserving further investigations and advances. Previous studies have reported the incorporation of carbon nanotubes (CNTs) into the TiO_2 film in order to achieve higher conversion efficiency. Many studies have focused on utilizing single-walled carbon nanotubes-SWCNTs for DSSC applications [126] [127] [128] [129] [130]. Recently a virus template approach was employed for more efficient SWCNTs distribution and attachments [131]. Their work revealed a high efficiency of 10.6% . Multi-walled carbon nanotubes-MWCNTs have also been studied as an integrated part of the TiO_2 mesoporous layer in order to improve the DSSC performance [132] [133].

Among the carbon nanotube family, double-walled carbon nanotubes - DWCNTs have attracted widespread attention due to the predominantly metallic behavior as compared to the case of SWNTs for which the nanotubes are often a mixture of semiconductor nanotubes and metallic nanotubes. Such metallic behavior of DWCNTs is highly desirable for electrical conduction related applications of carbon nanotubes [134] [135] [136]. Therefore, DWCNTs can be a good candidate material for incorporation into the TiO_2 layer of the DSSC anodes for improved electrical properties such as electron collection efficiency. So far, there have been no reports using DWCNTs in the active TiO_2 film anodes to our knowledge; although there are a few publications showing improved performance of DSSC devices with the DWCNT incorporated in the cathode counter electrodes [136] [137].

In this study, we have prepared TiO_2/DWCNTs nanocomposites for use in the photo anodes of dye sensitized solar cells. This one dimensionally elongated nanostructure of DWCNTs, typically a few nanometer in diameter and often less than $\sim$20-50 nm in diameter even in the agglomerated configuration, having the lengths in the micrometer regime, exhibits extremely high aspect ratio of hundreds to thousands. The DWCNTs in the nanocomposite are thus expected to get some-

what tangled with physical and electrical contacts among themselves unavoidable (and also with TiO_2 nanoparticles), although the degree of contacts would depend heavily on the amount of the carbon nanotubes. Furthermore, the problem of microcracking and local separations of the TiO_2 anode material layer often observed after drying of the doctor blade coated anode layer paste (containing TiO_2 nanoparticles, binder polymer and solvent) could be alleviated with the addition of long stringers such as DWCNTs. While the physical contacts of the DWCNTs are random and the direct effect of conductivity enhancement on DSSC properties is unclear, the mechanical locking of the TiO_2 anode layer due to the addition of high aspect ratio DWCNT fillers is expected to substantially reduce micro-cracking problem (which may be described as a "dry mud cracking"). We have actually observed a dramatic reduction of microcracks and associated improvements in DSSC characteristics as reported in this work. We have also investigated the effect of preparation methods of the TiO_2/DWCNTs nanocomposite paste, including the sequence of mixing and subsequent annealing treatments.

3.2 Experimental Procedures

3.2.1 Synthesis of TiO_2 nanoparticles (NPs) and paste preparation

The details of the general sol-gel synthesis of TiO_2 nanoparticles (NPs) and paste preparation have been well established by previous researchers, for example, as described by Jeong, et al. [138]. In brief, TiO_2 NPs were made by hydrolysis of mixed solution of titanium (IV) isopropoxide (TIP) in isopropanol and aqueous solution tetrabutylammonium hydroxide (TBAOH), followed by hydrothermal reaction to obtain the crystalline nanometer-sized particles. A standard TiO_2 nanoparticles paste has been prepared by combining 3.1 g of crystalline TiO_2 nanoparticles (NP) suspended in 9 g of ethanol in a vial. In another vial, 1.4 g of α-terpineol (96%, Alfa-Aesar), a viscosity enhancing alcohol, was added to 1.0 g of 10 wt% HPC-Ethanol solution. The HPC (hydroxyl propyl cellulose) is the binder

material utilized in the TiO_2 nano particles paste, which is dissolved in ethanol. The diluted NP suspension was transferred to the HPC- α-terpineol solution in drop-wise fashion. The mixture was stirred with a magnetic bar until a viscous paste formed. This paste is marked as Paste D in this report.

3.2.2 Preparation of CNT incorporated with TiO_2 nanoparticles

0.1 g of the surfactant solution (Nanosperse AQ procured from NanoLab, Inc) was mixed with 100 ml of deionized water, and then 0.1 g of DWCNTs powder (procured from NanoLab, Inc (with an average nanotube diameter $\sim$4 nm, average length $\sim$3 μm (1-5 μm range), and a purity >95%) was added into the surfactant-containing DI water to make a DWCNTs suspension. The suspension was stirred and ultrasonicated for several hours prior to using it in order to ensure the solution was uniform and the nanotubes well dispersed.

For preparation of the anode samples, different sequences of how DWCNTs were incorporated with TiO_2 NPs paste were investigated and named as Paste A, B, and C (Figure 3.2(a)). The well dispersed DWCNT suspension (containing surfactant and DI water) was mixed with the TiO_2 nanoparticles (NPs) suspension in ethanol first, then the composite suspension was added to the mixed solution of (HPC polymer binder + α-terpineol) and stirred for several hours until the paste is formed. This paste was labeled as Paste A. The final concentration of the DWCNTs in TiO_2 was adjusted to be 0.2 wt% ($\sim$0.4 vol %). This is a similar carbon nanotubes composition as studied by X. Dang et al [131].

Paste B was obtained by mixing the well dispersed DWCNTs suspension with the standard TiO_2 paste (described as Paste D earlier).The final concentration of the DWCNTs in TiO_2 was adjusted to be 0.2 wt % ($\sim$0.4 vol %). Paste C was made by adding as-received, non-dispersed DWCNTs powder into the TiO_2 nanoparticles (Paste D) followed by manual mechanical stirring for several hours for uniformity. The final concentration of the DWCNTs in TiO_2 in the Paste C was also 0.2 wt % ($\sim$0.4 vol %).

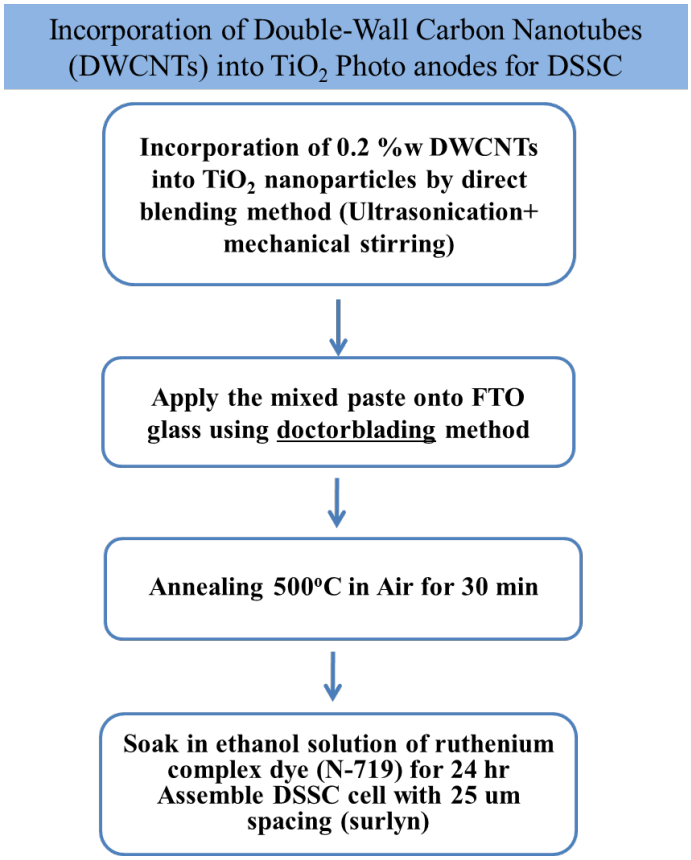

Figure 3.1: The processing sequence for the fabrication of the TiO_2/DWCNT nanocomposite photoanode.

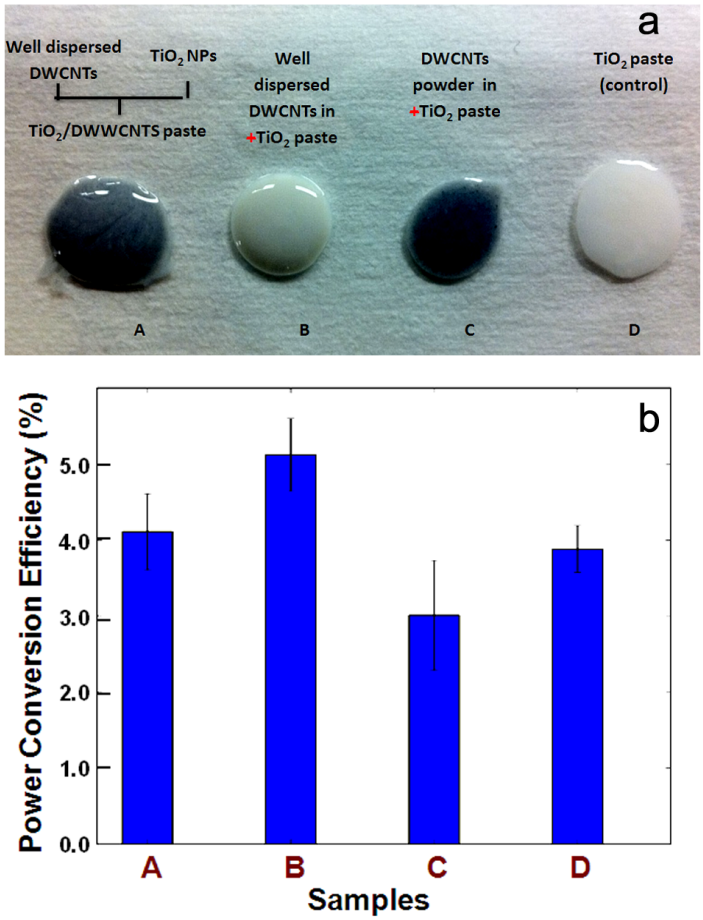

Figure 3.2: (a) Photographs of the TiO_2 pastes with different mix sequences. (A) adding TiO_2 nanoparticles to the well dispersed DWCNTs suspension + adding the binder and solvent, (B) adding well dispersed DWCNTs suspension to the already prepared TiO_2 paste containing TiO_2 nanoparticles + binder + solvent, (C) adding as-received dry DWCNTs powder into prepared TiO_2 paste, and (D) as-prepared TiO_2 paste. (b) Dependence of power conversion efficiency under AM 1.5 solar illumination on various paste mixing sequences of A to D.

3.2.3 Preparation of TiO_2/DWCNTs photoelectrodes

The standard FTO glass (15 Ω/square, Hartford Glass) was first scrubbed and ultrasonicated in detergent for 15 min, and subsequently ultrasonicated in ethanol for another 15 min, and dried by N_2 gas. The cleaned glass was treated with 0.04 M $TiCl_4$ aqueous solution at 70°C for 30 min in order to make good mechanical and electrical contacts between the applied active oxide layer and conducting layer.

The prepared TiO_2/DWCNTs paste (Paste A, B and C) was applied to the $TiCl_4$-treated conducting glass by the doctor-blade method with an active area of 0.16 cm^2. A single layer of adhesive tape was used as the doctor blading spacer to control the thickness of the coated layer. Two-step coated layers led to a thickness of 15 μm after annealing as determined by SEM analysis. To improve the uniformity of the surface, each applied layer was dried at ambient temperature for 3 min, and then placed on a hotplate at 120°C for 5 min. The TiO_2 NPs paste without DWCNTs (Paste D) was also applied on the FTO glass by the identical procedures.

The prepared anodes were annealed with three different conditions. The first two conditions were for annealing at either 375°C or 450°C for 1 hour then transferred to quartz tube furnace for further annealing at 500 °C for 30 min in argon gas to protect DWCNTs from burning. The third condition was to gradually heat from room temperature to 500 °C for 1 hour under air atmosphere in order to burn away the polymer and binder contained in the paste, as well as to transform the as-fabricated titanate to anatase TiO_2 phase. After annealing,TiCl4 treatment was repeated (0.04 M $TiCl_4$ aq. for 30 min at 70°C, rinse with water and ethanol, dry with N_2) and firing at 500 °C for 30 min to improve interconnections between TiO_2 nanoparticles. Finally, the anodes were immersed overnight in a 0.3 mM solution of [Ru(4-carboxylic acid-4´-carboxylate-2-2´ bipyridyl)2(NCS)2]-[tetrabutylammonium]2 (N719 dye, solaronix) in dry ethanol. The anode was washed with ethanol to remove excess dye material, followed by drying with N2 before DSSC device fabrication. The cathode counter-electrodes were fabricated by placing a small drop of 5 mM H_2PtCl_6 (from Sigma) in isopropanol onto cleaned FTO glass, followed by firing at 385°C for 15 min.

3.2.4 Fabrication of dye-sensitized solar cells

The prepared photoanodes and counter-electrodes were put together into sandwich cell type and sealed with hot-melt gasket of 25 μm Surlyn. The aperture of the Surlyn frame was 2 mm larger than TiO_2/DWCNTs area. The internal space was filled with a drop of electrolyte and the cell was placed in a small vacuum

chamber to remove inside air and let the electrolyte goes in. The electrolyte was composed of 0.6 M 1-butyl-3-methylimidazolium iodide (BMII), 0.03 M I_2, 0.1 M guanidinium thiocyanate, 0.5 M 4-tert-butylpyridine in acetonitrile and valeronitrile (85:15, v/v) [118]. The surface concentration of N719 dye in photoanode was determined by keeping the dyed-coated photoanode in 0.1 mol dm^{-3} NaOH solution in a mixed solvent (water/ethanol=1:1,v,v) [139]. for 24 hours to complete the desorption. The UV-Vis spectrum from the solution was used to determine the amount of dyes absorbed at the photoanode surface.

The morphology of TiO_2 and TiO_2/DWCNT after annealing were determined with an ultrahigh resolution scanning electron microscope (UHR SEM,FEI XL30), and the photocurrent density-voltage (J-V) curves were measured under AM 1.5 G illumination with 450 W Xenon lamp equipped with an AM 1.5 global filter (Newport 81094).

3.3 Results and Discussion

The experimental results and analysis include the study of the effect of paste incorporation sequence, the morphology of consolidated TiO_2 /DWCNTs anode, DSSC performance of TiO_2/DWCNTs nanocomposite photo-electrode, and the effect of process conditions such as the annealing conditions.

3.3.1 The effect of paste incorporation sequence

Since there has been no report showing the effect of the sequence of mixing CNTs with TiO_2 , we have investigated the effect of process parameters and have shown here that the different results can be obtained when the sequence of adding DWCNTs into the TiO_2 paste is altered. Figure 3.2(a) displays the characteristics of various TiO_2 /DWCNTs pastes, which were made by changing the order of adding DWCNTs into TiO_2 nanoparticles or pastes as described in the Experimental section. The dark grey color observed from Paste A and the black color of Paste C may result from the nonuniform and perhaps agglomerated configurations of DWCNTs in the paste. However, it was surprising to see that the Paste B (con-

taining nanotubes in surfactant) exhibited a rather light color, which may indicate the well-separated and uniform distribution of the nanotubes in the paste, since nano-dimensioned structures much less than the wavelength of the light should in principle have much reduced light absorption.

Figure 3.2(b) presents the plot of DSSC power conversion efficiency values obtained for the samples with different processing and materials parameters in Figure 3.2(a), under AM 1.5 G illumination. The sample size of the active area was maintained identical for all the samples throughout this research, ∼0.4 cm x 0.4 cm. The power conversion efficiency value of the paste A was 4.11%. It is noted that the highest DSSC power conversion efficiency of 5.3% was obtained from the paste B. This efficiency is higher than that for the standard TiO_2 NPs paste (Paste D), which was ∼3.9%. The lowest efficiency of 3.69% was obtained from paste C in which non-dispersed DWCNTs were simply added and manually mixed into the TiO_2 paste, with a likelihood of nanotubes agglomeration and light blocking as is evident from the more black color of the Paste C.

3.3.2 The morphology of consolidated TiO_2 /DWCNTs anode

Figure 3.3 shows the microscopic images of the annealed TiO_2 (Figure 3.3(a)) and TiO_2/DWCNTs (Figure 3.3(b)) films characterized by SEM. The annealed TiO_2 has a grain size (particle size) of approximately 20 nm as shown in Figure 3.3(a). Shown in Figure 3.3(b) is the DWCNTs dispersed well in TiO_2 nanoparticles matrix. Note that this particular sample for this image consisted of an intentionally higher concentration (10 wt%) of DWCNTs in TiO_2 paste for the purpose of obtaining a clearer image of DWCNTs distributed in TiO_2. To investigate the effect of DWCNTs on DSSC performance, the actual DSSC cells were constructed using a much lower concentration of 0.2 wt % (∼0.4 vol%). (DWCNTs, in this case it was not always easy to locate the nanotubes during SEM microscopy.)

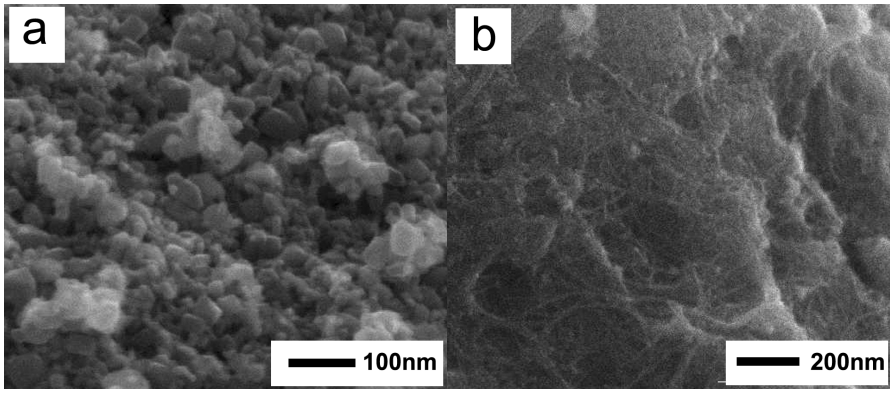

Figure 3.3: SEM images showing the surface morphology of (a) annealed TiO_2 film in the photoanode and (b) TiO_2/DWCNTs films with intentionally increased nanotube concentration for microscopic examination.

3.3.3 DSSC performance of TiO_2/DWCNTs nanocomposite photoelectrode

The comparative photocurrent-voltage (J-V) characteristic of the TiO_2 vs DWCNT-containing DSSC devices are shown in Figure 3.4(a). Compared to the devices with only TiO_2 NPs paste, the device with the DWCNTs incorporated into TiO_2 NP paste exhibited a much higher photocurrent density (J_{sc}) of ∼13.7 mA/cm^2, with a substantial increase J_{sc} value by ∼43%, as compared to that for the pure TiO_2 device (∼9.6 mA/cm^2). The open-circuit voltages from both types of devices were similar (∼0.8 V) and the fill factors were also similar at ∼0.6. Therefore, the only major difference was the photocurrent density (J_{sc}). As can be seen in the J-V characteristic curves (Figure3.4), it is obvious that the incorporation of a small amount of DWCNTs facilitated charge transport in some way in the composite TiO_2/DWCNTs film resulting in significantly higher electron collection efficiency.

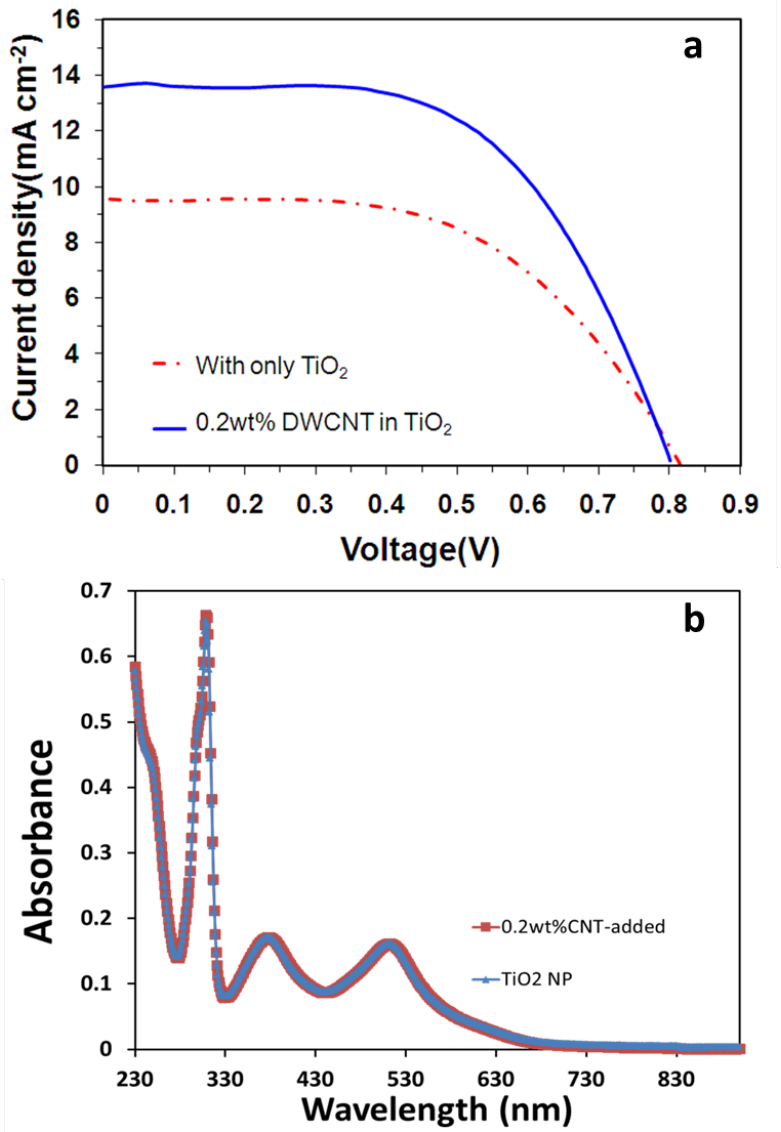

Figure 3.4: (a) J-V curves of TiO_2 device vs. TiO_2/DWCNTs device under AM 1.5 solar illumination. (b) UV-vis absorption spectra of N719-coated, TiO_2 nanoparticle (blue line) and 0.2 wt% DWCNT added (red line).

However, a comparative N719 dye analysis indicates that there is no noticeable difference in the amount of adsorbed dye molecules in the TiO_2 NP sample vs the TiO_2 NP with 0.2 wt% CNT sample, as shown in the UV-vis absorption spectra data in Figure 3.4(b), for example, at the wavelength of 515 nm having a molar extinction coefficient of 1.41×10^4 dm^3 mol^{-1} cm^{-1}, which is commonly used for dye adsorption comparison [29]. The adsorbed amount of dye at the anode

surface of TiO_2 NP and TiO_2 NP with 0.2 wt% DWCNT added is estimated to be 2.26×10^{-7} and 2.27×10^{-7} mol cm^{-2}, respectively. It means that the increased J_{sc} value in the DWCNT-containing sample does not result from an increased dye amount adsorbed on the photoanode surface.This may be understandable since the amount of DWCNT is small (only 0.2 wt%, equivalent to or ∼0.4 vol%), and hence the increase in the total surface area is also estimated to be relatively small.

There could be two possible interpretations for the effect of DWCNTs on enhanced J_{sc}. One is the noticeably reduced microcracking in the DWCNTs-containing TiO_2 devices compared to the nanotube-free TiO_2 devices, as is apparent in SEM micrographs shown in Figure 3.5. The very-high-aspect-ratio nanotubes combined with the well-known high strength of the nanotubes could serve as the mechanically strengthening elements in the nanocomposite (in a sense analogous to the rebar-reinforced concrete) which minimizes the microcracking during drying and sintering of the TiO_2 nanoparticles.

Another possible interpretation for the enhanced DSSC performance by the nanotube addition is that the electrically conductive DWCNTs providing a path for easier electron transport, and reduced charge recombination. The charge carrier recombination could be minimized if the electrons transported from the TiO_2 conduction band were able to quickly transport to the DWCNTs conduction band, and then get collected by the collecting electrode [131] [138]. This can be related to the improved interconnectivity between the TiO_2 and DWCNTs due to the overall enhanced electrical conductivity. However, since the amount of the nanotubes used here was rather small (∼0.2 wt% or ∼0.4 vol%), the reduced microcracking by nanotubes addition is considered to be a more important factor than the conductivity path enhancement by nanotubes. Additional electrical/electrochemical analysis such as AC impedance measurements would be useful for understanding of the exact cause of the J_{sc} improvement by the nanotube addition.

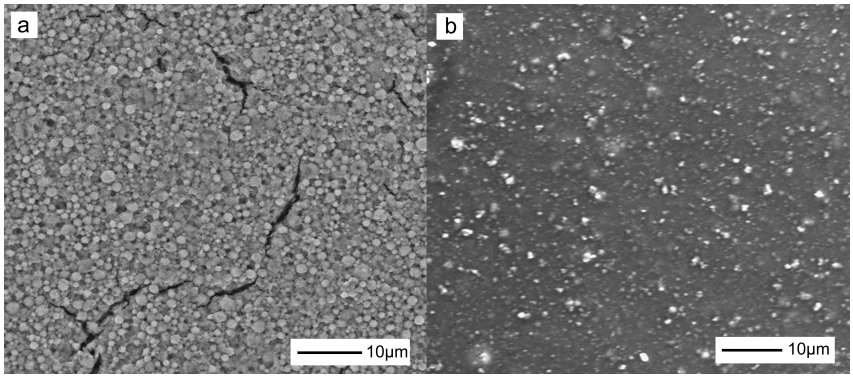

Figure 3.5: SEM images of (a) annealed TiO_2 and (b) TiO_2 - 0.2 wt% DWCNTs films, showing the drastic difference in the microcracking tendency of frequent cracks in the pure TiO_2 layer vs few microcracks in the nanotube-containing TiO_2 layer.

3.3.4 The effect of annealing conditions

It is seen that the DSSC performance is dependent on the annealing temperature for the TiO_2 layer. In order to understand the effect of the annealing temperature, the J-V curve characteristics, power conversion efficiencies and fill factors were also measured as a function of annealing temperature in Figure 3.6. All of the devices in Figure 3.6 were prepared by using paste B because this paste indicated the best performance compared to different pastes. The data in Figure 3.6(a) shows the J-V characteristic of the devices annealed at three different temperatures with the DSSC performance evaluated under AM 1.5 G illumination.

When annealed at 375° C for 1 hour in air followed by additional annealing in argon atmosphere for 30 min, the efficiency obtained was the lowest at 4.8%. On elevated temperature annealing, the efficiencies increased to 5.5% and 6.4% for the annealing temperatures of 450° C and 500° C respectively. In other words, the efficiency increased with increasing temperature. The reason behind this might be because the polymer binder materials in the coated paste film could not be completely decomposed at the lower temperatures below 450° C. Figure 3.6(b) also reveals that the fill factor of the cell improves monotonically with annealing temperature, over the range of 350- 500° C investigated in the present work.

Comparing with the standard TiO_2 anode annealed at identical 500°C, the

carbon nanotube-containing TiO_2 anode exhibited much higher photocurrent density (J_{sc}) increased by 43% as shown in Figure 3.4. The DSSC power conversion efficiency was also improved from ∼3.9% in the case of carbon nanotube-free TiO_2 anode to as high as 6.4% with the addition of DWCNTs. The observed enhancement in the solar cell performance in the presence of the double wall carbon nanotubes is attributed primarily to the noticeable reduction in microcracking and associated robust electrical conduction.

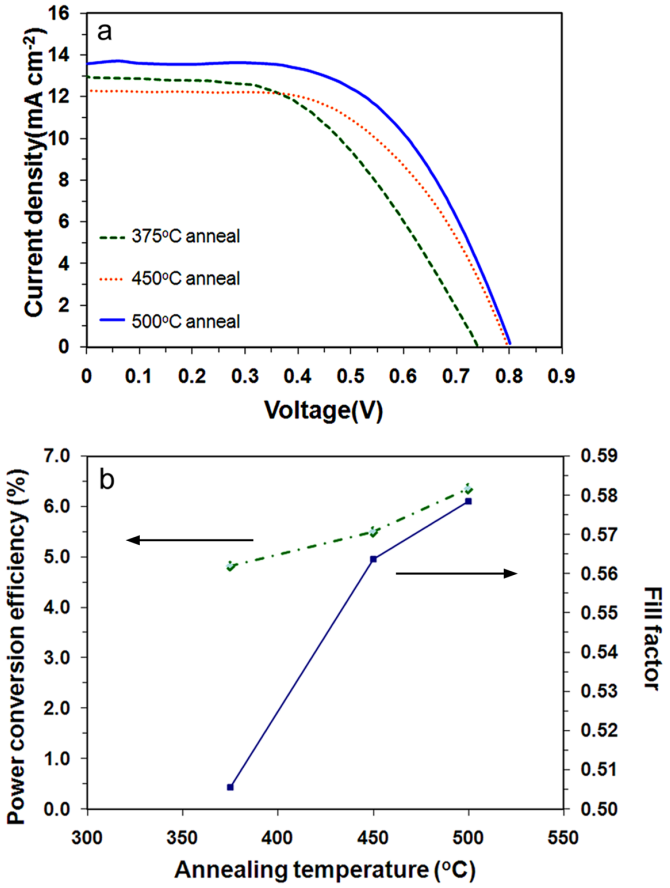

Figure 3.6: (a) Device performance; J-V curves of the DWCNTs-containing TiO_2 DSSC at various anode annealing conditions. (b) Dependence of power conversion efficiency of DSSC and fill factor on the different annealing temperature.

3.4 Conclusions

In summary, the incorporation of a small amount of double wall carbon nanotubes (DWCNTs) into the TiO_2 film in the dye sensitized solar cell photoanode resulted in a significant improvement in the solar cell performance. With the 0.2 wt% nanotubes addition, the photocurrent density was increased by ∼43%. Different types of pastes made by changing the mixing sequences of DWCNTs and TiO_2 NPs indicated the importance of the mixing order. Based on the photocurrent-voltage characteristic, our best TiO_2/DWCNTs devices exhibited a conversion efficiency of 6.4% under global AM 1.5 G solar illumination, with a significant improvement in conversion efficiency, and 43% increase in the current density (J_{sc}) relative to the cell without CNTs. The improved efficiency is attributed primarily to the dramatic decrease of microcracks in the nanotube-containing TiO_2 film, although some contributions by the enhanced electrical conduction through the nanotubes cannot be ruled out. It is also shown that the annealing condition plays an important role in improving the performance of the DSSC devices.

3.5 Note

This chapter, in full, is a reprint of the material as it appears in J. Renewable Sustainable Energy, vol.4, 2012. Jirapon Khamwannah, Sun Young Noh, Christine Frandsen, Yanyan Zhang, Hyunsu Kim, Seong Deok Kong, and Sungho Jin. The dissertation author was the primary investigator and author of this paper.

Chapter 4

Scale-up and FTO free Dye-sensitized solar cells

4.1 Introduction

Dye sensitized solar cells (DSSCs) have attracted considerable attention in recent years due to their low cost, high energy conversion efficiency, and relatively simple fabrication processes. Since the first report by O'Regan and Grätzel in 1991 [15], a number of investigations have been carried out to improve the performance of DSSCs [140] [141] [142] [64]. Over 11% energy conversion efficiency has been achieved in laboratory scale samples [141] [142]. Fluorine-doped tin oxide (FTO) glass has been widely used for the DSSC assembly as the transparent conducting oxide (TCO) because of its high visible light transmittance and good electrical conductivity. However, a noticeable size-dependent efficiency decrease is encountered when the solar cells are scaled up to larger areas for practical applications. As is well known, FTO glass exhibits a high sheet resistance, which causes ohmic loss and further leads to a significantly reduced efficiency [143]. In addition, FTO glass is also expensive, adding a substantial cost to the DSSC device [144]. Because of this size related problem, FTO glass based DSSCs are typically constructed with a stop-gap approach of fabricating about one centimeter wide parallel stripes and solder-bond stitching them together to produce larger area cells, for

example, with 10–30 cm dimensions. A single cell design without this stitching of narrower cells would be highly desirable for design simplicity and lower cost. Compared with FTO glass, highly conductive metal based electrodes could be a promising alternative to reduce the resistive loss, device weight and production cost of large size DSSCs. Fan et al., [145] utilized a stainless steel mesh as the cell photoanode to replace the FTO glass; however cells with very low energy conversion efficiencies of ∼1.49% were yielded. Onoda et al., investigated DSSCs with different substrates and they found that a nano-crystalline TiO_2 coated titanium substrate has a higher efficiency than stainless steel and FTO [146].

Metallic Ti has the advantages of low resistivity, low production cost and high temperature stability compared with FTO glass [81] [147] [148] [149]. The three-dimensional network film of interconnected TiO_2 nanoparticles has a porous structure and quite a large surface area. While some TiO_2 nanoparticles (TNP) paste tends to show poor adhesion on metal substrates, it has been reported that highly ordered TiO_2 nanotube arrays with a large internal surface area can be grown on Ti foils by an anodization process, and good energy conversion efficiencies have been reported [150] [151] [152] [153] [154]. Rustomji et al., utilized a woven Ti mesh with surface TiO_2 nanotubes as the anode basis to obtain ∼5% efficiency [124].

Here, we have employed a commercially available stainless steel mesh screen and modified the dimensions to be more suitable for DSSC anode structures. And we also combine low resistance Ti foil, vertically aligned TiO_2 nanotubes and porous film of nano-crystalline TiO_2 particles to reduce the resistive loss and enhance the energy conversion efficiency in larger size single piece DSSCs. The height of anodized, ordered TiO_2 nanotubes (TNTs) was controlled to be around 5 μm by controlled anodization of Ti foil, which was followed by coating with a thin layer of TNPs, about 7 μm thick. The Ti foil substrate gave good electrical conduction after DSSC assembly and the TNTs' nanostructure greatly enhanced the light scattering and the adhesion of the coated TNP paste. The coated TNP layer on top of the nanotubes had a large surface area which could absorb the desired amount of dye molecules. With scaled-up cell sizes from 0.25 to 9 cm^2, it is shown

that the size-dependent efficiency loss is substantially reduced in such a metal- and nanotube-containing composite structure in contrast to the traditional FTO glass based DSSC anode design.

4.2 Experimental procedure

4.2.1 Preparation of TiO_2 Composite of Embedded Stainless Steel Mesh for FTO-Free Photoanode

The commercially available Type 304 stainless steel mesh screen (3DLR6, SS Mesh, ∼40 um thick from Grainger) was too thick for use in the DSSC anode structure. Therefore we chemically etched the stainless steel mesh screen to optimally reduce the overall thickness, and also to reduce the grid wire diameter to increase the light transmission. Aqua Regia solution (HNO_3:HCl at 1:3 volume ratio) was used for 5 min to reduce the thickness to the desired level. The screen was then pressed to make it geometrically flat for easier assembly into DSSC cells. The final thickness of the stainless steel mesh was ∼30 um. Prior to the cell assembly, the mesh was cleaned in detergent solution, acetone and ethanol, using ultra-sonication for 10 min. Since the DSSC anodes using the bare stainless steel mesh screen gave a relatively poor performance with low DSSC efficiency, we added a dense 200 nm thick Ti metallic layer on the stainless steel mesh surface (both sides of the mesh screen). The Ti coating is naturally converted to a TiO_2 layer during subsequent processing for improved compatibility with the matrix TiO_2 nanoparticles material. The photoanode was fabricated by screen printing of TiO_2 paste (Solaronix, Swizerland), followed by annealing in air at 500°C/15 min, and soaked in a 0.3 mM solution of [Ru(4-carboxylic acid-4'-carboxylate-2-2 bipyridyl)2 (NCS)2]-[tetrabutylammonium]2 (N719 dye, from Solaronix) in ethanol for 24 h. A Pt- coated FTO glass substrate was employed as the counter electrode. The DSSC cell was constructed as shown in Figure 4.1.

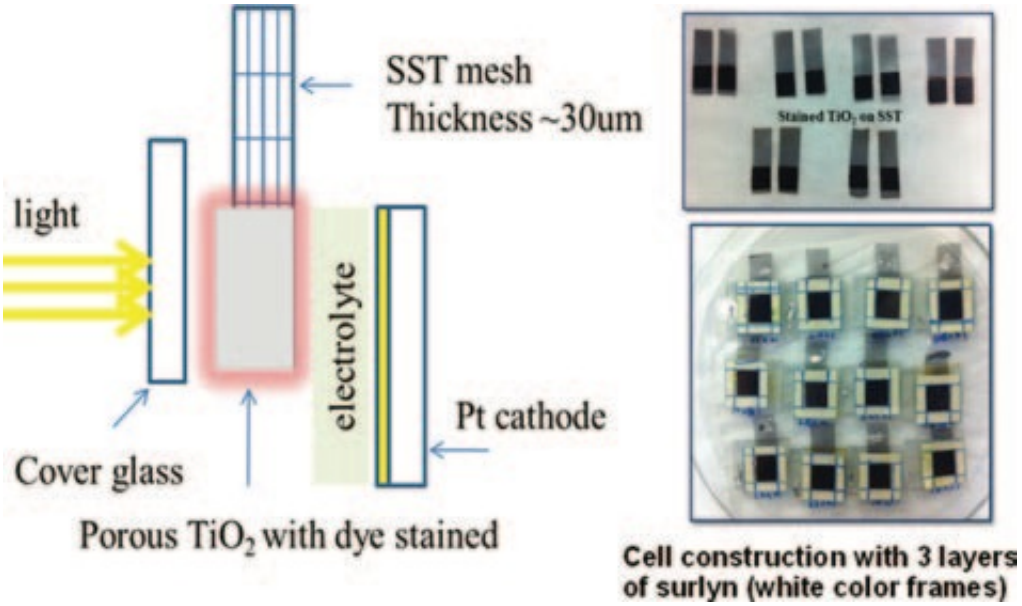

Figure 4.1: Schematic diagram of free-standing stainless steel mesh-based DSSCs (FTO-free anode).

4.2.2 Preparation of low resistance TiO_2 nanotubes on Ti-foil photoelectrodes

Synthesis of TiO_2 nanotubes (TNTs)

Highly ordered TiO_2 nanotube arrays were prepared by an anodization process in a two-electrode electrochemical bath. Ti foil (99.5% purity, 0.25 mm thick, Alfa Aesar) with square dimensions was used as a working electrode. Platinum foil was used as the counter-electrode. The voltage was applied by a DC power supply (Agilent, E3612A). A thin TiO_2 nanotube array layer was produced by anodizing the Ti foil in a solution of ethylene glycol (99.8%, JT Baker) containing 0.25% ammonium fluoride (NH4F, 96%, Alfa Aesar) and 2% H_2O at 60 V for 30 min.

Preparation of photoanodes

The TNP paste was synthesized by a sol–gel method which was described by previous researchers [155]. The TNP paste was coated onto the surfaces of different sized anodized TNT substrates using a doctor blading method and dried

at 130 °C for 10 min. Subsequently, all the samples were annealed in a furnace by gradual heating from room temperature to 500 °C (325 °C/5 min, 375 °C/5 min, 450 °C/15 min and 475 °C/15 min, with a 10 min ramping time between these steps). For comparison, TNP paste coating on bare Ti foil anodes was also carried out using similar processes. The samples were then treated in 0.04 M $TiCl_4$ aqueous solution at 70°C for 30 min in order to make good mechanical and electrical contacts between the active Ti oxide nano-particle layer and the conducting layer, followed by thermal treatment at 500 °C for 30 min.

Fabrication of dye sensitized solar cells

The prepared working-electrode (photo-anode) samples were soaked in N719 dye solution as in process described earlier. The cathode (counter-electrodes) were fabricated by placing a small drop of 5 mM H_2PtCl_6 (from Sigma Aldrich) in iso-propanol onto cleaned FTO glass, followed by firing at 400°C for 15 min. The prepared photo-anodes and counter-electrodes were put together into a sandwich cell type structure and sealed with hot-melt gasket of Surlyn. The cell's internal space was filled with electrolyte and the cell was placed in a vacuum chamber to remove the air from inside the cell space and allow the electrolyte to enter. The electrolyte was composed of 0.6 M 1-butyl-3-methylimidazolium iodide (BMII), 0.03 M I_2, 0.1 M guanidinium thiocyanate, 0.5 M 4-tert-butylpyridine in acetonitrile and valeronitrile (85:15, v/v). Four identical DSSC samples were made and tested for each condition.

Characterization

The morphologies of the TNTs and TNPs were determined using an ultrahigh resolution scanning electron microscope (UHR SEM, FEI XL30). The photocurrent density-voltage (J-V) curves were measured using a solar simulator under AM 1.5 G illumination with a 450 W xenon lamp equipped with an AM 1.5 global filter (Newport 81094) and coupled with a Keithley 2420 source meter. The illumination intensity (100 mW cm^{-2}) was calibrated by a standard Si cell.

4.3 Result and discussion

4.3.1 DSSC's performance of stainless steel mesh embedded photo-anodes for FTO free DSSCs

The J-V characteristics of the DSSCs made up of photoanode structure containing stainless steel mesh with an active area 1 cm^2 are shown in Figure 4.2. The photoconversion efficiency was very low (1.46%) for the anode with bare stainless steel mesh screen. Current density versus voltage relationship (J-V curves) of the DSSCs with different types of TiO_2 micropapers. However, the efficiency improved noticeably to 3.07% when 200 nm thick Ti was sputter coated on the surface of the stainless steel mesh screen.

The enhanced suppression of back electron transfer from the embedded stainless steel metal electrode to the electrolyte in the presence of the TiO_2-coated stainless steel mesh (since the metallic Ti coating will naturally oxidize to become TiO_2 during subsequent processing) could be one of the possible explanations of why the DSSCs cell performance was improved significantly with Ti coated stainless steel mesh than the bare stainless steel mesh. An alternative blocking layer coating such as Ti-sol solution could also be performed to improve the cell performance for the stainless steel mesh embedded photoanode structures.

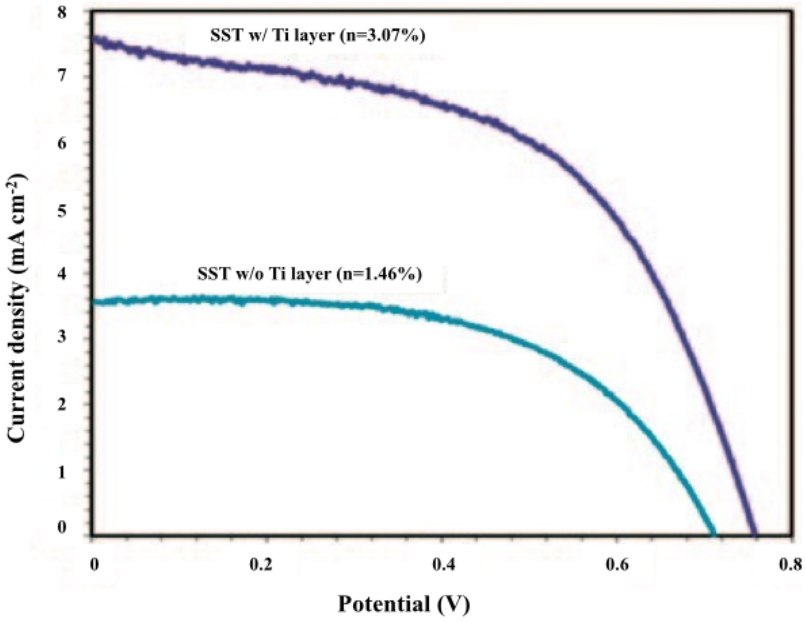

Figure 4.2: Current density versus voltage relationship (J –V curves) of the anodes containing embedded stainless steel mesh, with versus without 200 nm thick Ti sputter coating.

4.3.2 The morphology of the anodized TNTs and the TNP paste

Figures 4.3(a) and (b) show the morphology of the TiO_2 nanotubes grown by anodization and utilized as a substrate for coating with a TiO_2 nanoparticles paste layer to fabricate the DSSC solar cell. The vertically aligned TiO_2 nanotubes with ∼150 nm diameter and ∼5 μm length were produced by anodization treatment at 60 V for 30 min in a solution of ethylene glycol containing ammonium fluoride (NH_4F). After anodizing, the paste containing 25 nm size TiO_2 nanoparticles was coated on top of the TiO_2 nanotube layer, as shown in Figures 4.3(c) and (d). The total thickness of the nanotube and nanoparticles particles photoanode was around 12 μm (TNT layer 5 μm and TNP layer 7 μm). The crystal phase of the TiO_2 nanoparticles and TiO_2 nanotubes has been reported in our previous work [156] [157] to be predominantly the anatase phase after an 400–500°C annealing process. Anatase phase TiO_2 is still the main phase utilized in most DSSCs related

research and applications.

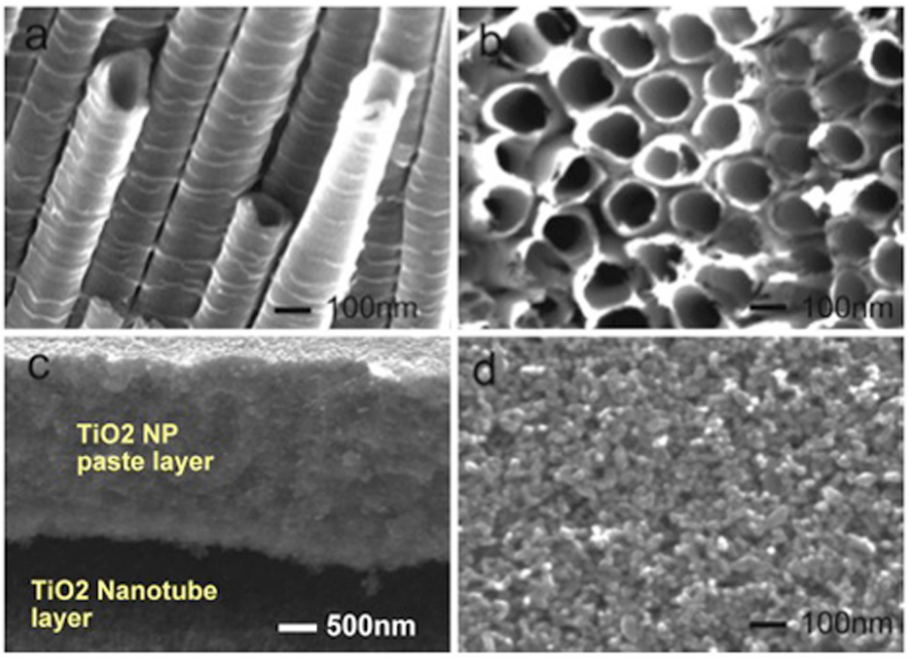

Figure 4.3: SEM images of anodized TiO_2 nanotubes and coated and baked TiO_2 nanoparticles paste. The TNTs were grown on a Ti foil at 60 V for 30 min. (a) 45°tilted view of the TNTs, (b) top view of the TNTs, (c) 45°tilted cross section of the coated and 500 °C baked paste, and (d) top view of the coated and baked paste.

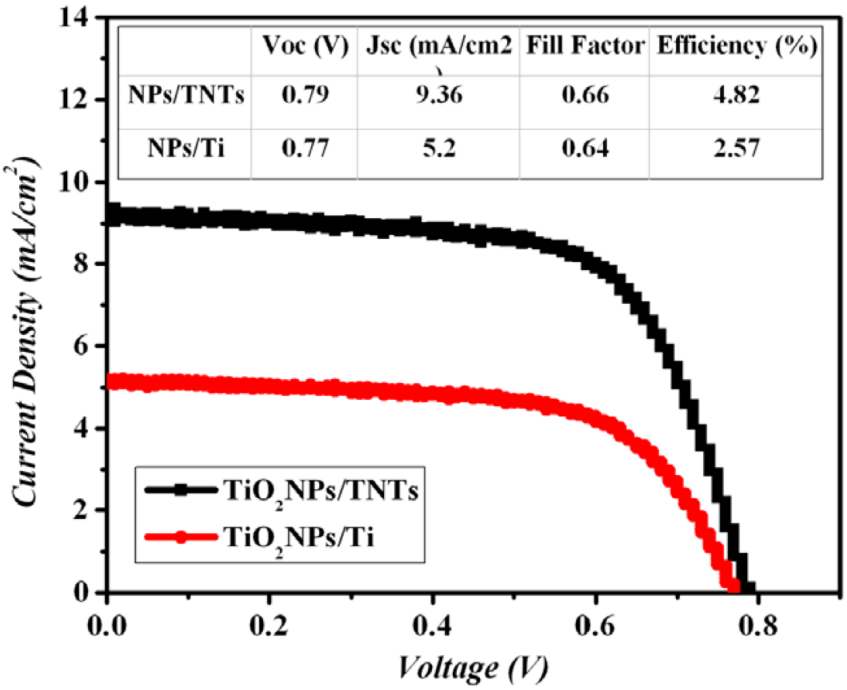

Figure 4.4: Comparative photocurrent density–voltage (J–V) characteristics of the (TNP-on-Ti foil) anode versus the (TNP-on-TNT on Ti foil) anode. The anode size is 0.5 × 0.5 cm^2 for both types of DSSC cell.

4.3.3 DSSCs performance of a TNP paste-on-Ti versus TNP paste-on-TNT anode

Figure 4.4 shows the typical, exemplary photocurrent density–voltage (J-V) characteristics of DSSC cells with TNPs coated on bare Ti foil substrate versus those on an anodized TiO_2 nanotube (TNT) layer. The inset shows the DSSC photovoltaic numerical performance data. In contrast to the J-V data for the TNP coated Ti foil (the lower curve in Figure 4.4), which indicates a relatively poor performance with a low short-circuit current density of J_{sc} = 5.20 mA cm^{-2}. The TNP coated TNT structure (the upper curve) exhibits a significantly enhanced photoanode current density of J_{sc} = 9.36 mA cm^{-2} (Four DSSC samples were made and tested for both types of sample, yielding generally comparable data). For example, the TNP coated Ti foil anode cells exhibited J_{sc} values ranging from 4.59 to 5.20 mA cm^{-2}, while the TNP coated TNT structure produced J_{sc} values

ranging from 6.56 to 9.90 mA cm^{-2}). The results indicate that the DSSC device with anodized TNTs exhibits almost two times higher J_{sc}. As is well known, the porous TNP film absorbs many N719 dye molecules on the large surface area of the 15-20 nm diameter TiO_2 nanoparticles within the TNP layer. There might be some extra dye molecules attached onto the surface of the TiO_2 nanotubes underneath as well; however the surface area of the ∼150 nm diameter nanotubes is expected to be much smaller than that of the TiO_2 nanoparticles in the samples investigated in this study.

The photoelectrons generated from the dye molecules are transferred to the TiO_2 nanoparticles for eventual collection by the conductive substrate to produce electric current and generate power. The improved DSSC performance by the addition of the TiO_2 nanotube layer between the traditional TiO_2 nanoparticles layer and the Ti foil (Figure 4.4) is tentatively attributed to one or more of the following factors.

(i) A more robust mechanical locking of the active TNP layer material (see the schematics of Figure 4.5) and less tendency for local micro-cracking or local delamination of the TNP layer from the Ti foil as the TNPs and metallic Ti have different elastic moduli and thermal expansion behavior.

(ii) TNTs, having fewer interfacial boundaries due to their vertically aligned array and continuous electrical conduction paths to the Ti metal conductor underneath, most likely allow more efficient electron transfer from the TiO_2 nanoparticles layer, thus reducing the chance of charge recombination, which also means that the electrons may have longer lifetimes to contribute to the higher photocurrent [158] [64].

(i) Increased sunlight absorption and reduced reflection due to the topographically rough, vertically aligned nanotube structure which may help to trap the sunlight better.

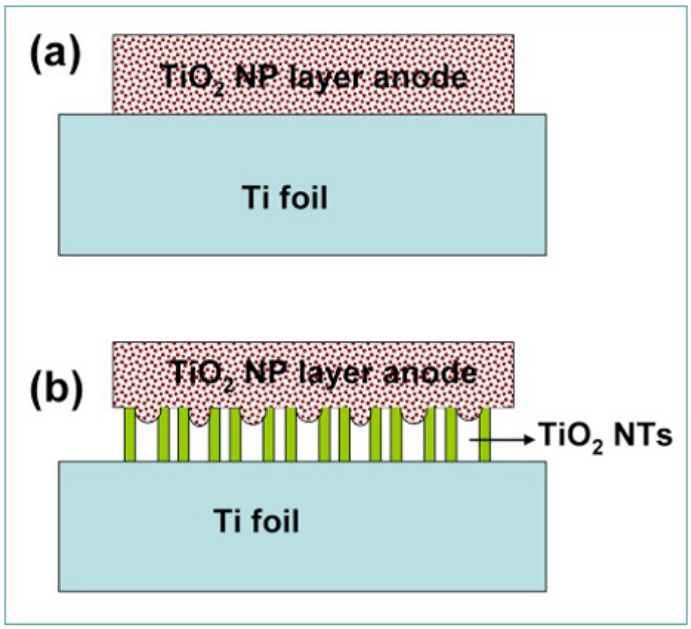

Figure 4.5: Schematic illustration of the mechanical and electrical connections of the TiO_2 anode layer to the Ti foil. (a) A TiO_2 nanoparticles (TNP) layer without a TiO_2 nanotube layer, and (b) with a TiO_2 nanotube (TNT) layer.

In order to consider the possible surface area effect that influences the amount of dye absorption and DSSC efficiency, we calculated the total surface area of the 5 μm tall nanotubes utilized and compared with that for the 7 μm thick TiO_2 nanoparticles layer. For the nanotubes, assuming an average OD (r_o, outer diameter) of 150 nm and ID (r_i, inner diameter) of 130 nm, and a 20 nm gap between adjacent nanotubes, the total inner surface area + outer surface area per 1 cm^2 area of the 5 μm tall TNT array structure is calculated to be $\sim$0.015 m^2. For the 7 μm thick nanoparticles layer, assuming a uniform 20 nm diameter and face-centered-cubic close packing, the total surface area is calculated to be 0.156 m^2, which is one order of magnitude larger than that for the 5 μm tall nanotubes. Therefore, even assuming that all the inner and outer surface of the nanotubes are coated with adsorbed dye and utilized, the contribution of the dye reaction from the nanotube portion is much smaller than that from the nanoparticles portion.

By substituting a part of the nanoparticles layer material with the nanotube material layer (i.e., instead of 12 μm thick TiO_2 nanoparticles, we used 5 μm thick nanotubes + 7 μm thick nanoparticles), we actually sacrificed about 40% of the

surface area. Nevertheless, we observed a significant improvement in the DSSC performance. We attributed this phenomenon to the enhanced light scattering by the presence of the TNT structure underneath the TNP structure, which is in agreement with Zhu et al's published results [23].

For the TNT-only DSSC cells without the TNP layer, we typically see ∼2–3% lower efficiency than for the TNP-only DSSC cells with a comparable material thickness (data not shown). As discussed above, the TNT layer that we utilize has an order of magnitude smaller surface area than the TNP layer and the dye absorption is thus expected to be much smaller than for the TNP cells, with the DSSC efficiency also expected to be somewhat limited. Further research is required to have a more thorough understanding of the mechanisms for the observed DSSC performance enhancement, and the possible contribution of each of the factors listed above.

Comparative schematic illustrations of the possible electron transfer and light paths for three types of anode structure—based on FTO, Ti metal, or anodized Ti substrates—are shown in Figure 4.6. In traditional FTO solar cells, light passes through the anode FTO glass, then some of the light is absorbed by the dye molecules. The transmitted sunlight is not utilized since it passes through the cell, as illustrated in Figure 4.6(a). In the Ti foil based solar cell, the photoanode substrate is replaced with a metallic titanium sheet, so some of the sunlight can be reflected by the Ti substrate and then be used again. For the anodized TNT based solar cell, the light can be scattered by the three-dimensional topography of the highly ordered TiO_2 nanotubes. This leads to an increase of the optical path length in the TiO_2 film, thus allowing more light to be recycled by the dye molecules for additional photocurrent generation. As reported previously [64], anodized TNTs show more light harvesting due to the enhanced light scattering off the oriented nanotube structure. This scattered light can be used again in the photo-anodes, which helps to improve the conversion efficiency. Furthermore, compared to the TiO_2 nanoparticles-based anode structure, the vertically aligned and continuous nanotubes have fewer interfaces for easier electron transport with a reduced chance of charge recombination, which could further enhance the conversion efficiency of

TNT based DSSCs.

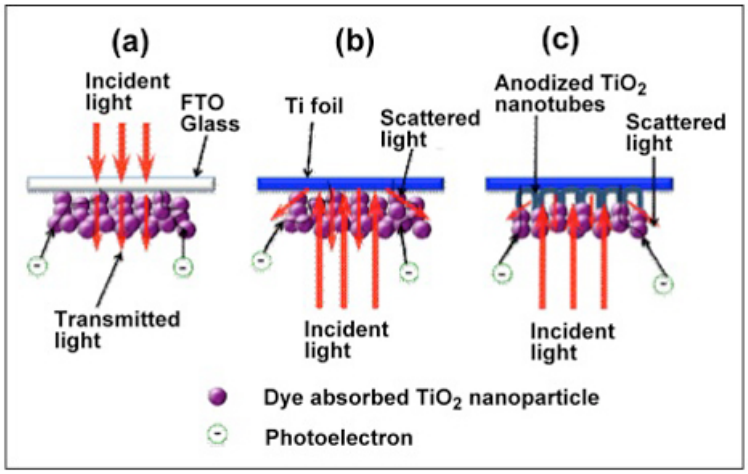

Figure 4.6: Schematic of the electron transfer paths and the utilization of incident light in the different substrate based DSSC anodes: (a) FTO glass, (b) Ti foil, and (c) anodized Ti (on Ti foil). More sunlight capture with reduced light transmission or reflection can be achieved by structure (c).

4.3.4 DSSC performance of different sized TNP paste-on-TNT cells

The photovoltaic characteristics of DSSCs with TNP paste coated on TNTs (Figure 4.6(c)) with four different active cell areas are shown in Figure 4.7 and Table 4.1. Four identical samples were prepared and tested for each cell size, with the results indicating comparable DSSC performance from sample to sample. The average data are shown in the Table 4.1. The typical example J–V curves shown in Figure 4.7 indicate that the TiO_2 nanoparticles coated, anodized TNT cells have efficiency values of 4.82%, 4.50% and 4.35% for cell sizes of 0.25 cm^2, 1 cm^2 and 4 cm^2, respectively. When the cell size is further increased to 9 cm^2, the efficiency is slightly lower (2.92%) than for the other three sizes. However, the fill factor (0.45) is improved by ∼80% compared to identical sized traditional FTO glass based photoanode solar cells as shown in Figure 4.8 and Table 4.2 due to the reduced series resistance of the Ti-containing photoanode.

Table 4.1: The photovoltaic performance of DSSCs with TNP paste coated on TNTs with four different active cell areas.

Active area (cm^2)	V_{oc}(V)	J_{sc}(mA/cm^2)	Efficiency(%)
0.25	0.79	9.36	4.82
1	0.75	9.69	4.50
4	0.73	9.68	4.35
9	0.67	9.72	2.92

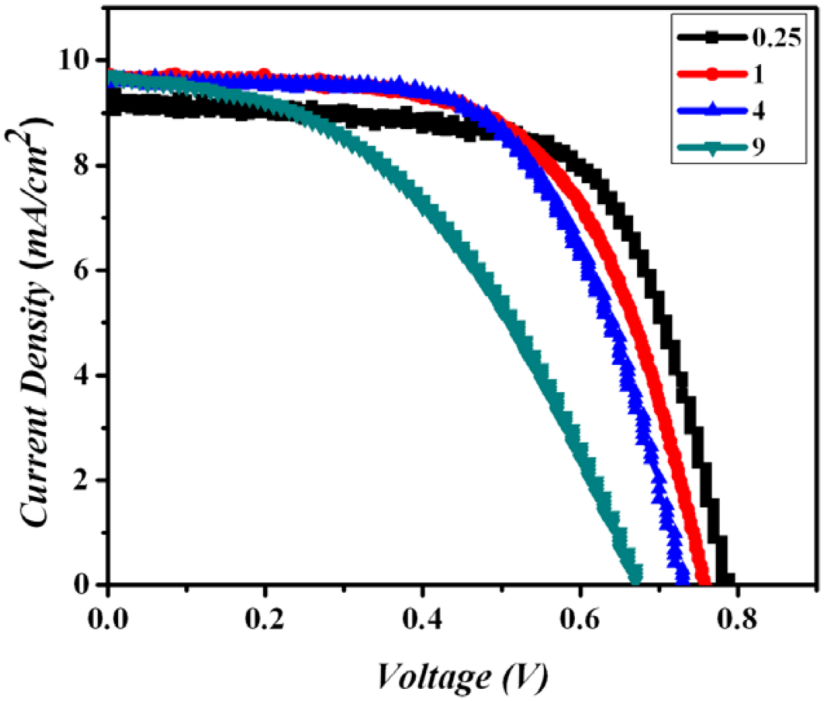

Figure 4.7: Photocurrent–voltage (J–V) characteristics of TiO_2 particles coated on different sized anodized TNT substrates. The cell sizes (in cm^2 active area) are marked in the inset.

Table 4.2: Photovoltaic characteristics of different size traditional FTO glass solar cells.

Active area (cm^2)	V_{oc}(V)	J_{sc}(mA/cm^2)	Efficiency(%)
0.25	0.81	17.90	7.92
1	0.82	14.70	6.56
4	0.80	13.20	2.96
9	0.77	5.99	1.18

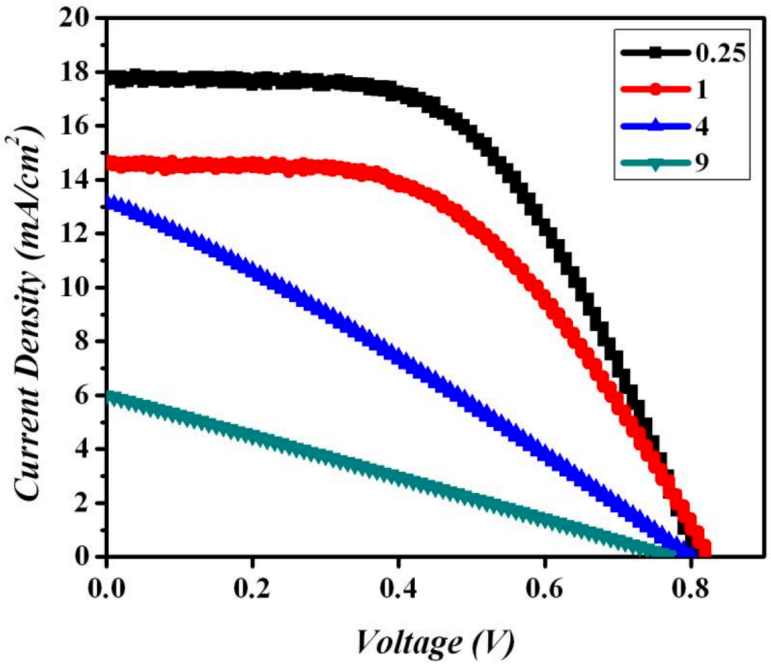

Figure 4.8: Photocurrent-voltage (J-V) characteristics of different size traditional FTO glass-solar cells with the cell size of 0.25, 1, 4, and 9 cm^2 area.

The noticeably higher fill factor results in almost 50% enhancement of the energy conversion efficiency over that of the same size traditional FTO glass solar cell. In contrast to FTO glass based TNP solar cells, the efficiency of the TNP anodized TNT–Ti foil solar cell does not exhibit a significant drop when the size of the solar cell is increased. For comparison, the photovoltaic characteristics of traditional DSSCs based on FTO glasses are presented in Figure 4.8 and Table 4.2. The samples in Figure 4.8 and Table 4.2 were fabricated in an essentially identical

manner to the cells with TNP paste on a Ti foil anode in this study, except that FTO glass was used in the anode without any Ti foil involved. The dependence of the DSSC photovoltaic performance of FTO and TNT based cells on the active area is shown in Figure 4.9.

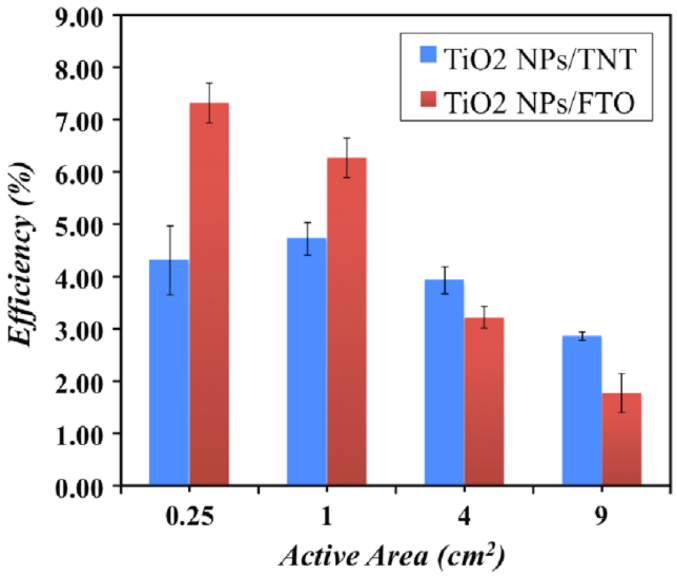

Figure 4.9: Photocurrent-voltage (J-V) characteristics of different size traditional FTO glass-solar cells with the cell size of 0.25, 1, 4, and 9 cm^2 area.

When the anode area is small, for example, 0.25 cm^2, the FTO based solar cell shows a much higher J_{sc} of 16.42 mA cm^{-2} than that for the TiO_2 nanotube/Ti foil based cell, exhibiting a J_{sc} value of 10.1 mA cm^{-2}. A similar behavior is seen for the 1 cm^2 size cells. However, when the size is increased the trend reverses at a cell area of 4 cm^2, at which point the nanotube-containing metal anode cell (TNP-on-TNT) already exhibits efficiency above that for the TNP on FTO cell. When the cell size is further increased to 9 cm^2, the J_{sc} of the FTO based cells dramatically decreases to 6 mA cm^{-2} (see Figure 4.8 and Table 4.2), while the nanotube-containing cell still maintains a higher efficiency than the FTO based cell. The fill factor of the FTO based cell also shows a noticeable decrease from 0.54 to 0.26. Furthermore, the power conversion efficiency of the FTO based cell drops remarkably from more than 7% to below 1.5% when the anode size is made larger. Therefore, it is shown that in order to prepare the desired, larger sized

DSSCs (a full sized cell, not a stitched line array cell), use of the TiO_2 nanotubes and removal of the FTO glass are very beneficial.

The sheet resistance of the FTO glass substrate is 12.4 Ω/sq at room temperature, which is increased to 15.4 after sintering at 450 °C for 30 min, while the Ti substrate maintains a low resistance of 1.0×10^{-3} Ω/sq which is four orders of magnitude smaller than that of the FTO glass [159]. The electrical resistance of the substrate plays a very important role in the factors determining the DSSC cell performance, especially when the cell size is scaled up.

Therefore, the efficiency of TNP coated, anodized Ti cells exhibits a much higher performance stability with respect to increased active area size than FTO based cells. It should be noted that while the anode FTO glass was eliminated in this work, the cathode structure still utilized FTO glass. Our ongoing research effort to also eliminate the cathode FTO glass and replace it with a metallic structure is likely to further reduce the size dependence of solar cell performance in larger DSSC cells, which will be reported in future publications.

4.4 Conclusions

In order to mitigate the severe performance deterioration in larger size dye sensitized solar cells, we have investigated the use of anodized TiO_2 nanotubes (TNTs) on Ti foil in combination with the standard TiO_2 nanoparticles coating. The presence of nanotubes in the DSSC anode as well as the removal of the FTO glass from the anode structure enabled a significant improvement in the size-dependent deterioration of the DSSC with a much milder decrease of the efficiency as a function of the cell dimensions up to 9 cm^2, greatly surpassing the performance of standard TiO_2 nanoparticles based solar cells. The observed improvement is partly attributed to the elimination of the highly resistive FTO glass in the anode structure, as well as the enhanced charge collection via the nanotubes coated Ti substrate, resulting from improved mechanical and electrical connections, electron conduction and possibly improved light trapping.

4.5 Note

This chapter, in full, is a reprint of the material as it appears in Nanotechnology, vol.24, 2012. Yanyan Zhang, Jirapon Khamwannah, Hyunsu Kim, Sun Young Noh, Haibin Yang, Sungho Jin. The dissertation author was the primary investigator and co-author of this paper.

This chapter, in part, is a reprint of the material as it appears in Journal of Nanoscience and Nanotechnology, vol.13, 2013. Jirapon Khamwannah, Hyunsu Kim, Yanyan Zhang, Tae Kyoung Kim and Sungho Jin. The dissertation author was the primary investigator and author of this paper.

Chapter 5

Conclusion and future outlook

5.1 Conclusion

The goal of this research was to develop a well-designed and economically competitive dye sensitized solar cell (DSSC) electrodes to further enhance the energy conversion efficiency of DSSCs. The major findings are as follows;

As discussed in Chapter 2, a composite of TiO_2 nanoparticles/8 nm TiO_2 nanotubes was successfully fabricated as a stand-alone, paper-like structure for photoanode of dye-sensitized solar cells by using a simple mechanical pressing method. Three types of TiO_2 micropaper photoanode were made and their microstructure and DSSC performances were compared. The measured photocurrent-voltage characteristics clearly indicated that the mixed of TiO_2 nanoparticle and 8 nm TiO_2 nanotube micropaper exhibited significantly improved photocurrent density (J_{sc}) as compared to the pure TiO_2 nanoparticle micropaper device, providing a much increased conversion efficiency. The best power conversion efficiency of 5.38% was for the solar cell under illumination of simulated AM 1.5 solar light. The combination of TiO_2 nanosphere-particles and 1D nanostructure leads to the effective electron transport and also provides the mechanical robustness for the overall structure while maintaining the transparency level. Additionally, the free-standing nature of the micropaper TiO_2 structure offers an interesting possibility of future simpler FTO-free anode could reduce the DSSC fabrication cost.

In Chapter 3, it was demonstrated that incorporation of double-walled car-

bon nanotubes (DWCNTs) into a TiO_2 photoanode layer resulted in significant improvement in the overall energy conversion in DSSC. Compared to the standard TiO_2 anode, the carbon nanotube-containing TiO_2 anode with 0.2 wt.% DWCNTs boosted up the photocurrent density (J_{sc}) by 43%. The DSSC power conversion efficiency was also improved from ∼3.9% in the case of carbon nanotube-free TiO_2 anode to as high as 6.4% with the addition of DWCNTs upon optimized anode annealing. The observed enhancement in the solar cell performance in the presence of the carbon nanotubes is attributed primarily to the noticeable reduction in microcracking and associated robust electrical conduction. Some contribution of the electrical conducting nature of the filler material (DWCNTs) to the improved DSSC properties may be possible; however, it is viewed as a minor effect, considering the small amount of nanotubes used.

In Chapter 4, the use of anodized TiO_2 nanotubes on Ti foil in combination with the standard TiO_2 nanoparticle paste coated anode structure has been investigated. Since, the typical DSSCs using TCO glass substrate exhibited a severe reduction of power conversion efficiency when the cell size was increased. A DSSC device based on a titanium foil photo-anode was developed. This type of anode structure enabled a significant mitigation of the size-dependent deterioration of the DSSC performance, with a much weaker decrease of the efficiency as a function of the cell dimension up to 9 cm^2. The observed improvement is partly attributed to the elimination of fluorine-doped tin oxide glass in the anode structure, as well as the enhanced charge collection via the nanotube-coated Ti substrate, resulting from enhanced mechanical and electrical connections and possibly improved light trapping. The introduction of TiO_2 nanotubes on the Ti foil substrate led to a substantial improvement of the J_{sc} current density.

5.2 Future work

5.2.1 A large-area and light-weight non-FTO dye-sensitized solar cell

For practical applications, the development of large-area and light-weight DSSCs are needed. The main structure of the DSSCs is the conductive substrate, but the conductive glass as a substrate is limited because of its rigidity, and plastic substrates are not applicable with the high temperature sintering process. Metal foils, on the other hand, can have good flexibility, low sheet resistance, high temperature endurance, and are inexpensive. Thus, they may be utilized as substrates in light-weight DSSCs. Although there are several candidates, such as stainless steel, silver, copper, etc., titanium is the most promising choice. Titanium as a substrate has high conductivity compared with a FTO (fluorine-doped tin oxide) substrate and has superior corrosion resistance to iodine electrolyte which is used in DSSCs [149] [159] [160].

In Chapter 4, the electrochemical anodized TiO_2-based DSSC was demonstrated, in which the titania nanotubes array was grown on titanium foil (Ti foil) and it was exploited as a photoanode [161]. The experimental results showed the anodized TiO_2-based anode structure enabled a significant mitigation of the size-dependent deterioration of the DSSC performance. Further study can be done by eliminating the fluorine-doped tin oxide (FTO) substrate and replacing it with a metal foil for both anode and counter electrode. The DSSC cell could be scaled up to 100 cm^2 by utilizing the all metal substrates structure.

The FTO glasses could be replaced with Ti-foil as the photoanode and Ti-mesh as the counter electrode. Due to the opaque nature of the Ti substrate, the cell can be illuminated through a transparent counter electrode. Figure 5.1 shows a schematic diagram of back-illuminated non-FTO DSSCs.

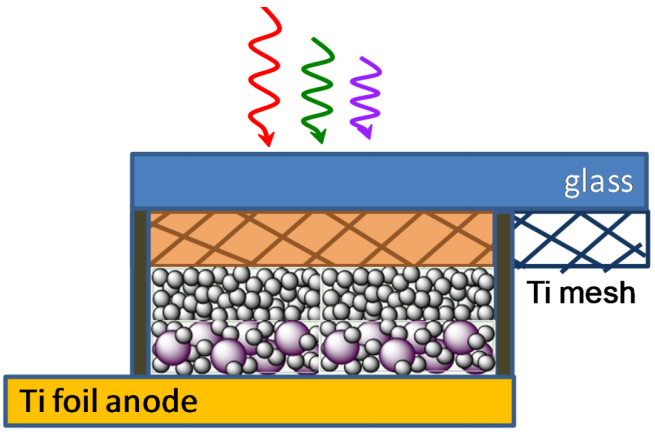

Figure 5.1: The schematic diagram of suggested back-illuminated large-area FTO-free DSSCs.

Preliminary study of a new design and fabrication of DSSC counter electrode for non-FTO DSSC

The counter electrode for the backside-illumination approach can be prepared from a platinized Ti mesh which has adequate transmittance for light to pass through. The optimum of the visible transmission of the Ti mesh should be in the range of 80-90% (comparable to FTO glass [162]). In this preliminary study, the tunable light transmission of patterned Ti was obtained via the method of low cost and high throughput printer-based fabrication of metal mesh followed by chemical etching of pattern-masked metal foils (see Figure 5.2). The pattern and size can be easily adjusted using a computer program. A large area of the patterned Ti foil can be obtained by this method as depicted in Figure 5.3. Careful design of the mesh opening size is important: the bigger the opening, the less conductive area of Ti substrate. Moreover when the opening is too large, the electrolyte diffusion path is longer, resulting in slower iodine regeneration which can occur at the counter electrode.

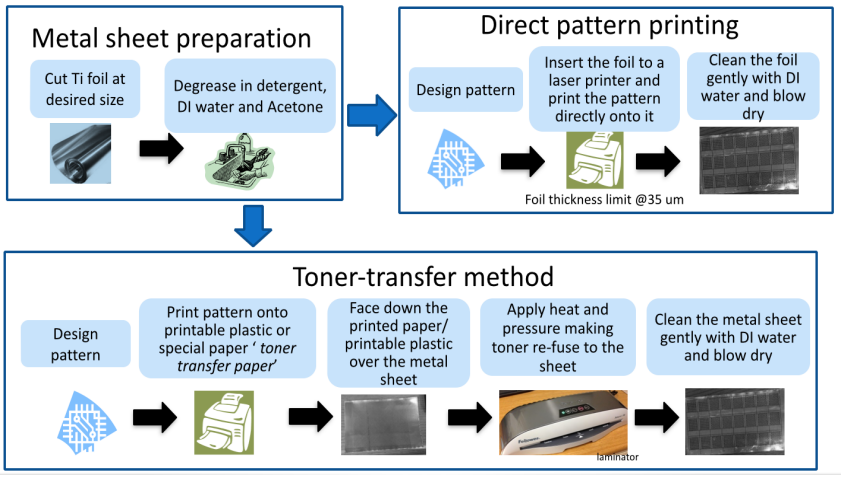

Figure 5.2: Low cost and high throughput printer-based fabrication for Ti mesh.

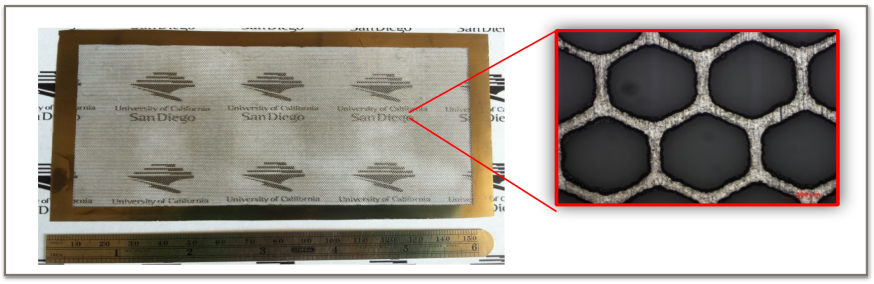

Figure 5.3: Large area (100 cm^2) Ti mesh obtained from printer-based fabrication.

A hexagonal pattern of Ti foil was obtained by printer-based fabrication and was used as a substrate for counter electrode. As shown in Figure 5.4, the SEM image shows a hexagonal pattern. The dimension of the hexagonal wire width is 185 μm and the opening size is about 445 μm. This pattern is calculated to have 50% light transmittance.

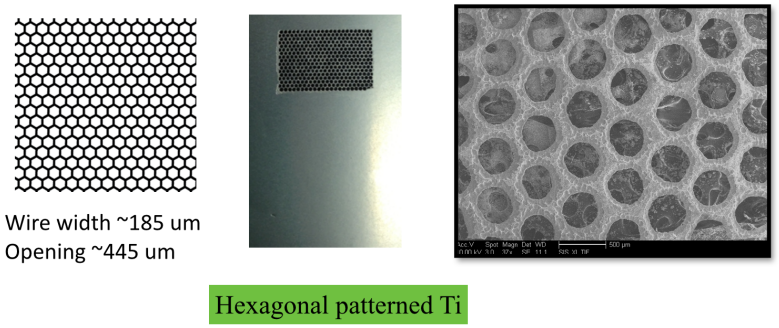

Figure 5.4: Hexagonal patterned Ti from printer-based fabrication.

In this experiment, platinum, which is the most efficient catalyst, was coated onto the patterned Ti foil by a sputtering process (Denton Discovery sputter/UCSD Nano3 system). The thickness of the nanoparticles Pt thin film layer was controlled to be 30 nm, 60 nm and 90 nm as the thicker layer will result in a continuous film. A DSSC photoanode was made from TiO_2 nanoparticles on FTO glass as previously explained in Chapter 4. A cell construction was similar to the traditional DSSC construction except at the counter electrode, in which the normal glass slide (not FTO) was used as a transparent supporting substrate. A standard FTO glass DSSCs were also built to compare the performance of the proposed structure. Figure 5.5 illustrates a structure of the patterned Ti mesh counter electrode DSSC.

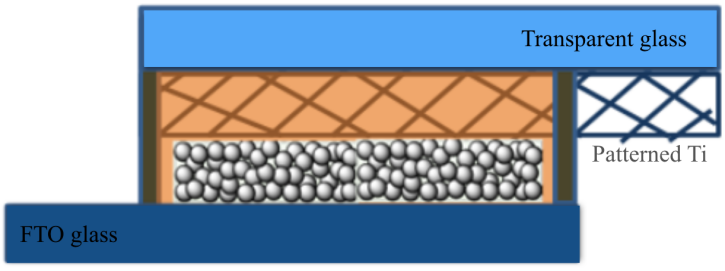

Figure 5.5: Schematic diagram Pt-sputtered on patterned Ti counter electrode DSSC.

The photovoltaic characteristics of DSSCs of the Pt-sputtered on a patterned Ti counter electrode DSSCs and traditional FTO DSSCs are shown in

Figure 5.6 and Table 5.1. Front-illumination via the photoanode and backside-illumination via the counter-electrode testing were performed. In the case of front illumination, the obtained performance from hexagonal pattern is good, which shows similar cell performance such as J_{sc}, V_{oc}, ff and efficiency, indicating the excellent catalytic activity of sputtered Pt, no matter what the thickness is. According to the backside illumination results, since the light loss through etched Ti patterned is much more than PT/FTO/Glass (transmittance of 71% at 550 nm), which is about 88% (transmittance of float glass) x 50% (transmittance of etched Ti foil) x 85% (transmittance of additional electrolyte between float glass and etched Ti foil), corresponding to 37.4% transmittance finally. Since the electrochemical activity of sputtered Pt is comparable with Pt/FTO/Glass, it is better to try the higher transmittance (>85%) of patterned Ti foil for further enhanced the cell performance of the backside-illumination FTO free DSSCs.

Table 5.1: The photovoltaic performance of standard FTO-DSSC vs Pt-sputtered on hexagonal patterned Ti DSSCs.

DSSC sample	Active area (cm^2)	V_{oc}(V)	J_{sc}(mA/cm^2)	Efficiency(%)
Standard-front	0.748	12.94	0.576	5.57
Standard-back	0.734	8.38	0.671	4.13
30nm-front	0.753	12.96	0.517	5.04
30nm-back	0.720	4.96	0.701	2.37
60nm-front	0.750	12.82	0.572	5.51
60nm-back	0.710	4.34	0.684	2.11
90nm-front	0.756	12.75	0.577	5.57
90nm-back	0.727	4.78	0.710	2.47

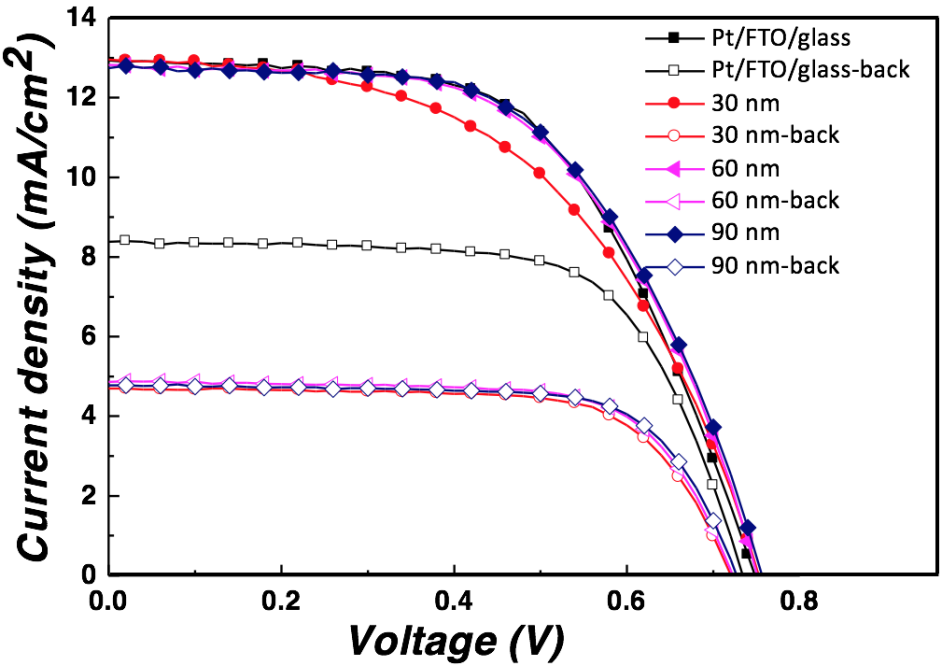

Figure 5.6: Photocurrent–voltage (J–V) characteristics of standard FTO-DSSC vs various thicknesses of Pt-sputtered on hexagonal patterned Ti DSSCs.

As Pt sputtering process requires high-cost equipment and it is also not practical for the scaled-up, larger production DSSCs, a counter electrode can be prepared by electrodepositing Pt on a patterned Ti using a current–time (chronoamperometry) technique from a H_2PtCl_6 (2 mM) aqueous solution containing HCl (0.50 M) [163].

An electrodeposition three-electrode cell was set up with Ti mesh as a working electrode, a Pt wire counter electrode and an Ag/AgCl reference electrode is shown in Figure 5.7. One example of Pt nanowire on a patterned Ti foil is shown in Figure 5.8.

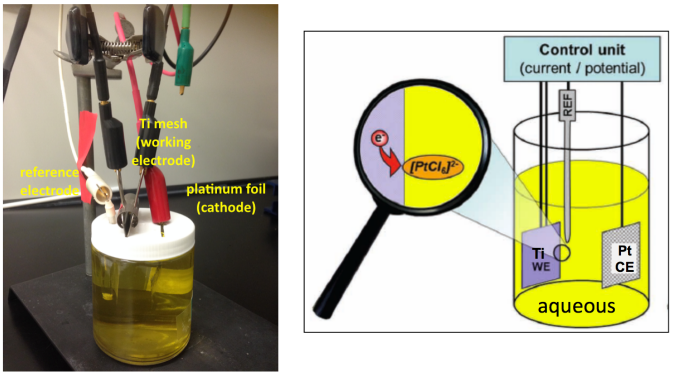

Figure 5.7: Electrodeposition set up for depositing Pt on counter electrode.

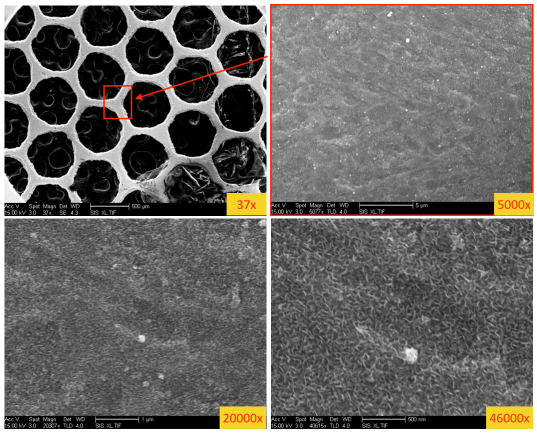

Figure 5.8: Electrodeposition of Pt nano size on hexagonal patterned Ti foil. Total applied current 60 mA/cm^2 , total applied charge density 540 mC/cm^2, the pulse 'on' 10 ms and the pulse 'off' 190 ms.

This study should be continued to evaluate these concepts more fully. The size, morphology, and loading of platinum nanoparticles should be studied in more detail, as well as the processing parameter, such as pH of the H_2PtCl_6 solution, current density, applied charge density and deposition time. A cyclic voltammetry measurement is required to evaluate the electrocatalytic activity of the Pt on a Ti surface in I_3^-/I^- redox reaction.

Bibliography

[1] Phillip Drachman. Third generation thin film solar photovoltaic technologies on track to breakthrough, http://www.solarserver.com/solar-magazine/solar-report/solar-report/third-generation-thin-film-solar-photovoltaic-technologies-on-track-to breakthrough.html.accessed 13 april 2015.

[2] Alexandre-Edmond Becquerel. Mémoire sur les effets électriques produits sous l'influence des rayons solaires. *Comptes Rendus*, 9(567):1839, 1839.

[3] Willoughby Smith. Effect of light on selenium during the passage of an electric current. *SPIE MILESTONE SERIES MS*, 56:3–3, 1992.

[4] Albert Einstein. Concerning an heuristic point of view toward the emission and transformation of light. *American Journal of Physics*, 33(5):367, 1965.

[5] Jan Czochralski. A new method for measuring the crystallization velocity of metals. *Z. Phys. Chem*, 92:219–221, 1918.

[6] DM Chapin, CS Fuller, and GL Pearson. A new silicon p-n junction photocell for converting solar radiation into electrical power. *Journal of Applied Physics*, (25):676–677, 1954.

[7] Holger Spanggaard and Frederik C Krebs. A brief history of the development of organic and polymeric photovoltaics. *Solar Energy Materials and Solar Cells*, 83(2):125–146, 2004.

[8] Zhang Wei. *Fabricataion of Dye Sensitized Solar Cells With Enhanced Energy Conversion Efficiency*. PhD thesis, 2011.

[9] National Renewable Energy Laboratory. Best research-cell efficiencies. golden, co: Nrel, efficiency_chart.jpg,accessed 13 april,2015.

[10] Paula Mints. Photovoltaic manufacturer shipments, capacity, & competitive analysis 2008/2009, 2009.

[11] Tatsuya Takamoto, Eiji Ikeda, Hiroshi Kurita, and Masamichi Ohmori. Over 30% efficient ingap/gaas tandem solar cells. *Applied Physics Letters*, 70(3):381–383, 1997.

[12] Alan Goodrich, Ted James, and Michael Woodhouse. Residential, commercial, and utilityscale photovoltaic (pv) system prices in the united states: current drivers and cost-reduction opportunities. *Contract*, 303:275–3000, 2012.

[13] Satyen K Deb. Recent developments in high-efficiency pv cells. In *World Renewable Energy Congress (WREC) VI, Brighton, UK*, pages 1–9, 2000.

[14] Antonio Luque and Steven Hegedus. *Handbook of photovoltaic science and engineering*. John Wiley & Sons, 2011.

[15] Brian O'regan and Michael Grätzel. A low-cost, high-efficiency solar cell based on dye-sensitized colloidal tio_2 films. 1991.

[16] Luís Moreira Gonçalves, Verónica de Zea Bermudez, Helena Aguilar Ribeiro, and Adélio Magalhães Mendes. Dye-sensitized solar cells: A safe bet for the future. *Energy & Environmental Science*, 1(6):655–667, 2008.

[17] Md K Nazeeruddin, Etienne Baranoff, and Michael Grätzel. Dye-sensitized solar cells: a brief overview. *Solar Energy*, 85(6):1172–1178, 2011.

[18] Michael Grätzel. Dye-sensitized solar cells. *Journal of Photochemistry and Photobiology C: Photochemistry Reviews*, 4(2):145–153, 2003.

[19] Juan Bisquert. Dye solar cell façade at swisstech convention center at epfl, by solaronix, https://juanbisquert.wordpress.com/2014/04/08/dye-solar-cell-facade-at-swisstech-covention-center-at-epfl-by-solaronix/. accessed 13 april 2015.

[20] Khalil Ebrahim Jasim. Dye sensitised solar cells-working principles, challenges and opportunities. *A chapter in Solar Cells/Book*, 2, 2011.

[21] Md K Nazeeruddin, A Kay, I Rodicio, R Humphry-Baker, E Müller, P_ Liska, N Vlachopoulos, and M Grätzel. Conversion of light to electricity by cis-x2bis (2, 2'-bipyridyl-4, 4'-dicarboxylate) ruthenium (ii) charge-transfer sensitizers (x= cl-, br-, i-, cn-, and scn-) on nanocrystalline titanium dioxide electrodes. *Journal of the American Chemical Society*, 115(14):6382–6390, 1993.

[22] Anders Hagfeldt and Michael Grätzel. Molecular photovoltaics. *Accounts of Chemical Research*, 33(5):269–277, 2000.

[23] A Karami. Synthesis of tio_2 nano powder by the sol-gel method and its use as a photocatalyst. *Journal of the Iranian Chemical Society*, 7(2):S154–S160, 2010.

[24] Akira Fujishima, Xintong Zhang, and Donald A Tryk. Tio_2 photocatalysis and related surface phenomena. *Surface Science Reports*, 63(12):515–582, 2008.

[25] A Kumar, R Jose, K Fujihara, J Wang, and S Ramakrishna. Structural and optical properties of electrospun tio_2 nanofibers. *Chemistry of Materials*, 19(26):6536–6542, 2007.

[26] JC Jamieson, Bart Olinger, F Dachille, PY Simons, and R Roy. Pressure-temperature studies of anatase, brookite rutile and tio_2 (ii)-a discussion, 1969.

[27] Stacey J Smith, Rebecca Stevens, Shengfeng Liu, Guangshe Li, Alexandra Navrotsky, Juliana Boerio-Goates, and Brian F Woodfield. Heat capacities and thermodynamic functions of tio_2 anatase and rutile: Analysis of phase stability. *American Mineralogist*, 94(2-3):236–243, 2009.

[28] A Beltran, L Gracia, and J Andres. Density functional theory study of the brookite surfaces and phase transitions between natural titania polymorphs. *The Journal of Physical Chemistry B*, 110(46):23417–23423, 2006.

[29] David O Scanlon, Charles W Dunnill, John Buckeridge, Stephen A Shevlin, Andrew J Logsdail, Scott M Woodley, C Richard A Catlow, Michael J Powell, Robert G Palgrave, Ivan P Parkin, et al. Band alignment of rutile and anatase tio_2. *Nature materials*, 12(9):798–801, 2013.

[30] Lianjun Liu, Huilei Zhao, Jean M Andino, and Ying Li. Photocatalytic co_2 reduction with h2o on tio_2 nanocrystals: Comparison of anatase, rutile, and brookite polymorphs and exploration of surface chemistry. *Acs Catalysis*, 2(8):1817–1828, 2012.

[31] Dorian AH Hanaor and Charles C Sorrell. Review of the anatase to rutile phase transformation. *Journal of Materials science*, 46(4):855–874, 2011.

[32] Thomas W Hamann, Rebecca A Jensen, Alex BF Martinson, Hal Van Ryswyk, and Joseph T Hupp. Advancing beyond current generation dye-sensitized solar cells. *Energy & Environmental Science*, 1(1):66–78, 2008.

[33] Jun Wang and Zhiqun Lin. Freestanding tio_2 nanotube arrays with ultra-high aspect ratio via electrochemical anodization. *Chemistry of Materials*, 20(4):1257–1261, 2008.

[34] David R Baker and Prashant V Kamat. Photosensitization of tio_2 nanostructures with cds quantum dots: particulate versus tubular support architectures. *Advanced Functional Materials*, 19(5):805–811, 2009.

[35] Jinting Jiu, Seiji Isoda, Fumin Wang, and Motonari Adachi. Dye-sensitized solar cells based on a single-crystalline tio_2 nanorod film. *The Journal of Physical Chemistry B*, 110(5):2087–2092, 2006.

[36] Soon Hyung Kang, S-H Choi, M-S Kang, J-Y Kim, H-S Kim, Taeghwan Hyeon, and Y-E Sung. Nanorod-based dye-sensitized solar cells with improved charge collection efficiency. *Advanced Materials*, 20(1):54–58, 2008.

[37] Jongmin Choi, Gyeongho Kang, and Taiho Park. A competitive electron transport mechanism in hierarchical homogeneous hybrid structures composed of tio_2 nanoparticles and nanotubes. *Chemistry of Materials*, 27(4):1359–1366, 2015.

[38] José Maçaira, Luísa Andrade, and Adélio Mendes. Review on nanostructured photoelectrodes for next generation dye-sensitized solar cells. *Renewable and Sustainable Energy Reviews*, 27:334–349, 2013.

[39] Neil Robertson. Optimizing dyes for dye-sensitized solar cells. *Angewandte Chemie International Edition*, 45(15):2338–2345, 2006.

[40] Saif A Haque, Emilio Palomares, Byung M Cho, Alex NM Green, Narukuni Hirata, David R Klug, and James R Durrant. Charge separation versus recombination in dye-sensitized nanocrystalline solar cells: the minimization of kinetic redundancy. *Journal of the American Chemical Society*, 127(10):3456–3462, 2005.

[41] Yasuo Chiba, Ashraful Islam, Yuki Watanabe, Ryoichi Komiya, Naoki Koide, and Liyuan Han. Dye-sensitized solar cells with conversion efficiency of 11.1%. *Japanese Journal of Applied Physics*, 45(7L):L638, 2006.

[42] Roberto Buscaino, Claudio Baiocchi, Claudia Barolo, Claudio Medana, Michael Grätzel, Md K Nazeeruddin, and Guido Viscardi. A mass spectrometric analysis of sensitizer solution used for dye-sensitized solar cell. *Inorganica Chimica Acta*, 361(3):798–805, 2008.

[43] K Hara, T Horiguchi, T Kinoshita, K Sayama, and H Arakawa. Influence of electrolytes on the photovoltaic performance of organic dye-sensitized nanocrystalline tio 2 solar cells. *Solar Energy Materials and Solar Cells*, 70(2):151–161, 2001.

[44] Naohiko Kato, Yasuhiko Takeda, Kazuo Higuchi, Akihiro Takeichi, Eiichi Sudo, Hiromitsu Tanaka, Tomoyoshi Motohiro, Toshiyuki Sano, and Tatsuo

Toyoda. Degradation analysis of dye-sensitized solar cell module after long-term stability test under outdoor working condition. *Solar Energy Materials and Solar Cells*, 93(6):893–897, 2009.

[45] ChunHung Law, Shehan C Pathirana, Xaioe Li, Assaf Y Anderson, Piers RF Barnes, Andrea Listorti, Tarek H Ghaddar, et al. Water-based electrolytes for dye-sensitized solar cells. *Advanced Materials*, 22(40):4505–4509, 2010.

[46] Ze Yu, Nick Vlachopoulos, Mikhail Gorlov, and Lars Kloo. Liquid electrolytes for dye-sensitized solar cells. *Dalton Transactions*, 40(40):10289–10303, 2011.

[47] Qingjiang Yu, Yinghui Wang, Zhihui Yi, Ningning Zu, Jing Zhang, Min Zhang, and Peng Wang. High-efficiency dye-sensitized solar cells: the influence of lithium ions on exciton dissociation, charge recombination, and surface states. *ACS nano*, 4(10):6032–6038, 2010.

[48] Aswani Yella, Hsuan-Wei Lee, Hoi Nok Tsao, Chenyi Yi, Aravind Kumar Chandiran, Md Khaja Nazeeruddin, Eric Wei-Guang Diau, Chen-Yu Yeh, Shaik M Zakeeruddin, and Michael Grätzel. Porphyrin-sensitized solar cells with cobalt (ii/iii)–based redox electrolyte exceed 12 percent efficiency. *science*, 334(6056):629–634, 2011.

[49] A Hauch, R Kern, J Ferber, A Georg, and J Luther. Characterization of the electrolyte-solid interfaces of dye-sensitized solar cells by means of impedance spectroscopy. In *2nd World Conference and Exhibition on Photovoltaic Solar Conversion, Vienna, Austria*, 1998.

[50] Dong Shi, Nuttapol Pootrakulchote, Renzhi Li, Jin Guo, Yuan Wang, Shaik M Zakeeruddin, Michael Gratzel, and Peng Wang. New efficiency records for stable dye-sensitized solar cells with low-volatility and ionic liquid electrolytes. *The Journal of Physical Chemistry C*, 112(44):17046–17050, 2008.

[51] Jiajia Gao, Muthuraaman Bhagavathi Achari, and Lars Kloo. Long-term stability for cobalt-based dye-sensitized solar cells obtained by electrolyte optimization. *Chemical Communications*, 50(47):6249–6251, 2014.

[52] N Papageorgiou, WF Maier, and M Grätzel. An iodine/triiodide reduction electrocatalyst for aqueous and organic media. *Journal of the electrochemical Society*, 144(3):876–884, 1997.

[53] Seok-Soon Kim, Yoon-Chae Nah, Yong-Young Noh, Jang Jo, and Dong-Yu Kim. Electrodeposited pt for cost-efficient and flexible dye-sensitized solar cells. *Electrochimica Acta*, 51(18):3814–3819, 2006.

[54] Xiaoming Fang, Tingli Ma, Guoqing Guan, Morito Akiyama, Tetsya Kida, and Eiichi Abe. Effect of the thickness of the pt film coated on a counter electrode on the performance of a dye-sensitized solar cell. *Journal of Electroanalytical Chemistry*, 570(2):257–263, 2004.

[55] Sara Thomas, TG Deepak, GS Anjusree, TA Arun, Shantikumar V Nair, and A Sreekumaran Nair. A review on counter electrode materials in dye-sensitized solar cells. *Journal of Materials Chemistry A*, 2(13):4474–4490, 2014.

[56] Michael Grätzel. Solar energy conversion by dye-sensitized photovoltaic cells. *Inorganic chemistry*, 44(20):6841–6851, 2005.

[57] Pablo Docampo, Stefan Guldin, Tomas Leijtens, Nakita K Noel, Ullrich Steiner, and Henry J Snaith. Lessons learned: from dye-sensitized solar cells to all-solid-state hybrid devices. *Advanced Materials*, 26(24):4013–4030, 2014.

[58] Akshay Kumar, Anuj R Madaria, and Chongwu Zhou. Growth of aligned single-crystalline rutile tio2 nanowires on arbitrary substrates and their application in dye-sensitized solar cells. *The Journal of Physical Chemistry C*, 114(17):7787–7792, 2010.

[59] Suresh Gubbala, Harry B Russell, Hemant Shah, Biswapriya Deb, Jacek Jasinski, Heather Rypkema, and Mahendra K Sunkara. Surface properties of sno 2 nanowires for enhanced performance with dye-sensitized solar cells. *Energy & Environmental Science*, 2(12):1302–1309, 2009.

[60] Bin Liu and Eray S Aydil. Growth of oriented single-crystalline rutile tio_2 nanorods on transparent conducting substrates for dye-sensitized solar cells. *Journal of the American Chemical Society*, 131(11):3985–3990, 2009.

[61] Alex BF Martinson, Jeffrey W Elam, Joseph T Hupp, and Michael J Pellin. Zno nanotube based dye-sensitized solar cells. *Nano letters*, 7(8):2183–2187, 2007.

[62] Matt Law, Lori E Greene, Justin C Johnson, Richard Saykally, and Peidong Yang. Nanowire dye-sensitized solar cells. *Nature materials*, 4(6):455–459, 2005.

[63] L Forro, O Chauvet, D Emin, L Zuppiroli, H Berger, and F Levy. High mobility n-type charge carriers in large single crystals of anatase (tio_2). *Journal of Applied Physics*, 75(1):633–635, 1994.

[64] Kai Zhu, Nathan R Neale, Alexander Miedaner, and Arthur J Frank. Enhanced charge-collection efficiencies and light scattering in dye-sensitized solar cells using oriented tio2 nanotubes arrays. *Nano letters*, 7(1):69–74, 2007.

[65] Xiaoyan Gan, Xiaomin Li, Xiangdong Gao, Fuwei Zhuge, and Weidong Yu. Zno nanowire/tio 2 nanoparticle photoanodes prepared by the ultrasonic irradiation assisted dip-coating method. *Thin Solid Films*, 518(17):4809–4812, 2010.

[66] Cheng-Yu Kuo and Shih-Yuan Lu. Fabrication of a multi-scale nanostructure of tio_2 for application in dye-sensitized solar cells. *Nanotechnology*, 19(9):095705, 2008.

[67] Stefan Guldin, Pablo Docampo, Morgan Stefik, Gen Kamita, Ulrich Wiesner, Henry J Snaith, and Ullrich Steiner. Layer-by-layer formation of block-copolymer-derived tio_2 for solid-state dye-sensitized solar cells. *Small*, 8(3):432–440, 2012.

[68] Joseph Kalowekamo and Erin Baker. Estimating the manufacturing cost of purely organic solar cells. *Solar Energy*, 83(8):1224–1231, 2009.

[69] Bo Wang and Lei L Kerr. Dye sensitized solar cells on paper substrates. *Solar Energy Materials and Solar Cells*, 95(8):2531–2535, 2011.

[70] Yaoming Xiao, Jihuai Wu, Gentian Yue, Jianming Lin, Miaoliang Huang, Zhang Lan, and Leqing Fan. Electrodeposition of high performance pedot/ti counter electrodes on ti meshes for large-area flexible dye-sensitized solar cells. *Electrochimica Acta*, 85:432–437, 2012.

[71] Kati Miettunen, Xiaoli Ruan, Tapio Saukkonen, Janne Halme, Minna Toivola, Huang Guangsheng, and Peter Lund. Stability of dye solar cells with photoelectrode on metal substrates. *Journal of The Electrochemical Society*, 157(6):B814–B819, 2010.

[72] Min Ju Yun, Seung I Cha, Seon Hee Seo, and Dong Y Lee. Highly flexible dye-sensitized solar cells produced by sewing textile electrodes on cloth. *Scientific reports*, 4, 2014.

[73] Fuzhi Huang, Dehong Chen, Yang Chen, Rachel A Caruso, and Yi-Bing Cheng. Mesoporous titania beads for flexible dye-sensitized solar cells. *Journal of Materials Chemistry C*, 2(7):1284–1289, 2014.

[74] AR Yugis, RF Mansa, and CS Sipaut. Review on metallic and plastic flexible dye sensitized solar cell. In *IOP Conference Series: Materials Science and Engineering*, volume 78, page 012003. IOP Publishing, 2015.

[75] Takeshi Yamaguchi, Nobuyuki Tobe, Daisuke Matsumoto, Takuma Nagai, and Hironori Arakawa. Highly efficient plastic-substrate dye-sensitized solar cells with validated conversion efficiency of 7.6%. *Solar Energy Materials and Solar Cells*, 94(5):812–816, 2010.

[76] Hasitha C Weerasinghe, Prasad M Sirimanne, George P Simon, and Yi-Bing Cheng. Cold isostatic pressing technique for producing highly efficient flexible dye-sensitised solar cells on plastic substrates. *Progress in Photovoltaics: Research and Applications*, 20(3):321–332, 2012.

[77] Takurou N Murakami, Yujiro Kijitori, Norimichi Kawashima, and Tsutomu Miyasaka. Uv light-assisted chemical vapor deposition of tio_2 for efficiency development at dye-sensitized mesoporous layers on plastic film electrodes. *Chemistry Letters*, 32(11):1076–1077, 2003.

[78] Dongshe Zhang, Tsukasa Yoshida, Ken Furuta, and Hideki Minoura. Hydrothermal preparation of porous nano-crystalline tio 2 electrodes for flexible solar cells. *Journal of Photochemistry and Photobiology A: Chemistry*, 164(1):159–166, 2004.

[79] Larissa Grinis, Sveta Kotlyar, Sven Rühle, Judith Grinblat, and Arie Zaban. Conformal nano-sized inorganic coatings on mesoporous tio_2 films for low-temperature dye-sensitized solar cell fabrication. *Advanced Functional Materials*, 20(2):282–288, 2010.

[80] André Sarto Polo, Melina Kayoko Itokazu, and Neyde Yukie Murakami Iha. Metal complex sensitizers in dye-sensitized solar cells. *Coordination Chemistry Reviews*, 248(13):1343–1361, 2004.

[81] Seigo Ito, Guido Rothenberger, Paul Liska, Pascal Comte, Shaik M Zakeeruddin, Péter Péchy, Mohammad Khaja Nazeeruddin, Michael Grätzel, et al. High-efficiency (7.2%) flexible dye-sensitized solar cells with ti-metal substrate for nanocrystalline-tio 2 photoanode. *Chemical Communications*, (38):4004–4006, 2006.

[82] Jong Hyeok Park, Yongseok Jun, Ho-Gyeong Yun, Seung-Yup Lee, and Man Gu Kang. Fabrication of an efficient dye-sensitized solar cell with stainless steel substrate. *Journal of the Electrochemical Society*, 155(7):F145–F149, 2008.

[83] Heng Li, Qing Zhao, Hui Dong, Qianli Ma, Wei Wang, Dongsheng Xu, and Dapeng Yu. Highly-flexible, low-cost, all stainless steel mesh-based dye-sensitized solar cells. *Nanoscale*, 6(21):13203–13212, 2014.

[84] Byung-wook Park, Takafumi Inoue, Yuhei Ogomi, Akari Miyamoto, Shinsuke Fujita, Shyam S Pandey, and Shuzi Hayase. Electron injection from linearly linked two dye molecules to metal oxide nanoparticles for dye-sensitized solar cells covering wavelength range from 400 to 950 nm. *Applied physics express*, 4(1):012301, 2011.

[85] AJ Nozik. Quantum dot solar cells. *Physica E: Low-dimensional Systems and Nanostructures*, 14(1):115–120, 2002.

[86] Jin-Wook Lee, Dae-Yong Son, Tae Kyu Ahn, Hee-Won Shin, In Young Kim, Seong-Ju Hwang, Min Jae Ko, Soohwan Sul, Hyouksoo Han, and Nam-Gyu Park. Quantum-dot-sensitized solar cell with unprecedentedly high photocurrent. *Scientific reports*, 3, 2013.

[87] Meidan Ye, Xiaoru Wen, Mengye Wang, James Iocozzia, Nan Zhang, Changjian Lin, and Zhiqun Lin. Recent advances in dye-sensitized solar cells: from photoanodes, sensitizers and electrolytes to counter electrodes. *Materials Today*, 2014.

[88] P Sudhagar, Emilio J Juárez-Pérez, Yong Soo Kang, and Iván Mora-Seró. Quantum dot-sensitized solar cells. In *Low-cost Nanomaterials*, pages 89–136. Springer, 2014.

[89] Alexander H Ip, Susanna M Thon, Sjoerd Hoogland, Oleksandr Voznyy, David Zhitomirsky, Ratan Debnath, Larissa Levina, Lisa R Rollny, Graham H Carey, Armin Fischer, et al. Hybrid passivated colloidal quantum dot solids. *Nature nanotechnology*, 7(9):577–582, 2012.

[90] Jeong Ah Chang, Sang Hyuk Im, Yong Hui Lee, Hi-jung Kim, Choong-Sun Lim, Jin Hyuk Heo, and Sang Il Seok. Panchromatic photon-harvesting by hole-conducting materials in inorganic–organic heterojunction sensitized-solar cell through the formation of nanostructured electron channels. *Nano letters*, 12(4):1863–1867, 2012.

[91] Akihiro Kojima, Kenjiro Teshima, Yasuo Shirai, and Tsutomu Miyasaka. Organometal halide perovskites as visible-light sensitizers for photovoltaic cells. *Journal of the American Chemical Society*, 131(17):6050–6051, 2009.

[92] Jeong-Hyeok Im, Chang-Ryul Lee, Jin-Wook Lee, Sang-Won Park, and Nam-Gyu Park. 6.5% efficient perovskite quantum-dot-sensitized solar cell. *Nanoscale*, 3(10):4088–4093, 2011.

[93] Hui-Seon Kim, Chang-Ryul Lee, Jeong-Hyeok Im, Ki-Beom Lee, Thomas Moehl, Arianna Marchioro, Soo-Jin Moon, Robin Humphry-Baker, Jun-Ho Yum, Jacques E Moser, et al. Lead iodide perovskite sensitized all-solid-state submicron thin film mesoscopic solar cell with efficiency exceeding 9%. *Scientific reports*, 2, 2012.

[94] Michael M Lee, Joël Teuscher, Tsutomu Miyasaka, Takurou N Murakami, and Henry J Snaith. Efficient hybrid solar cells based on meso-superstructured organometal halide perovskites. *Science*, 338(6107):643–647, 2012.

[95] James M Ball, Michael M Lee, Andrew Hey, and Henry J Snaith. Low-temperature processed meso-superstructured to thin-film perovskite solar cells. *Energy & Environmental Science*, 6(6):1739–1743, 2013.

[96] Nam Joong Jeon, Hag Geun Lee, Young Chan Kim, Jangwon Seo, Jun Hong Noh, Jaemin Lee, and Sang Il Seok. o-methoxy substituents in spiro-ometad for efficient inorganic–organic hybrid perovskite solar cells. *Journal of the American Chemical Society*, 136(22):7837–7840, 2014.

[97] Nam-Gyu Park. Organometal perovskite light absorbers toward a 20% efficiency low-cost solid-state mesoscopic solar cell. *The Journal of Physical Chemistry Letters*, 4(15):2423–2429, 2013.

[98] Mohammad K Nazeeruddin, Peter Pechy, Thierry Renouard, Shaik M Zakeeruddin, Robin Humphry-Baker, Pascal Comte, Paul Liska, Le Cevey, Emiliana Costa, Valery Shklover, et al. Engineering of efficient panchromatic sensitizers for nanocrystalline tio_2-based solar cells. *Journal of the American Chemical Society*, 123(8):1613–1624, 2001.

[99] Daibin Kuang, Peng Wang, Seigo Ito, Shaik M Zakeeruddin, and Michael Grätzel. Stable mesoscopic dye-sensitized solar cells based on tetracyanoborate ionic liquid electrolyte. *Journal of the American Chemical Society*, 128(24):7732–7733, 2006.

[100] Jihuai Wu, Sanchun Hao, Zhang Lan, Jianming Lin, Miaoliang Huang, Yunfang Huang, Pingjiang Li, Shu Yin, and Tsugio Sato. An all-solid-state dye-sensitized solar cell-based poly (n-alkyl-4-vinyl-pyridine iodide) electrolyte with efficiency of 5.64%. *Journal of the American Chemical Society*, 130(35):11568–11569, 2008.

[101] Stefan Guldin, Sven Hüttner, Priti Tiwana, M Christopher Orilall, Burak Ülgüt, Morgan Stefik, Pablo Docampo, Matthias Kolle, Giorgio Divitini, Caterina Ducati, et al. Improved conductivity in dye-sensitised solar cells through block-copolymer confined tio 2 crystallisation. *Energy & Environmental Science*, 4(1):225–233, 2011.

[102] Gerald J Meyer. The 2010 millennium technology grand prize: dye-sensitized solar cells. *ACS nano*, 4(8):4337–4343, 2010.

[103] Mateja Hočevar, Urša Opara Krašovec, Marko Berginc, Goran Dražič, Nina Hauptman, and Marko Topič. Development of tio_2 pastes modified with pechini sol–gel method for high efficiency dye-sensitized solar cell. *Journal of sol-gel science and technology*, 48(1-2):156–162, 2008.

[104] Mateja Hočevar, Marko Berginc, Marko Topič, and Urša Opara Krašovec. Sponge-like tio_2 layers for dye-sensitized solar cells. *Journal of Sol-Gel Science and Technology*, 53(3):647–654, 2010.

[105] Ryohei Mori, Tsutomu Ueta, Kazuo Sakai, Yasuhiro Niida, Yasuko Koshiba, Li Lei, Katsuhiko Nakamae, and Yasukiyo Ueda. Organic solvent based tio_2 dispersion paste for dye-sensitized solar cells prepared by industrial production level procedure. *Journal of materials science*, 46(5):1341–1350, 2011.

[106] Tianyou Peng, De Zhao, Ke Dai, Wei Shi, and Kazuyuki Hirao. Synthesis of titanium dioxide nanoparticles with mesoporous anatase wall and high photocatalytic activity. *The Journal of Physical Chemistry B*, 109(11):4947–4952, 2005.

[107] Hun Park, Woong-Rae Kim, Hyo-Tae Jeong, Jae-Joon Lee, Ho-Gi Kim, and Won-Youl Choi. Fabrication of dye-sensitized solar cells by transplanting highly ordered tio 2 nanotube arrays. *Solar Energy Materials and Solar Cells*, 95(1):184–189, 2011.

[108] Yoshinori Ohsaki, Naruhiko Masaki, Takayuki Kitamura, Yuji Wada, Takumi Okamoto, Toru Sekino, Kohichi Niihara, and Shozo Yanagida. Dye-sensitized tio 2 nanotube solar cells: fabrication and electronic characterization. *Physical Chemistry Chemical Physics*, 7(24):4157–4163, 2005.

[109] Seigo Ito, Takurou N Murakami, Pascal Comte, Paul Liska, Carole Grätzel, Mohammad K Nazeeruddin, and Michael Grätzel. Fabrication of thin film dye sensitized solar cells with solar to electric power conversion efficiency over 10%. *Thin solid films*, 516(14):4613–4619, 2008.

[110] L Dloczik, O Ileperuma, I Lauermann, LM Peter, EA Ponomarev, G Redmond, NJ Shaw, and I Uhlendorf. Dynamic response of dye-sensitized nanocrystalline solar cells: characterization by intensity-modulated photocurrent spectroscopy. *The Journal of Physical Chemistry B*, 101(49):10281–10289, 1997.

[111] N Kopidakis, EA Schiff, N-G Park, J Van de Lagemaat, and AJ Frank. Ambipolar diffusion of photocarriers in electrolyte-filled, nanoporous tio_2. *The Journal of Physical Chemistry B*, 104(16):3930–3936, 2000.

[112] Anita Solbrand, Henrik Lindström, Håkan Rensmo, Anders Hagfeldt, Sten-Eric Lindquist, and Sven Södergren. Electron transport in the nanostructured tio_2-electrolyte system studied with time-resolved photocurrents. *The Journal of Physical Chemistry B*, 101(14):2514–2518, 1997.

[113] Heli Wang, Jianjun He, Gerrit Boschloo, Henrik Lindström, Anders Hagfeldt, and Sten-Eric Lindquist. Electrochemical investigation of traps in a nanostructured tio_2 film. *The Journal of Physical Chemistry B*, 105(13):2529–2533, 2001.

[114] S Nakade, M Matsuda, S Kambe, Y Saito, T Kitamura, T Sakata, Y Wada, H Mori, and S Yanagida. Dependence of tio_2 nanoparticle preparation methods and annealing temperature on the efficiency of dye-sensitized solar cells. *The Journal of Physical Chemistry B*, 106(39):10004–10010, 2002.

[115] Kehan Yu and Junhong Chen. Enhancing solar cell efficiencies through 1-d nanostructures. *Nanoscale Research Letters*, 4(1):1–10, 2009.

[116] Tomoko Kasuga, Masayoshi Hiramatsu, Akihiko Hoson, Toru Sekino, and Koichi Niihara. Formation of titanium oxide nanotube. *Langmuir*, 14(12):3160–3163, 1998.

[117] Chien-Cheng Tsai and Hsisheng Teng. Chromium-doped titanium dioxide thin-film photoanodes in visible-light-induced water cleavage. *Applied Surface Science*, 254(15):4912–4918, 2008.

[118] Nathan R Neale, Nikos Kopidakis, Jao van de Lagemaat, Michael Grätzel, and Arthur J Frank. Effect of a coadsorbent on the performance of dye-sensitized tio_2 solar cells: shielding versus band-edge movement. *The Journal of Physical Chemistry B*, 109(49):23183–23189, 2005.

[119] Seigo Ito, Md Nazeeruddin, Paul Liska, Pascal Comte, Raphaël Charvet, Péter Péchy, Marie Jirousek, Andreas Kay, Shaik M Zakeeruddin, Michael Grätzel, et al. Photovoltaic characterization of dye-sensitized solar cells: effect of device masking on conversion efficiency. *Progress in photovoltaics: research and applications*, 14(7):589–601, 2006.

[120] Xiaobo Chen and Samuel S Mao. Titanium dioxide nanomaterials: synthesis, properties, modifications, and applications. *Chemical reviews*, 107(7):2891–2959, 2007.

[121] Seung I Cha, Kyu H Hwang, SH Seo, and Dong Y Lee. Tio_2 paper-inserted sinter-free electrode for dye-sensitized solar cells. *Nanoscience and Nanotechnology Letters*, 3(3):295–299, 2011.

[122] Mi Yeon Song, Do Kyun Kim, Kyo Jin Ihn, Seong Mu Jo, and Dong Young Kim. Electrospun tio_2 electrodes for dye-sensitized solar cells. *Nanotechnology*, 15(12):1861, 2004.

[123] Daibin Kuang, Cedric Klein, Zhipan Zhang, Seigo Ito, Jacques-E Moser, Shaik Zakeeruddin, Michael Grätzel, et al. Stable, high-efficiency ionic-liquid-based mesoscopic dye-sensitized solar cells. *Small*, 3(12):2094–2102, 2007.

[124] Cyrus S Rustomji, Christine J Frandsen, Sungho Jin, and Michael J Tauber. Dye-sensitized solar cell constructed with titanium mesh and 3-d array of

tio$_2$ nanotubes†. *The Journal of Physical Chemistry B*, 114(45):14537–14543, 2010.

[125] Hoda Hafez, Zhang Lan, Qinghua Li, and Jihuai Wu. High efficiency dye-sensitized solar cell based on novel tio$_2$ nanorod/nanoparticle bilayer electrode. *Nanotechnology, science and applications*, 3:45, 2010.

[126] Song-Rim Jang, R Vittal, and Kang-Jin Kim. Incorporation of functionalized single-wall carbon nanotubes in dye-sensitized tio$_2$ solar cells. *Langmuir*, 20(22):9807–9810, 2004.

[127] Anusorn Kongkanand, Rebeca Martínez Domínguez, and Prashant V Kamat. Single wall carbon nanotube scaffolds for photoelectrochemical solar cells. capture and transport of photogenerated electrons. *Nano Letters*, 7(3):676–680, 2007.

[128] Patrick Brown, Kensuke Takechi, and Prashant V Kamat. Single-walled carbon nanotube scaffolds for dye-sensitized solar cells. *The Journal of Physical Chemistry C*, 112(12):4776–4782, 2008.

[129] F Bonaccorso. Debundling and selective enrichment of swnts for applications in dye-sensitized solar cells. *International Journal of Photoenergy*, 2010, 2010.

[130] Michael J O'connell, Sergei M Bachilo, Chad B Huffman, Valerie C Moore, Michael S Strano, Erik H Haroz, Kristy L Rialon, Peter J Boul, William H Noon, Carter Kittrell, et al. Band gap fluorescence from individual single-walled carbon nanotubes. *Science*, 297(5581):593–596, 2002.

[131] Xiangnan Dang, Hyunjung Yi, Moon-Ho Ham, Jifa Qi, Dong Soo Yun, Rebecca Ladewski, Michael S Strano, Paula T Hammond, and Angela M Belcher. Virus-templated self-assembled single-walled carbon nanotubes for highly efficient electron collection in photovoltaic devices. *Nature nanotechnology*, 6(6):377–384, 2011.

[132] Thanyarat Sawatsuk, Anon Chindaduang, Chaiyuth Sae-Kung, Sirapat Pratontep, and Gamolwan Tumcharern. Dye-sensitized solar cells based on tio 2–mwcnts composite electrodes: Performance improvement and their mechanisms. *Diamond and Related Materials*, 18(2):524–527, 2009.

[133] Tae Young Lee, PS Alegaonkar, and Ji-Beom Yoo. Fabrication of dye sensitized solar cell using tio 2 coated carbon nanotubes. *Thin Solid Films*, 515(12):5131–5135, 2007.

[134] DW Zhang, XD Li, S Chen, F Tao, Z Sun, XJ Yin, and SM Huang. Fabrication of double-walled carbon nanotube counter electrodes for dye-sensitized solar sells. *Journal of Solid State Electrochemistry*, 14(9):1541–1546, 2010.

[135] Seung Chul Lyu, Bao Chun Liu, Cheol Jin Lee, Hee Kwang Kang, Cheol-Woong Yang, and Chong Yun Park. High-quality double-walled carbon nanotubes produced by catalytic decomposition of benzene. *Chemistry of materials*, 15(20):3951–3954, 2003.

[136] Dingwen Zhang, Xiaodong Li, Si Chen, Zhuo Sun, Xi Jiang Yin, and Sumei Huang. Performance of dye-sensitized solar cells with various carbon nanotube counter electrodes. *Microchimica Acta*, 174(1-2):73–79, 2011.

[137] Jinquan Wei, Yi Jia, Qinke Shu, Zhiyi Gu, Kunlin Wang, Daming Zhuang, Gong Zhang, Zhicheng Wang, Jianbin Luo, Anyuan Cao, et al. Double-walled carbon nanotube solar cells. *Nano letters*, 7(8):2317–2321, 2007.

[138] Nak Cheon Jeong, Omar K Farha, and Joseph T Hupp. A convenient route to high area, nanoparticulate tio_2 photoelectrodes suitable for high-efficiency energy conversion in dye-sensitized solar cells. *Langmuir*, 27(5):1996–1999, 2011.

[139] Zhong-Sheng Wang, Hiroshi Kawauchi, Takeo Kashima, and Hironori Arakawa. Significant influence of tio 2 photoelectrode morphology on the energy conversion efficiency of n719 dye-sensitized solar cell. *Coordination chemistry reviews*, 248(13):1381–1389, 2004.

[140] Michael Grätzel. Conversion of sunlight to electric power by nanocrystalline dye-sensitized solar cells. *Journal of Photochemistry and Photobiology A Chemistry*, 164:3–14, 2004.

[141] Mohammad K Nazeeruddin, Filippo De Angelis, Simona Fantacci, Annabella Selloni, Guido Viscardi, Paul Liska, Seigo Ito, Bessho Takeru, and Michael Grätzel. Combined experimental and dft-tddft computational study of photoelectrochemical cell ruthenium sensitizers. *Journal of the American Chemical Society*, 127(48):16835–16847, 2005.

[142] Michael Grätzel. Photovoltaic performance and long-term stability of dye-sensitized meosocopic solar cells. *Comptes Rendus Chimie*, 9(5):578–583, 2006.

[143] Kenichi Okada, Hiroshi Matsui, Takuya Kawashima, Tetsuya Ezure, and Nobuo Tanabe. 100 mm$\times$ 100 mm large-sized dye sensitized solar cells. *Journal of Photochemistry and Photobiology A: Chemistry*, 164(1):193–198, 2004.

[144] Helena Greijer, Lennart Karlson, Sten-Eric Lindquist, and Anders Hagfeldt. Environmental aspects of electricity generation from a nanocrystalline dye sensitized solar cell system. *Renewable Energy*, 23(1):27–39, 2001.

[145] Xing Fan, Fuzhi Wang, Zengze Chu, Lin Chen, Chao Zhang, and Dechun Zou. Conductive mesh based flexible dye-sensitized solar cells. *Applied physics letters*, 90(7):073501, 2007.

[146] Minna Toivola, Fredrik Ahlskog, and Peter Lund. Industrial sheet metals for nanocrystalline dye-sensitized solar cell structures. *Solar energy materials and solar cells*, 90(17):2881–2893, 2006.

[147] Yaoming Xiao, Jihuai Wu, Gentian Yue, Guixiang Xie, Jianming Lin, and Miaoliang Huang. The preparation of titania nanotubes and its application in flexible dye-sensitized solar cells. *Electrochimica Acta*, 55(15):4573–4578, 2010.

[148] Vishnuvardhanan Vijayakumar, Aurelien Du Pasquier, and Dunbar P Birnie. Electrical and optical studies of flexible stainless steel mesh electrodes for dye sensitized solar cells. *Solar Energy Materials and Solar Cells*, 95(8):2120–2125, 2011.

[149] Kinji Onoda, Supachai Ngamsinlapasathian, Takuya Fujieda, and Susumu Yoshikawa. The superiority of ti plate as the substrate of dye-sensitized solar cells. *Solar Energy Materials and Solar Cells*, 91(13):1176–1181, 2007.

[150] Dawei Gong, Craig A Grimes, Oomman K Varghese, Wenchong Hu, RS Singh, Zhi Chen, and Elizabeth C Dickey. Titanium oxide nanotube arrays prepared by anodic oxidation. *Journal of Materials Research*, 16(12):3331–3334, 2001.

[151] Qingyun Cai, Maggie Paulose, Oomman K Varghese, and Craig A Grimes. The effect of electrolyte composition on the fabrication of self-organized titanium oxide nanotube arrays by anodic oxidation. *Journal of Materials Research*, 20(01):230–236, 2005.

[152] Maggie Paulose, Karthik Shankar, Sorachon Yoriya, Haripriya E Prakasam, Oomman K Varghese, Gopal K Mor, Thomas A Latempa, Adriana Fitzgerald, and Craig A Grimes. Anodic growth of highly ordered tio_2 nanotube arrays to 134 μm in length. *The Journal of Physical Chemistry B*, 110(33):16179–16184, 2006.

[153] Karthik Shankar, Gopal K Mor, Haripriya E Prakasam, Sorachon Yoriya, Maggie Paulose, Oomman K Varghese, and Craig A Grimes. Highly-ordered tio_2 nanotube arrays up to 220 μm in length: use in water photoelectrolysis and dye-sensitized solar cells. *Nanotechnology*, 18(6):065707, 2007.

[154] Jan M Macak, Hiroaki Tsuchiya, Luciano Taveira, Saule Aldabergerova, and Patrik Schmuki. Smooth anodic tio_2 nanotubes. *Angewandte Chemie International Edition*, 44(45):7463–7465, 2005.

[155] Hyung-Jun Koo, Jihee Park, Beomjin Yoo, Kicheon Yoo, Kyoungkon Kim, and Nam-Gyu Park. Size-dependent scattering efficiency in dye-sensitized solar cell. *Inorganica Chimica Acta*, 361(3):677–683, 2008.

[156] Yanyan Zhang, Wuyou Fu, Haibin Yang, Qi Qi, Yi Zeng, Tong Zhang, Ruixia Ge, and Guangtian Zou. Synthesis and characterization of tio 2 nanotubes for humidity sensing. *Applied Surface Science*, 254(17):5545–5547, 2008.

[157] Jirapon Khamwannah, Yanyan Zhang, Sun Young Noh, Hyunsu Kim, Christine Frandsen, Seong Deok Kong, and Sungho Jin. Enhancement of dye sensitized solar cell efficiency by composite tio 2 nanoparticle/8nm tio 2 nanotube paper-like photoelectrode. *Nano Energy*, 1(3):411–417, 2012.

[158] Ho-Gyeong Yun, Jong Hyeok Park, Byeong-Soo Bae, and Man Gu Kang. Dye-sensitized solar cells with tio 2 nano-particles on tio 2 nano-tube-grown ti substrates. *Journal of Materials Chemistry*, 21(11):3558–3561, 2011.

[159] Hai Wang, Yong Liu, Hong Huang, Minyi Zhong, Hui Shen, Yuanhao Wang, and Hongxing Yang. Low resistance dye-sensitized solar cells based on all-titanium substrates using wires and sheets. *Applied Surface Science*, 255(22):9020–9025, 2009.

[160] Yuanhao Wang, Hongxing Yang, Yong Liu, Hai Wang, Hui Shen, Jin Yan, and Hongmei Xu. The use of ti meshes with self-organized tio2 nanotubes as photoanodes of all-ti dye-sensitized solar cells. *Progress in Photovoltaics: Research and Applications*, 18(4):285–290, 2010.

[161] Yanyan Zhang, Jirapon Khamwannah, Hyunsu Kim, Sun Young Noh, Haibin Yang, and Sungho Jin. Improved dye sensitized solar cell performance in larger cell size by using tio_2 nanotubes. *Nanotechnology*, 24(4):045401, 2013.

[162] Dong-Joo Kwak, Byung-Ho Moon, Don-Kyu Lee, Cha-Soo Park, and Youl-Moon Sung. Comparison of transparent conductive indium tin oxide, titanium-doped indium oxide, and fluorine-doped tin oxide films for dye-sensitized solar cell application. *Journal of Electrical Engineering & Technology*, 6(5):684–687, 2011.

[163] Jihuai Wu, Yaoming Xiao, Qunwei Tang, Gentian Yue, Jianming Lin, Miaoliang Huang, Yunfang Huang, Leqing Fan, Zhang Lan, Shu Yin, et al. A large-area light-weight dye-sensitized solar cell based on all titanium substrates with an efficiency of 6.69% outdoors. *Advanced Materials*, 24(14):1884–1888, 2012.